

# *Development of a cellulose acetate hollow-fine-fibre membrane*

by

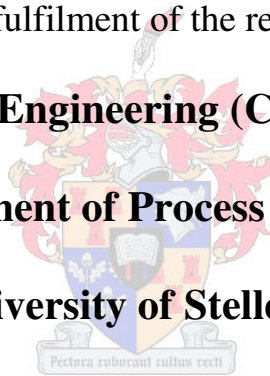
**Akram Tawari**

Thesis submitted in partial fulfilment of the requirements for the degree of

**Master of Science in Engineering (Chemical Engineering)**

**in the Department of Process Engineering at**

**the University of Stellenbosch**



*Supervised by*

**Study leaders**

**Prof SM Bradshaw**

**Prof EP Jacobs**

STELLENBOSCH

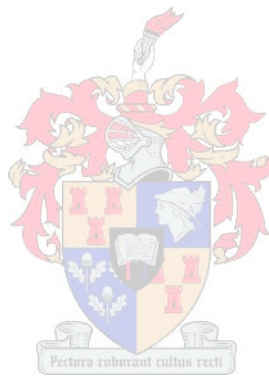
(March 2010)

## ***Declaration***

I, the undersigned, hereby declare that the work contained in this thesis is my own original work and that I have not previously in its entirety or in part submitted it at any university for a degree.

.....  
Signature

.....  
Date



## *Abstract*

The goal of this study is to produce cellulose acetate (CA) hollow-fine-fibre membranes with good water flux performance in the 95 – 96% salt retention range for brackish water desalination from first principles. First, the acceptable range of fibre dimensions was determined by means of a collapse pressure calculation using the elastic buckling pressure equation (thin shell assumption). Second, the pressure drop across the fibre wall in the hollow-fine fibre was determined by using the Hagen-Poiseuille equation, in order to determine how this would affect the chosen fibre dimensions. It was determined that the acceptable range of fibre dimensions was 222 – 247  $\mu\text{m}$ , and the wall thickness was 50  $\mu\text{m}$ . Fibres with these dimensions exhibited a high resistance to brackish water operating pressure of 20 – 25 bar, without collapse. The pressure drop calculations of these dimensions showed a sufficiently low pressure drop across the fibres.

A dry-wet spinning technique was used for the preparation of the hollow-fine-fibre membranes. Hollow-fine fibres were spun using CA dissolved in a suitable solvent and non-solvent mixture comprising acetone and formamide.

The effects of the dope composition and spinning parameters such as solvent to non-solvent ratio, bore fluid ratio, take-up speed, dope extrusion rate and heat treatment on the membrane morphology and performance were investigated. The spun fibres showed a good morphological structure, with no macrovoids (sponge-like structure), which is favourable for reverse osmosis (RO) applications. The hollow-fine-fibre membranes showed a good brackish water desalination performance within brackish water operating conditions.

Statistical analysis was used to generate a fabrication formulation for producing cellulose acetate hollow-fine-fibre membrane for brackish water desalination with improved salt retention and flux. A three-level three-factor factorial was used to the study of the effect of spinning parameters (solvent to non-solvent ratio, bore fluid ratio and air gap distance). A regression equation was successfully established and was used to predictably produce membranes with good performance within the limits of the factors studied. RO performance of these hollow-fine-fibre membranes was good: The salt retention ranged from 96 to 98% and the permeate flux ranged from 60 to 46  $\text{L}/\text{m}^2\cdot\text{d}$  (2 000 ppm, NaCl, 20 bar, 24 °C).

## *Opsomming*

Die studie het ten doel gehad om selluloseasetaat holveselmembrane vanaf eerste beginsels vir brakwaterontsouting te ontwikkel. Die ontsoutingsvlakke van die membrane moet tussen 95 en 96% lê met 'n aanvaarbare waterproduksievermoë. Aanvaarbare deursnee vir die holvesels is eerstens bepaal deur platval-berekeninge met behulp van die inmekaarvou-vergelyking uit te voer (dunwand aanname). Hierna is drukval oor die wand van die holvesel met behulp van die Hagen-Poiseuille vergelyking bepaal ten einde vas te stel hoe dit die gekose dimensies sal beïnvloed. Daar is vasgestel dat vesel deursnee tussen 222 en 247  $\mu\text{m}$  met 'n 50  $\mu\text{m}$  wand aanvaarbaar is. Vesels met hierdie dimensies het 'n hoë weerstand teen inval getoon by brakwater opereringsdrukke tussen 20 en 25 bar.

'n Droë-nat spintegniek is in die voorbereiding van die holveselmembrane gebruik. Holvesel membrane is met 'n selluloseasetaat stroop gespin wat uit 'n oplosmiddel (asetoon) en nie-oplosmiddel (formamied) bestaan het.

Die effek van die spinstroop samestelling en spinparameters soos die oplosmiddel tot nie-oplosmiddel verhouding, lumen-vloeistof verhouding, opneempoed, spinstroop ekstrusie tempo en hittebehandeling op membraan morfologie en werkverrigting is ondersoek. Die gespinde vesels toon 'n sponsagtige struktuur sonder die teenwoordigheid van enige mikro-leemtes wat voordelig is vir tru-osmose toepassings. Die holvesel membrane het aanvaarbare brakwater ontsoutings werkverrigting.

Statistiese analise is gebruik in die generasie van produksieformulasies vir die produksie van brakwater ontsoutingsmembrane met verbeterde retensie en vloed. 'n Drie-vlak drie-faktoriaal ontwerp is tydens die studie gebruik om die effek van spinparameters (oplosmiddel tot nie-oplosmiddel verhouding, lumen vloeistof verhouding, en lug-gaping) te ondersoek. 'n Regressie vergelyking is suksesvol daargestel en gebruik om voorspelbaar membrane met goeie werkverrigting binne die limiete van die studie te produseer. Die tru-osmose werkverrigting van die membrane was goed: die sout retensie het tussen 96 en 98% gelê en die permeaatvloed tussen 60 en 46  $\text{L}/\text{m}^2 \cdot \text{d}$  (2 000 ppm NaCl, 20 bar, 24°C).



## *Acknowledgements*

I would like to express my deep and sincere appreciation to the strong influence of my supervisor Prof Steven Bradshaw, for his valuable advice, enthusiasm, encouragement and patience throughout this study. I am gratefully indebted to my co-supervisor Prof Ed Jacobs for his limitless supply of ideas, advice and support throughout this research.

I also would like to express my gratitude to Prof Ron Sanderson for his assistance and time that gave to me.

A special thank to Dr Ian Goldie, my mentor, for his persistent guidance, and the friendly and patient manner in which he advised and assisted me in various ways during my research. Thanks to Dr Margie Hurndall, for her time and help with the editing of my thesis. I would like to acknowledge Deon Koen for his help in my research with the good experience in membrane field.

I express my gratitude to my family. They provided me with support, enthusiasm and encouragement.

Finally, I am extremely appreciative of the National Bureau of Research and Development in Libya, for financial support for this research and University of Stellenbosch.

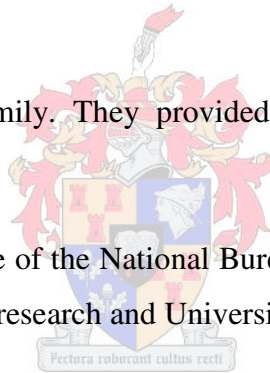


## *Table of contents*

<i>Declaration</i> .....	<b>ii</b>
<i>Abstract</i> .....	<b>iii</b>
<i>Opsomming</i> .....	<b>iv</b>
<i>Acknowledgements</i> .....	<b>v</b>
<i>Table of contents</i> .....	<b>vi</b>
<i>List of figures</i> .....	<b>ix</b>
<i>List of tables</i> .....	<b>xii</b>
<i>List of Symbols and abbreviations</i> .....	<b>xiii</b>
<b><i>Chapter 1: Introduction and objectives</i></b> .....	<b>1</b>
1.1 Introduction.....	2
1.2 Objectives .....	5
<b><i>Chapter 2: Theoretical background and literature review</i></b> .....	<b>7</b>
2.1 General considerations.....	8
2.2 Theory of RO .....	8
2.3 Membrane types.....	8
2.3.1 Symmetrical (isotropic) membranes .....	8
2.3.2 Asymmetrical (anisotropic) membranes .....	9
2.4 Applications of RO membranes.....	9
2.5 Transport phenomena across RO membranes .....	10
2.6 RO membrane materials .....	11
2.6.1 Thin-film composite membranes (TFC) .....	12
2.6.2 CA asymmetric membrane materials .....	12
2.6.3 Noncellulosic asymmetric membrane materials .....	14
2.7 Method of membrane fabrication by the phase inversion process.....	14
2.7.1 Solubility parameter .....	15
2.7.2 Wet phase-inversion process .....	18
2.8 Hollow-fibre membrane technology.....	22
2.8.1 The spinning process .....	24
2.8.2 Effect of spinning parameters on membrane morphology.....	26
2.9 Conclusion .....	32
<b><i>Chapter 3: The dimensional requirement for CA hollow-fine-fibre by means of Collapse and pressure drop calculations</i></b> .....	<b>33</b>

3.1	The resistance of hollow fibres to external pressure.....	34
3.1.1	Introduction .....	34
3.1.2	Elastic collapse pressure on cylindrical shells subjected to external pressure .....	34
3.2	Pressure drop across the wall of a hollow-fine-fibre membranes.....	35
3.2.1	Introduction .....	35
3.2.2	Pressure drop across the fibre wall of the hollow-fine-fibre membranes .....	35
3.3	Collapse pressure calculations .....	36
3.4	Pressure drop across the wall of a hollow-fine-fibre membrane .....	41
3.4.1	Fluid pressure drop equations .....	41
3.4.2	Material balance equation .....	42
3.4.3	Membrane transport equations .....	43
3.4.4	Numerical analysis to determine the pressure drop .....	45
3.5	Conclusion .....	47
<b>Chapter 4: Experimental techniques .....</b>		<b>48</b>
4.1	Introduction.....	49
4.2	Materials .....	49
4.2.1	Polymer .....	49
4.2.2	Low molecular mass components .....	50
4.2.3	Fibre mounting adhesive.....	51
4.3	Hollow-fibre spinning.....	51
4.3.1	Preparation of the spinning solution.....	51
4.3.2	Description of the spinning apparatus.....	51
4.3.3	The spinning process.....	53
4.4	Storage of hollow fibres.....	57
4.5	Hollow-fine-fibre analysis .....	58
4.5.1	Determination of membrane morphology by scanning electron microscopy .....	58
4.5.2	Measurement of hollow-fine-fibre dimensions .....	59
4.5.3	Determination of mechanical properties of hollow-fine fibres .....	59
4.6	Preparation of a membrane bundle .....	61
4.7	Post-treatment of hollow-fine fibres .....	62
4.8	Evaluation of hollow-fine fibres .....	62
4.8.1	Determination of RO performance (flux and salt retention).....	62
4.8.2	Determination of collapse pressure .....	63
<b>Chapter 5: Investigations into the effects of dope solution and spinning process for use in statistical analysis .....</b>		<b>64</b>

5.1	Introduction.....	65
5.2	Solvent to non-solvent ratio.....	65
5.3	Bore fluid.....	69
5.4	Dope extrusion rate.....	72
5.5	Take-up speed.....	72
5.6	Collapse pressure determination of the produced fibre dimensions.....	74
5.7	Effect of heat treatment.....	76
5.8	Conclusion.....	78
<b>Chapter 6: Statistical analysis using factorial design experiments for developing CA hollow-fine-fibre membranes .....</b>		<b>79</b>
6.1	Introduction.....	80
6.2	Experimental design .....	80
6.3	Results and discussion .....	82
6.3.1	Analysis of variance (ANOVA).....	82
6.3.2	Checking the adequacy of both regression models .....	83
6.3.3	Effect of factors and interactions on the performance of CA hollow-fine-fibre membranes.....	88
6.4	Model validation.....	92
6.5	Conclusions.....	93
<b>Chapter 7: Conclusions and recommendations .....</b>		<b>94</b>
7.1	Conclusions.....	95
7.2	Recommendations for future work .....	96
<b>References.....</b>		<b>98</b>
<b>Appendix A: Solubility parameters of solvents with reference to Figure 2-6.....</b>		<b>105</b>
<b>Appendix B: FORTRAN Codes .....</b>		<b>106</b>
<b>Appendix C: Results of the tensile test .....</b>		<b>107</b>

## *List of figures*

Figure 2-1: Diagrammatic presentation of the process of osmosis. <sup>11</sup> .....	8
Figure 2-2: Diagrammatic presentation of the process of reverse osmosis. <sup>11</sup> .....	8
Figure 2-3: Schematic representation of symmetric sub-structure.....	9
Figure 2-4: Schematic representation of asymmetric sub-structure.....	9
Figure 2-5: Water permeability of CA membranes as a function of the acetyl content of CA. <sup>18</sup> .....	13
Figure 2-6: Solubility diagram of cellulose acetate $\delta_p$ versus $\delta_h$ .....	17
Figure 2-7: Schematic of a Loeb-Sourirajan asymmetric membrane (finger-like structure). <sup>9</sup> .....	19
Figure 2-8: Schematic of a Loeb-Sourirajan membrane (sponge-like structure). <sup>9</sup> .....	19
Figure 2-9: Representative phase diagram for mixtures of polymer, a solvent and non-solvent, indicating the spinodal and binodal curves, and the tie lines. <sup>1</sup> .....	20
Figure 2-10: Schematic presentation of a hollow-fine-fibre module (Du Pont B9 Permeator). .....	23
Figure 2-11: Schematic presentation of typical hollow-fibre membrane spinning process... ..	25
Figure 2-12: Effect of various solvents on the porosity of CA membranes cast from 15% (m/m). <sup>84</sup> .....	27
Figure 2-13: Schematic diagrams of tow pores at low and high degree of orientation.....	29
Figure 2-14: Typical flux and NaCl retention of Asymmetric CA membrane. <sup>111</sup> .....	32
Figure 3-1: Collapse pressure of hollow fibre, calculated using both values of Young's modulus (0.114 and 0.094 GPa).....	40
Figure 3-2: Schematic diagram of single hollow-fine fibre. ....	41
Figure 3-3: Pressure drop across the fibre wall of hollow-fine-fibre membranes.....	46
Figure 4-1: Molecular structure of CA.....	49
Figure 4-2: Acetone. Formamide. ....	50
Figure 4-3: Schematic diagram of the dry-wet solution spinning apparatus.....	523
Figure 4-4: Tube-in-orifice spinneret used in the production of hollow-fine fibres. ....	544
Figure 4-5: Photographs showing apparatus used during the dry-wet spinning process. ....	566

Figure 4-6: Photographs of the preservation tanks containing fibres.....	577
Figure 4-7: Photograph of hollow-fine fibres mounted on stubs for SEM analysis. ....	59
Figure 4-8: Schematic diagram of a hollow-fine-fibre membrane bundle.....	61
Figure 4-9: Schematic of hollow-fine-fibre membrane test rig plant.....	63
Figure 5-1: SEM images of hollow-fine fibre spun from dope containing 27% CA, 49% acetone and 24% formamide. (acetone: formamide ratio 2.04). ....	666
Figure 5-2: SEM images of hollow-fine fibre spun from dope containing 27% CA, 43.2% acetone and 29.8 % formamide. (acetone: formamide ratio 1.447). ....	68
Figure 5-3: SEM images of hollow-fine fibre spun from dope solution containing 27% CA, 39% acetone and 34% formamide. (acetone: formamide ratio 1.147). ....	68
Figure 5-4: SEM images of hollow-fine fibre spun from dope solution containing 27% CA, 44% acetone and 29 % formamide, with water as bore fluid.....	70
Figure 5-5: SEM images of hollow-fibre fibre spun from dope solution containing 27% CA, 44% acetone and 29 % formamide, with 80 % acetone and 20% water as bore fluid. ....	711
Figure 5-6: SEM images of hollow-fine fibre spun from dope solution containing 27% CA, 44% acetone and 29% formamide with 20% acetone and 80% water as bore fluid. ....	711
Figure 5-7: SEM images of hollow-fine fibre spun from dope solution containing 27% CA, 44% acetone and 29% formamide with 70% acetone and 30% water as bore fluid. ....	71
Figure 5-8: SEM images of hollow-fine-fibre membrane with different dimensions (M1 to M4). ....	73
Figure 5-9: SEM images of hollow-fine-fibre membrane spun using lower take-up speeds (a) 60 r/min (b) 40 r/min respectively.....	744
Figure 5-10: Collapse pressures of CA hollow-fine fibre with different ID/OD ratios. ....	75
Figure 5-11: Effect of heat treatment on CA hollow-fine-fibre membrane performance. ....	76
Figure 5-12: Effect of annealing time on CA hollow-fine-fibres membrane performance at the second annealing temperature at 86 °C. ....	77
Figure 6-1: Normal plot of residuals for retention (left) and flux (right). ....	87
Figure 6-2: Plots of residuals verses predicted response values for retention (right) and flux (left). ....	87
Figure 6-3: Effect of solvent/non-solvent and bore fluid ratio on salt retention.....	89
Figure 6-4: Effect of solvent/non-solvent and bore fluid ratio on water flux. ....	89

Figure 6-5: Response surface plot of the effects of solvent/non-solvent ratio and air gap distance on salt retention of CA hollow-fine-fibre membranes. .... 90

Figure 6-6: Response surface plot of the effects of solvent/non-solvent ratio and air gap distance on water flux of CA hollow-fine-fibre membranes..... 90

Figure 6-7: Response surface plot of the effects of air gap distance and bore fluid ratio on salt retention of CA hollow-fine-fibre membranes..... 91

Figure 6-8: Response surface plot of the effects of air gap distance and bore fluid ratio on flux of CA hollow-fine-fibre membranes. .... 91



## *List of tables*

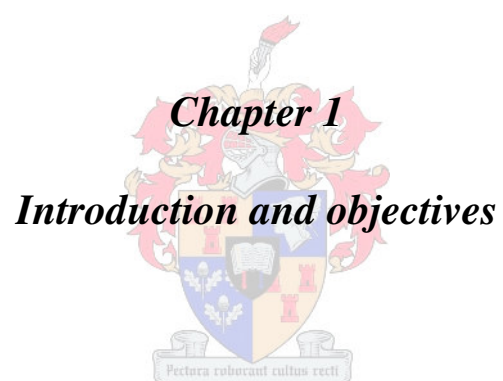
Table 2-1: Performance achieved by commercial membranes to various applications .....	10
Table 3-1: Hollow-fine-fibre collapse pressure (Young's modulus 0.114 GPa, wall thickness 50 $\mu\text{m}$ ) .....	39
Table 3-2: Hollow-fine-fibre collapse pressure (Young's modulus 0.094 GPa, wall thickness 50 $\mu\text{m}$ ) .....	39
Table 4-1: Properties of CA used in this study .....	50
Table 4-2: Properties of acetone and formamide used in this study .....	51
Table 4-3: Typical spinning conditions used to prepare CA hollow-fine-fibre membranes by statistical analysis .....	58
Table 5-1: Temperature changes associated with heat of mixing .....	65
Table 5-2: Temperature changes associated with heat of mixing .....	677
Table 5-3: The viscosities of 27% (m/m) CA polymer spinning solution with different solvent/non-solvent ratio (Zero shear rate at 23.4 $^{\circ}\text{C}$ ) .....	67
Table 5-4: Effect of dope extrusion rate on retention and flux of CA hollow-fine-fibre membranes for brackish water desalination .....	72
Table 5-5: Mechanical properties and fibre diameters as function of take-up speed.....	733
Table 5-6: Calculated and measured collapse pressure values .....	75
Table 6-1: Factors and levels for $3^3$ levels factorial design .....	80
Table 6-2: Design data of the experiments and their replication with response values .....	81
Table 6-3: Analysis of variance of the regression model for retention .....	82
Table 6-4: Analysis of variance of the regression model for flux.....	83
Table 6-5: Comparison of the actual and predicted responses of retention and flux .....	86
Table 6-6: Confirmation runs with their responses .....	92
Table 6-7: Actual and predicted responses of retention and flux for the confirmation runs....	93



## *List of Symbols and abbreviations*

Å	Angstrom
A, B, C	Factors (defined as feature of a designed experiment)
ANOVA	Analysis of variance
CA	Cellulose acetate
cm	Centimetre
DMF	N-dimethyl formamide
DMAc	N-dimethyl acetamide
df	Degree of freedom
GPa	Gigapascal
h	Hours
L/m <sup>2</sup> .d	Litre per square meter day
MF	Microfiltration
m/m	Mass ratio
MPa	Mega Pascal
ml/min	Millilitre per minute
NMP	N-methyl-2-pyrrolidone
ppm	Parts per million
Prob>F	Probability
RO	Reverse osmosis
r/min	Revolution per minute
TFC	Thin film composite membrane
UF	Ultrafiltration





## 1.1 Introduction

About 60% of the land surface of the earth is arid, and most of this dry portion of the earth's surface is near to or has available sources of saline water. These arid regions in the world, including North Africa, Arabian Gulf and Middle East, are actively searching for supplementary sources of fresh water to help fulfil future demands. This quest includes new sources of fresh water such as the desalination of brackish and seawater.

According to the World Health Organization<sup>1</sup> drinking water should not contain more than 500 ppm dissolved salts and water containing more than 1000 ppm should not be used for human consumption. Water containing 1000 – 5000 ppm dissolved solids is classified as brackish. Sea water contains about 35000 ppm dissolved solids.

The technology of desalination was designed for the creation of new sources of fresh water, as the seas and inland brackish supplies offer great unlimited sources of water. The use of desalination of sea and inland brackish water by a pressure-driven separation process, which included the use of reverse osmosis (RO) membranes, was proposed 50 years ago, and this use has been widely studied from the basic mechanism to the design of industrial scale plants.<sup>2-4</sup>

Membrane separations processes are attractive for several reasons:<sup>3</sup>

- there is no phase change as in the other conventional thermal desalination processes, which reduces the energy requirements;
- the process is inherently simple: a pressurized feed solution (usually water) passes through a semipermeable barrier from the side with higher solute concentration to the side with lower solute concentration;
- membranes processes can be applied, with almost the same principles, to a wide variety of problems in many different fields, like desalination, waste treatment, food products, and pharmaceutical products; and
- the operation is essentially at ambient temperature, which is very important in certain applications especially where temperature-sensitive substances are involved.

RO is a membrane permeation process for separating relatively pure water (or other solvent) from a less pure solution. The solution is passed over the surface of an appropriate semipermeable membrane at a pressure in excess of the effective osmotic pressure of the feed

solution. The permeating liquid is collected which the product and the concentrated feed solution is generally discarded.<sup>4</sup>

A practical RO membrane for water purification application should possess several characteristics:

- it must be highly permeable to water in preference to all other components in the feed solution and highly impermeable to solutes;
- the rate of permeation of water per unit surface (water flux) must be high enough to produce reasonable product volumes per unit time;
- the membrane must be durable, physically, chemically and biologically to have a reasonable extended life; and
- the membrane must be able to withstand substantial pressure gradients on its own or with some porous backing or support material. Finally, the membrane should be easily fabricated into the configuration necessary for use and preferably have an asymmetric structure, so as to provide a membrane with high permeability and selectivity.<sup>5</sup>

One of the most common membrane types in use is the asymmetric flat-sheet cellulose acetate (CA) membrane. These membranes were developed in the early 1960s by Loeb and Sourirajan.<sup>6</sup> The asymmetric CA membrane was considered to be the leading commercial membrane at that time, when Reid proved that CA was able to retain salts in 1959.<sup>15</sup> The reason this membrane performs as well as it does is the structure of the CA material which has about 2.5 acetyl groups per repeat unit and consists of a very thin, dense skin, 0.15 – 0.25  $\mu\text{m}$  in thickness, on top of a highly porous substructure.<sup>7</sup> It should be noted that the RO properties of the membrane are determined by the thin dense layer. CA membranes are also mechanically and chemically stable, they can withstand low concentration levels of chlorine typically 1 ppm, as well as other oxidants. This is a significant advantage over other membrane types, such as polyamide and thin-film composite membranes which are susceptible to degradation by even ppm of chlorine concentration.<sup>8</sup>

RO technology was further advanced during the 1970s by introduction of hollow-fibre membranes. Hollow-fibre membranes have played an important role in the membrane separation technology since the earliest development of reverse osmosis membranes for sea water desalination, primarily due to its large surface area, typically  $10^4 \text{ m}^2/\text{m}^3$  per unit volume, which exceeds other membrane module configurations. They are also self-supported

(there is no need for supporting material). Hollow-fibre membranes for RO desalination are typically of small fibre dimensions in the range of 300 – 500  $\mu\text{m}$  outside diameter to be able to withstand high operating pressure for RO applications without collapse.

When the fibre diameter ranges from 50 to 500  $\mu\text{m}$ , the fibres are usually called hollow-fine fibres. They have the ability to withstand high feed pressure (20 bar or more) applied from the outside. This property makes them suitable for RO or high-pressure gas separation.<sup>9</sup> This study will focus on producing a RO hollow-fine-fibre membrane within the range of these diameters. When the fibre diameters are greater than 500  $\mu\text{m}$ , the hollow fibres are commonly used for MF or UF, which do not require high operating pressure.<sup>9</sup>

Various spinning techniques have been used to prepare hollow-fibre membranes, such as melt spinning, dry spinning and dry-wet spinning. The dry-wet spinning process is commonly used to prepare hollow-fibre membranes. This spinning process can be employed to obtain almost every known membrane morphology by controlling the phase separation processes that take place.

In the current study, CA hollow-fine-fibre membranes were prepared using the dry-wet spinning technique. The preparation process in this study involved using a mixture of solvent and water as internal coagulant. Using a mixture of solvent and water as bore fluid had two advantages: (1) to control the inside structure of nascent fibre to obtain the desirable structure; (2) to allow the nascent fibres to be drawn to a smaller dimensions, as the inside fibre takes some time to be completely set. Other parameters were also investigated in this study to develop the asymmetric structure of CA hollow-fine-fibre membranes with good water flux in the 95 – 96% salt retention range for brackish water desalination. Furthermore, the hollow-fine-fibre membranes in the current study were operated from outside by applying a feed pressure for brackish water applications in the range of 20 – 25 bar.

The basis of this work relies on the concept of creating an efficient RO hollow-fibre membrane that should provide a high product water flow rate at low energy expenditure. The membrane and the processes that it will be used for should meet the following requirements:- (the suggested means by which the requirements can be met are given in brackets):

- high water permeability with low salt permeability (CA material was found as good material for this property);

- large membrane surface area (producing hollow-fine-fibre membranes should be able to meet this requirement, smaller fibre dimensions offer larger surface area);
- high resistant fibres for RO operating pressure of brackish water desalination (collapse pressure calculations should meet this requirement);
- low pressure drop across the membrane (determining the acceptable range of fibre dimensions for brackish water applications by pressure drop calculations should be able to meet this requirement); and
- defect-free asymmetric RO membranes (adopting the dry-wet spinning technique to control the phase separation that happens from both sides should meet this requirement).

## 1.2 Objectives

The objectives of this study were the following:

- To determine the acceptable range of fibre diameters for brackish water desalination by means of collapse pressure analysis, using the elastic buckling pressure equation for a thin shell under external pressure (thin shell assumption).
- To determine the pressure drop ( $\Delta P$ ) along the fibre bore in the hollow-fine-fibre by using the Hagen-Poiseuille equation in order to determine how  $\Delta P$  affects the chosen fibre dimensions.
- To investigate the effect of spinning parameters on membrane performance and morphology for use in the statistical analysis to prepare CA hollow-fine fibre membranes for brackish water based on the dimensional requirement determined above.
- To perform collapse pressure tests on produced fibres to validate the calculated fibre dimensions data.
- To perform a statistical analysis to study the effect of the dry-wet spinning parameters in order to develop CA hollow-fine-fibre membranes with good water flux performance in the 95 – 96% salt retention range.

## Outline of the thesis

Chapter 2 contains a theoretical background and literature review on the basic principles of RO, membrane types and materials, applications of RO, transport across the RO membrane and methods of membrane fabrication by the wet phase-inversion process. The last part

describes the hollow-fibre membrane technology and the effect of various fabrication parameters on hollow-fibre membrane morphology.

Chapter 3 contains the collapse and pressure drop calculations used to determine an acceptable range of fibre dimensions.

Chapter 4 contains the material used and the experimental layout for the preparation of CA hollow-fine-fibre membranes, potting of hollow-fine-fibre in membrane bundles, heat treatment and determination of fibre morphology by scanning electron microscopy, measurement of fibre dimensions and determination of mechanical properties. The last part deals with the evaluation of membrane performance and determination of collapse pressure of the resultant fibres.

Chapter 5 concerns the spinning parameters involved in fabrication of hollow-fine-fibre membranes. Under investigation are bore fluid type, solvent to non-solvent ratio, air gap distance, dope extrusion rate, take-up speed and finally the determination of membrane collapse pressure.

Chapter 6 contains results of the  $3^3$  factorial design experiments conducted on the fabrication of membrane. Here three major factors mainly are solvent/non-solvent ratio, air gap distance and bore fluid ratio are presented and discussed. The regression equations created and thereafter the model validation was carried out. The excellent fit to the model is discussed.

Chapter 7 contains the overall conclusions as they relate to the stipulated objectives.

## ***Chapter 2***

### ***Theoretical background and literature review***





## 2.1 General considerations

## 2.2 Theory of RO

When a solution of a chemical substance, which therefore has a chemical potential, is separated from pure water by a semipermeable membrane, the membrane will allow the passage of water, but not salt. The pure water, as it flows through the membrane will increase the chemical potential of the salt solution (Figure 2-1). This process will continue until equilibrium of chemical potential is restored or until the hydrostatic pressure of the salt solution is sufficiently high to arrest the process. This hydrostatic pressure is known as the osmotic pressure of the salt solution. Use of this phenomenon in the opposite direction will result in water being forced through the membrane from the concentrated solution to the more dilute solution side. This reverse flow is achieved by applying a pressure higher than the osmotic pressure of the concentrated solution to the concentrate side of the membrane (Figure 2-2).<sup>10</sup>

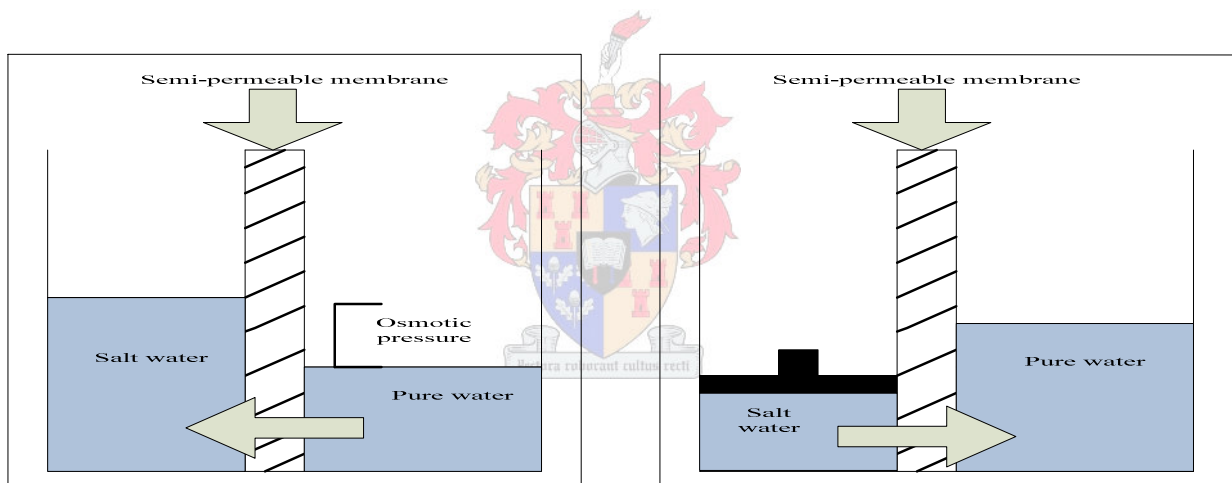


**Figure 2-1:** Diagrammatic presentation of the process of osmosis.<sup>11</sup>

**Figure 2-2:** Diagrammatic presentation of the process of reverse osmosis.<sup>11</sup>

## 2.3 Membrane types

Two types of morphological membrane structures can be distinguished, symmetrical and asymmetrical membranes.

### 2.3.1 Symmetrical (isotropic) membranes

When a membrane sub-structure shows symmetry perpendicular to the membrane surface, the membrane is said to be symmetric (uniform structure) Figure 2-3. The resistance to mass transfer in the symmetrical membranes is determined by the entire thickness of the membrane,

which in turn affects the membrane permeation rate. A decrease in membrane thickness increase mass transfer and the permeation rate increases.



**Figure 2-3:** Schematic representation of a symmetric sub-structure.

### 2.3.2 Asymmetrical (anisotropic) membranes

Reid made the first membrane from CA, for use in RO studies.<sup>15</sup> He proved that CA membranes were semipermeable. These membranes were symmetric in structure and dense. Loeb and Sourirajan were the first to improve on these CA membranes. Their breakthrough was to produce asymmetric membranes.<sup>12</sup> Asymmetrical membranes comprise a layered structure with a thin finely porous or dense permselective top-layer supported on a much thicker, highly permeable but integrated microporous layer (Figure 2-4). An advantage of asymmetric membrane lies in their internally layered structure, where each layer can be optimized so that these membranes provide high flux and retention.<sup>12</sup> The asymmetric membranes almost completely displaced the symmetrical membranes because of their superior flux and retention performances.

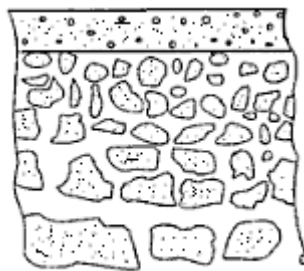


**Figure 2-4:** Schematic representation of an asymmetric sub-structure.

## 2.4 Applications of RO membranes

The main application of RO technology is the desalination of sea and brackish water for producing fresh potable water of good quality.<sup>13</sup> The amount of salt present in brackish water is between 1000 and 5000 ppm and the operating pressure required is about 20 – 25 bar. Therefore up to 90% of the salt must be removed from these levels for brackish water to be useful as potable water. In sea water the salt concentration is about 35000 ppm and

the operating pressure required is about 40 – 80 bar. Thus up to 99.9% of seawater salts must be removed from these levels. The performances achieved by commercial membranes of various applications such as high-pressure sea water membrane, medium-pressure brackish water membrane and low pressure nanofiltration membranes are tabulated in Table 2-1. RO can be used for a wide range of applications in many other fields, for example:<sup>14</sup>

- for the electronics industry;
- pharmaceutical and medical industry;
- textile and dye industry;
- treatment of domestic and municipal water;
- paper and pulp industry;
- petrochemical, steel and machine industry;
- electroplating operations;
- food and beverage industries;
- nuclear power industry; and
- power generation.

**Table 2-1: Performance achieved by commercial membranes to various applications**

Parameter	Sea water	Brackish water	Nanofiltration
Pressure (bar)	40 – 80	20 – 25	6 – 10
Solution concentration % (m/m)	1 – 5	0.2 – 0.5	0.05
Retention (%)			
NaCl	99.9	97	60
MgCl <sub>2</sub>	99.9	99	89
MgSO <sub>4</sub>	99.9	99.9	99
Na <sub>2</sub> SO <sub>4</sub>	99.8	99.1	99
NaSO <sub>3</sub>	90	90	45
Ethylene glycol	70	-	-
Glycerol	96	-	-
Ethanol	-	20	20
Sucrose	100	99.9	99.0

## 2.5 Transport phenomena across RO membranes

The choice of membrane material and the phase separation process play important roles in determining the pore size distribution throughout a membrane, which in turn affect the trans-membrane flux. There are three models describing the transport phenomena of the water and solutes through RO membranes.

(1) The bound water pore-type diffusion model (water clustering). This model is applicable to CA membranes that contain polar groups (carboxyl). Hydrogen bonding of water molecules will tend to bond with the carboxyl groups at the interface between the solution and

the membrane and create an absorbed film. Then the bound water will dissolve and translate through the membrane pore from one hydrogen-bonding site to another under the effect of the driving force.<sup>15</sup> Not every solute component in an aqueous solution can dissolve in bound water. In this model a solute component that does not form a hydrogen bond can be passed through a pore in a membrane structure.<sup>15</sup>

(2) The porous capillary-diffusion model. This model was established on the assumption that the RO membrane has a fine porous skin and heterogeneous structure, in which the flow of water will take place through the pores. If the characteristic of membrane surface has indicated negative adsorption of each solute at the membrane-solution interface, the solute is then excluded because of the low dielectric constant. Therefore, solute concentration decreases rapidly in the vicinity of the membrane-solution interface, and a preferential thin sorption layer of pure water is formed at the membrane-solution interface. This preferential water sorption layer will move through the capillaries of the membranes under the pressure gradient. This module is applicable for material such as CA and polyamide that involve the preferential sorption of substances at the interface.<sup>16, 17</sup>

(3) The solution-diffusion model. This model is based on the assumptions that membranes have a homogeneous nonporous surface layer and all molecular species will dissolve and diffuse through the membrane by a solid- or liquid-diffusion mechanism in an uncoupled manner. In this model both the concentration and the pressure gradient across the membranes work as driving forces for the matter to be transported from one side to the other.<sup>18, 19</sup> This model applies to thin-film composite membranes (Section 2.6.1) and not to CA membranes.

## 2.6 RO membrane materials

Many different types of membrane materials have been used to fabricate RO membranes. The ultimate target of RO membranes and performance is to provide fresh water from sea water (which contains 3.5% (m/m) ions of dissolved salts). This demands of membranes to have a salt retention greater than 99.3% and a permeate of less than 500 ppm salt. Early membranes could meet this target only when operated at very high pressure up to 100 bar but as membranes with improved performance became available this pressure has decreased to 55 – 68 bar. Recently the need for desalination membranes has shifted more towards brackish water with salt concentrations of 0.2 – 0.5% (m/m), working at operating pressures

up to 27 bar, and providing salt retentions of 96 – 98%, because the energy consumption is proportional to the salt content in the source water.<sup>9,20</sup>

An important consideration in polymer material is hydrophobicity or hydrophilicity. Hydrophilicity is favoured in RO membranes, as it could enhance the diffusion of water molecules through the membrane.<sup>21</sup> However RO membranes can only be made from materials that have the right hydrophilic/hydrophobic balance, since it is important for water to be able to interact with the membranes as seen from the earlier discussion on models.

### **2.6.1 Thin-film composite membranes (TFC)**

The first commercialized true TFC membrane was developed in 1972.<sup>22</sup> A TFC membrane can be defined as a multilayer membrane which was developed as an alternative means of producing an ultrathin semipermeable membrane layer on top of a more porous support layer. TFC membrane can be made from an aqueous solution of a reactive prepolymer, such as a polyamine. This layer is first deposited in the pores of a microporous support membrane, typically a polysulfone ultrafiltration membrane after which it is cross-linked to insolubilise it. The advantage of TFCs is that the roles of the active separating layer and the support can be separated. The semipermeable coating can be optimized for water flux and solute retention, while the microporous sublayer can be optimized for porosity and mechanical strength. TFC membranes have significantly higher salt retention and flux compared to integrally skinned membranes such as asymmetric CA and polyamide membranes, because of the ultrathin selective skin layer deposited on the top of the more porous support layer. TFC membranes are susceptible to degradation by chlorine and oxidants. Thus the exposure to trace levels of chlorine or hypochlorite disinfectants cause rapid permanent loss in selectivity in TFC membranes.<sup>8</sup> An other disadvantage of TFC membranes, is that the negative membrane surface will attract coagulants and cationic polymers.<sup>23</sup>

### **2.6.2 CA asymmetric membrane materials**

The first asymmetric RO membranes were developed by Loeb and Sourirajan.<sup>12, 24</sup> These flat-sheet CA membrane were cast at 0 °C from casting solutions containing 15 – 25% (m/m) CA dissolved in a solvent system consisting of acetone with water and magnesium perchlorate as non-solvent. Formamide is now used as non-solvent instead of water and magnesium perchlorate. Due to its amorphous structure CA dissolves in most of the convenient solvents such as acetone, dioxane, N-dimethyl formamide (DMF), N-methyl-2-pyrrolidone (NMP) and N-dimethyl acetamide (DMAc).

An important characteristic of CA membrane is the dependence of water and solute permeabilities on degree of substitution. The water and solute permeabilities of CA membranes are sensitive to the degree of acetylation. With increasing degree of acetylation, the solubility of water in the membrane decreases as does the water permeability.<sup>18</sup> Figure 2-5 shows the effect of the degree of the acetylation on the salt and water permeability of CA membranes. Most commercial CA membrane uses a polymer containing about 40% (m/m) acetate with a degree of acetylation of 2.7.

CA combines the three essential requirements for an efficient RO membrane: (1) it is highly permeable to water, (2) its permeability to most water-soluble compounds is low, and (3) it is an excellent film-former.<sup>5</sup> CA also has additional advantages that include the following: ease of fabrication, low-cost, a sustainable resource, CA membranes are nonionic and have less tendency to attract ionically charged substances such as coagulants in RO pretreatment, mechanical stability, resistance to degradation by chlorine and other oxidants. CA membranes are chlorine tolerant up to 1 ppm and therefore work well in systems where biological fouling attacks must be controlled.

Asymmetric RO membranes are also made from other derivatives of cellulosic materials, such as cellulose triacetate and cellulose diacetate, or blends of both.

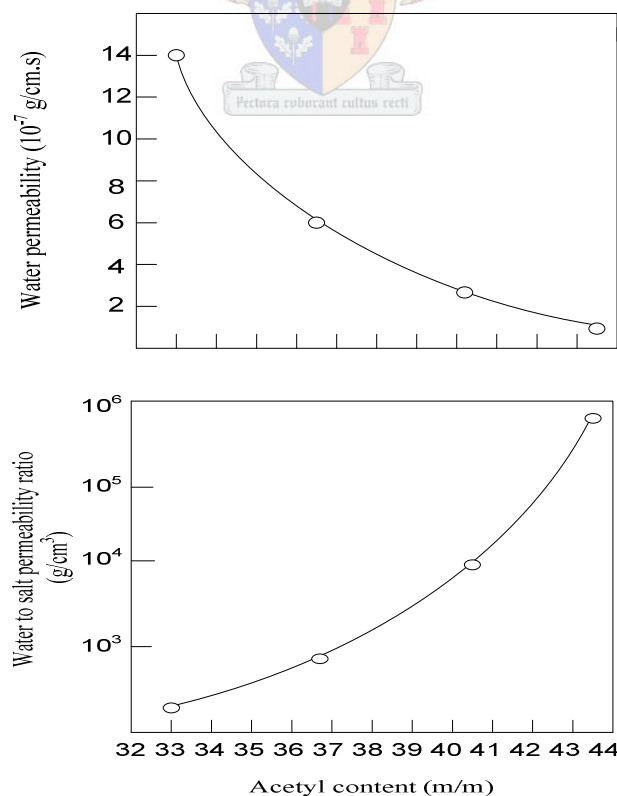


**Figure 2-5:** Water permeability of CA membranes as a function of the acetyl content of CA.<sup>18</sup>

### 2.6.3 Noncellulosic asymmetric membrane materials

Many different noncellulosic materials have been used for fabricating RO membranes,<sup>25</sup> such as aromatic polyamide. Aromatic polyamide asymmetric membranes, in particular, were developed by several chemical groups.<sup>26,27</sup> These membranes were all in the form of hollow-fibres and have a good solute retention 99.5%. Polyamide membranes like TFC, are also susceptible to degradation by chlorine because of their amide bonds. Thus chlorine removal is necessary, while in the case of CA membranes, the presence of chlorine protects against bacterial attacks.

### 2.7 Method of membrane fabrication by the phase inversion process

In the following section the fundamentals of membrane fabrications will be discussed. Phase inversion is one of the most important preparation processes in membrane technology; it is also known as polymer precipitation.<sup>28</sup> Phase inversion is a process by which a homogeneous polymer solution decomposes into two phases during the immersion of the solution in a non-solvent bath. A solid, polymer-rich phase that will become the rigid membrane structure forms the matrix, and a liquid, polymer-lean phase forms the voids and interconnecting pores.

Phase inversion membranes can be prepared from any polymer mixture that forms under certain conditions of temperature and composition in which the free energy of mixing of the polymer system must be negative.<sup>28</sup> The demixing of a composition can be processed by a break of the thermodynamic homogeneous condition of the solution through a change in the solution composition or a change in the solution temperature. The final morphology of a solidified membrane is determined by the kinetics of the phase transition during demixing.<sup>28</sup> There are four techniques that can be used to induce the phase inversion:- (i) polymer precipitation by evaporation of a volatile solvent from a homogeneous solution,<sup>29, 30</sup> (ii) polymer precipitation by immersion of homogeneous solution into a coagulation bath (wet phase-inversion process),<sup>31, 32</sup> (iii) the thermal inversion process,<sup>31, 33</sup> and (iv) the polymer assisted phase inversion process.<sup>34</sup> The majority of the commercially available membranes are produced by the wet phase-inversion process. The work of this thesis involved the use of the wet phase-inversion process, so only the details of the wet phase-inversion will be examined here. Before introducing the wet phase-inversion process, the solubility parameter concept, which relates to the polymer/solvent system in terms of their miscibility and compatibility, will be discussed first.



### 2.7.1 Solubility parameter

The solubility parameters was first articulated by Hilderbrand and Scott.<sup>35</sup> It is a parameter to express the nature and magnitude of interaction between molecules. Dissolution of polymeric materials is accompanied by free energy change, which can be written as:

$$\Delta G_M = \Delta H_M - T\Delta S_M \quad (2.1)$$

where  $\Delta G_M$  is the change in Gibbs free energy on mixing,  $T$  is the absolute temperature, and  $\Delta S_M$  is the entropy of mixing. A negative value of  $\Delta G_M$  implies that solvent/polymer system forms a homogenous solution, that is, the two components are miscible.<sup>36</sup> The term  $T\Delta S_M$  is always positive because there is an increase in the entropy on mixing. (But, note the negative sign). Therefore the sign of  $\Delta G_M$  depends on the magnitude of  $\Delta H_M$ , the enthalpy of mixing.

A method has been proposed to predict the solubility behaviour of polymers by the relationship of Hilderbrand who connected the Gibbs free energy of mixing of two compounds to their respective heat of vapourization.<sup>35</sup>

$$\Delta H_M = V_M v_1 v_2 \left[ \left( \frac{\Delta E_1}{V_1} \right)^{1/2} - \left( \frac{\Delta E_2}{V_2} \right)^{1/2} \right]^2 \quad (2.2)$$

Where  $\Delta H_M$  is the total heat of mixing (J/mol),  $V_M$  represents the total molar volume of the mixture,  $\Delta E$  represents the energy of vapourization (J/mol),  $V$  represents the molar volume of both components 1 and 2 ( 1 = solvent, 2 = polymer ) and  $v$  represents the volume fraction of components 1 and 2 of the solution mixture. The quantity  $\frac{\Delta E}{V}$  represents the energy of vapourization per unit volume. This term is called the cohesive energy density and relates to the cohesive forces that keep the molecules of the solution together. The square root of the cohesive energy density is widely known as the solubility parameter,  $\delta$ :

$$\delta = \left( \frac{\Delta E}{V} \right)^{1/2}$$



Thus the heat of mixing of two components can be arranged now in terms of solubility parameters:

$$\frac{\Delta H_M}{(V_M v_1 v_2)} = (\delta_1 - \delta_2)^2 \quad (2.3)$$

according to equation (2.3). A polymer becomes more soluble in a solvent when their respective solubility parameters are close to each other. If a solvent and polymer have the same solubility parameters, the heat of mixing is zero and they are therefore miscible in all proportions. The lower the solubility parameter difference, the larger the tendency for miscibility. On the other hand, a polymer becomes less soluble in a solvent when the difference in their solubility parameters increases.

Hansen<sup>37</sup>, assumed that the total energy of evaporation,  $\Delta E_M$ , was an additive quantity:

$$\Delta E_M = \Delta E_d + \Delta E_p + \Delta E_h \quad (2.4)$$

$\Delta E_d$ , the energy required to overcome dispersion forces;  $\Delta E_p$ , the energy required to overcome polar forces; and  $\Delta E_h$ , the energy required to break the hydrogen bonding forces. Dividing equation 2.4 by the molar volume  $V$ , yields the parallel equation in terms of the solubility parameters:

$$\delta_T^2 = \delta_d^2 + \delta_p^2 + \delta_h^2 \quad (2.5)$$

where  $\delta_T^2$  is the total Hilderbrand solubility parameter.

Hansen found that in many cases the two dimensional coordinates based on only the  $\delta_p$  (polar force) and  $\delta_h$  (hydrogen bonding) values were adequate to describe the solubility boundary of a given polymer. In practice, the solubility of the polymer is determined in a series of solvents whose locations on a two or three dimensional grid are represented by the ordered pairs given by their solubility parameters.<sup>38</sup> To find the optimum solvent for polymer using solubility parameters, it is most desirable to have the solubility

parameters for polymer, matching the parameters for already existing solvent or combination of solvents.

CA has been characterized very well in the literature, both in terms of its solubility and in terms of the asymmetric sub-structure. In Figure 2-6 the boundaries of solubility for CA based on data obtained from literature are shown.<sup>39, 40</sup> To simplify the diagram, solvents have been assigned numbers and these are tabulated in (Appendix A). With very few exceptions most of the solvents are encompassed within the area designated, and most, if not all non-solvents, are excluded from the area. For a homogeneous polymer, the diagram will describe a region containing the solvents for the specific polymer. Non-solvents for the polymer are located outside the region. It can be seen from the figure below that acetone lies within the area of solubility for CA and is therefore as a suitable solvent. Water and formamide lie outside the area of solubility for CA and are used as non-solvents.

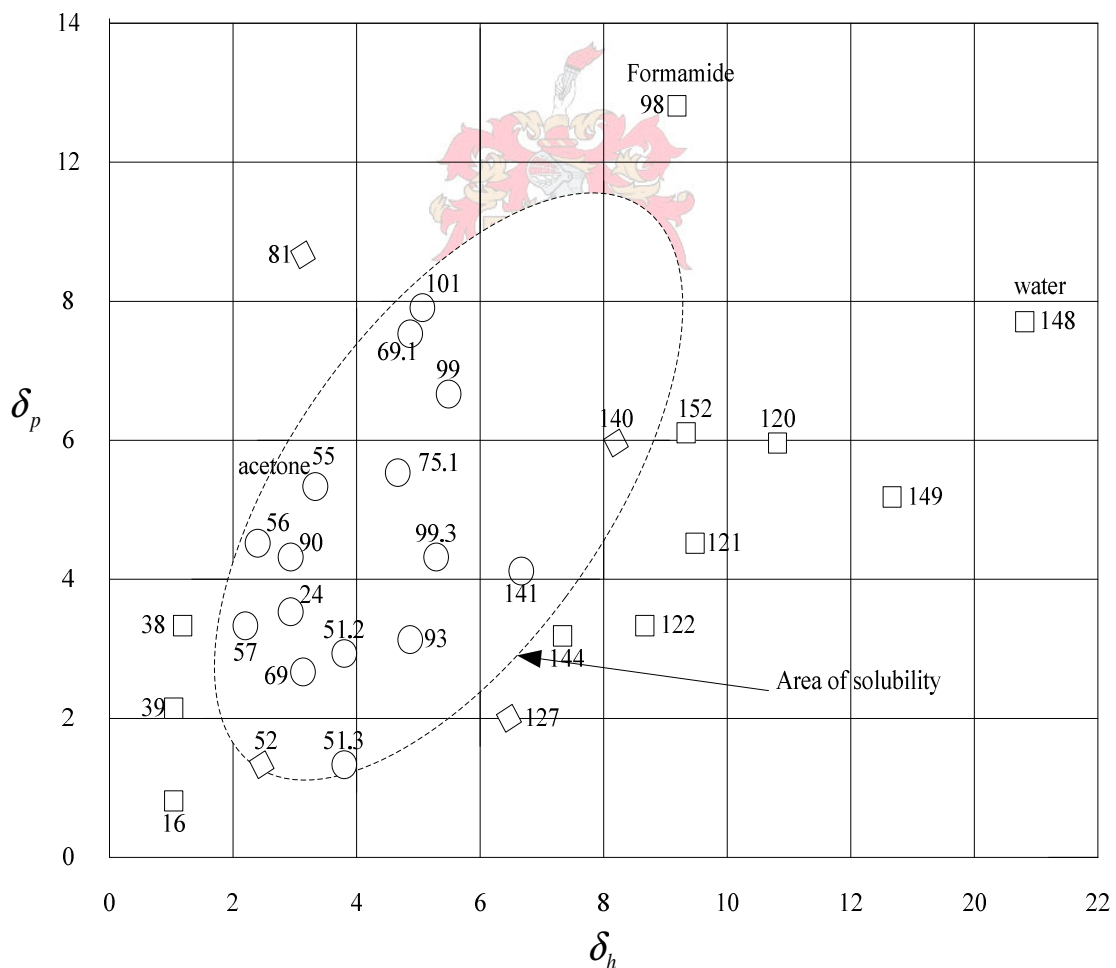


**Figure 2-6:** Solubility diagram of cellulose acetate  $\delta_p$  versus  $\delta_h$ .<sup>39, 40</sup>

Legend in the figure represents: ○ soluble, ◇ partially soluble and □ insoluble

## 2.7.2 Wet phase-inversion process<sup>31, 32</sup>

The preparation of asymmetric membranes by means of immersion precipitation of a casting solution started with the development of RO membranes by the Loeb-Sourirajan process.<sup>6</sup> The immersion precipitation technique is also used for making the supporting layer of thin-film composite (TFC) membranes. This technique remains one of the most important inventions in the membrane-making process. Changing the membrane structure, from typical RO characteristics to UF or MF characteristics, can be done by varying the process parameters in the membrane preparation or by adding extra components to the casting solution or to the precipitation bath. The choice of polymer is also important since RO membranes can not be made from hydrophobic polymers.

The procedure to prepare a wet phase inversion membrane by immersion precipitation can be spilt into five essential steps:

- preparation of the casting solution, which includes mixing of the polymer into the solvent or solvent system, with or without additives such as formamide or magnesium perchlorate;
- casting or extruding the solution using an appropriate procedure (for flat-sheets or hollow fibres);
- allowing some of the solvent to evaporate by exposing the nascent membrane to the air for a certain period of time;
- coagulation in a non-solvent medium, where the nascent membrane is immersed and precipitated in a fluid medium (usually water), which is a non-solvent for the polymer but is completely miscible with the polymer solvent and other additives; and
- post treatment (annealing, pressurization, etc.)

The membrane formation process can be split into two parts:

- Alteration of the polymer solution composition prior to immersion into a coagulation bath, by an evaporation step. It has commonly been established that during the evaporation step, the solvent will evaporate from the surface of the nascent membrane and then the polymer concentration in the top layer of the polymer solution will be increased.<sup>41, 42</sup>

- Composition changes in the dope solution during the immersing into a coagulation bath usually water by demixing processes, which takes place when the composition of the polymer solution becomes metastable.<sup>43, 44</sup>

Schematics of a Loeb-Sourirajan membrane prepared by immersion precipitation are shown in Figures 2-7 and 2-8.

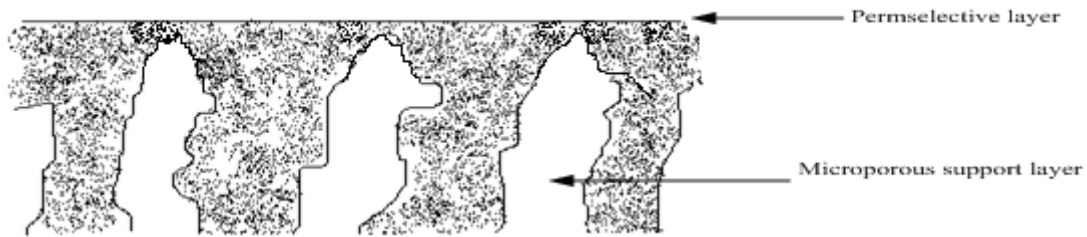


**Figure 2-7:** Schematic of a Loeb-Sourirajan asymmetric membrane (finger-like structure).<sup>9</sup>

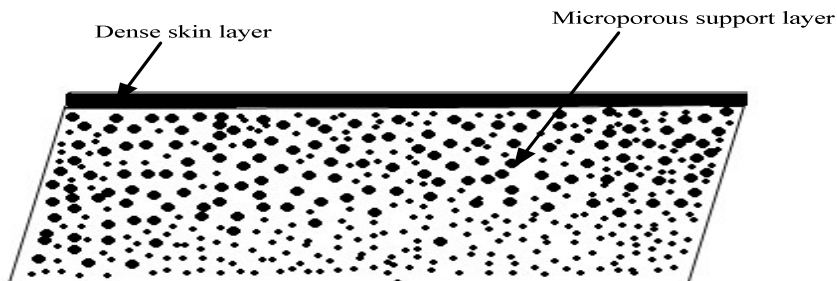


**Figure 2-8:** Schematic of a Loeb-Sourirajan membrane (sponge-like structure).<sup>9</sup>



Membrane formation by the phase immersion process is illustrated in Figure 2-9, using an isothermal phase diagram, which is divided into homogeneous, metastable and liquid-liquid demixing regions, and where each point in the triangle represents one of three mixtures of a polymer, a solvent and a non-solvent (water). For practical purposes it is convenient to subdivide the liquid-liquid demixing gap into a region of spinodal demixing and a region of nucleation and growth of the polymer-rich and polymer-poor phase.<sup>45, 46</sup>

During immersion of the dope solution the homogenous solution becomes thermodynamically unstable by crossing the binodal boundary. This brings the dope solution into a metastable two-phase region, where the composition of the solution in this region will not precipitate unless well-nucleated. The metastable region in the phase diagrams of low-molecular-mass materials is very small, but can be larger for high-molecular-mass materials. As more solvent diffuses out and more non-solvent diffuses in, the composition crosses into another

region of the phase diagram in which a one-phase region is always thermodynamically unstable. In this region compositions separate into two phases: a solid polymer-rich phase and a liquid polymer-poor phase, connected by tie lines in the phase.<sup>1, 47</sup>

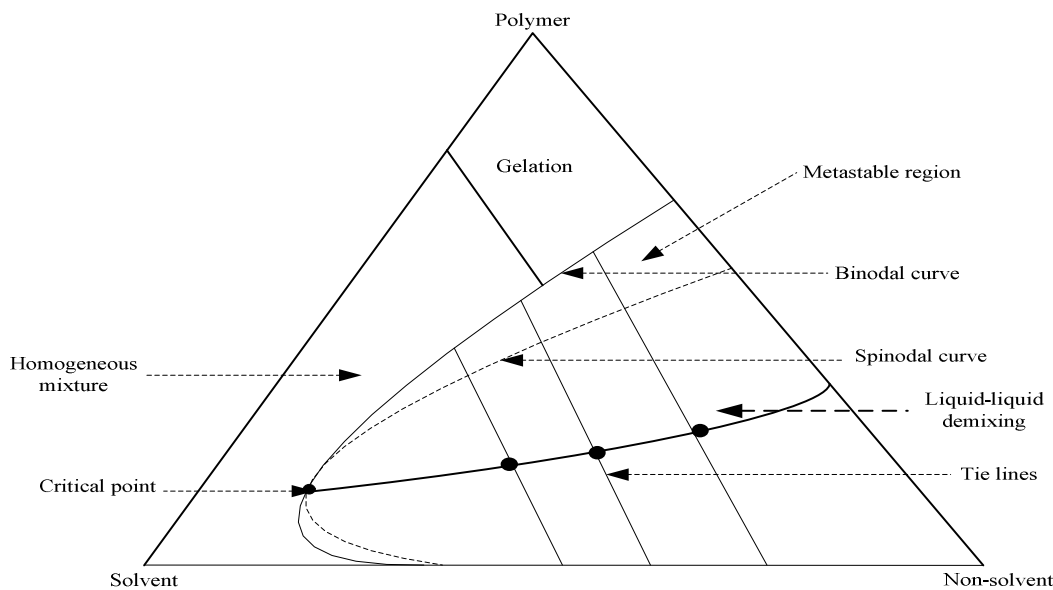
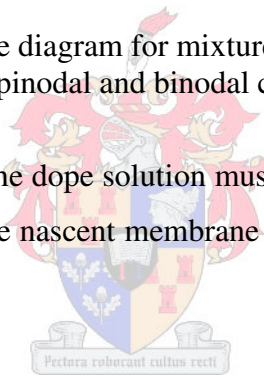


**Figure 2-9:** Representative phase diagram for mixtures of polymer, a solvent and non-solvent, indicating the spinodal and binodal curves, and the tie lines.<sup>1</sup>

In the wet phase-inversion process the dope solution must be relatively viscous at the point of immersion in the non-solvent, so the nascent membrane can maintain its integrity throughout the formation process.<sup>28</sup>



During the wet phase-inversion process, the membrane structure can be determined by two different mechanisms, the skin top layer is formed first by a gelation process and the substructure underneath the skin is formed second by a liquid-liquid demixing mechanism discussed below.

## Gelation

Gelation process is a phenomenon of considerable importance during membrane formation especially for the top layer to form a defect free polymeric network. Gelation can be physically defined as a network of entangled polymer chains with solvent trapped in the network.<sup>48</sup> Several investigators ascribe the skin formation of asymmetric membranes to a transformation of fluid polymer solution to a gel state having infinite viscosity caused by the evaporation of a volatile solvent.<sup>49, 50</sup> This explanation has been widely accepted in the dry-wet phase inversion process. Various types of intermolecular interactions can, in

principle, give rise to an interconnected polymer network in solution. Microcrystallites, ionic interaction, hydrogen bonding, dipolar interactions, hydrophobic interactions and solvent bridging may induce the formation of gels.<sup>51, 52</sup>

### **Liquid-liquid demixing**

At the immersion of a homogeneous polymer solution in a non-solvent (coagulation) bath, the solution lowers its free enthalpy by separating into two liquid equilibrium phases. There are two ways for this demixing to occur: by nucleation and growth of droplets of the second phase or by instantaneous spinodal demixing.<sup>53, 54</sup> The spinodal demixing gap is surrounded by the composition area where phase separation by nucleation and growth takes place. Liquid-liquid demixing takes place by nucleation and growth of droplets of a polymer poor phase when the original composition of the solution is located at polymer concentrations higher than that of the critical point. The solution demixes by nucleation and growth of droplets of a polymer rich phase when the polymer concentration is lower than that of the critical point. Once formed the droplet can grow because of the presence of a concentration gradient towards the droplet.<sup>55, 56</sup>

During the growth stages of a nucleation and growth process, nuclei of the new phase form progressively larger droplets, which are dispersed in the second phase. A highly supersaturated solution will lead to a larger number of nuclei compared to those formed from a barely supersaturated solution, thereby affecting the morphology of the resultant microphase separated structure.<sup>57</sup> During the course of phase separation, the size of droplets evolved from a highly supersaturated system will be much smaller than for those formed from barely supersaturated solution, since there are more centers competing for phase separating material.<sup>57</sup>

Phase separation by nucleation and growth generally leads to a random distribution of droplet sizes and positions in the surrounding phase.<sup>58</sup> Two structures can be distinguished by the liquid-liquid demixing mechanism. One is a sponge-like structure which results from delayed liquid-liquid demixing and the other is a finger-like structure (macrovoids) that results from instantaneous liquid-liquid demixing.<sup>59, 48</sup> In the case of the former the composition path crosses the binodal curve in the phase diagram immediately after immersion in the non-solvent bath to form a membrane with a finger-like structure. In the case of the latter it takes some time before the composition path crosses the binodal curve to configure a membrane

with a sponge-like structure.<sup>44, 60</sup> In the case of instantaneous liquid-liquid demixing, the nuclei of the polymer-poor phase are those responsible for macrovoid formation. The growth of these nuclei takes place because of the diffusional flow of solvent from polymer solution into nuclei is larger than the flow of non-solvent from the nuclei into the polymer solution. A nucleus can only grow if a stable composition is induced in front of it by diffusion. In this way nuclei continues to grow to form the macrovoids until the polymer concentration at the macrovoid wall becomes so high that solidification occurs.<sup>59, 48</sup> On the other hand, growth will cease if a new stable nucleus are being generated in front of the first formed nucleus. In the case of delayed onset liquid-liquid demixing, nucleation is not possible until a certain period of time has passed. In the meantime the polymer concentration has increased in the top layer with the extension of the delay time. After a finite period, the nucleation of the polymer-poor phase sets in, starting in the layer beneath the top layer, there will be an interfacial layer where nuclei cannot be formed anymore and a membrane with a dense top layer is the result.<sup>59, 48</sup> There are many parameters that influence the onset of liquid-liquid demixing, which can also determine the membrane structures. The main parameter is the affinity between solvent/non-solvent, other parameters include the addition of additives to the dope solution, the addition of solvent to the coagulation and increasing the polymer concentration of the dope solution.

## 2.8 Hollow-fibre membrane technology

Hollow-fibre membranes are of high commercial importance. Their fabrication by spinning dopes or mixtures containing membrane forming materials (polymers) has been described in a series of patents by Mahon (1966), assigned to the Dow Chemical Company.<sup>61, 62</sup>

Hollow-fibre membranes were developed to be used for a wide range of applications, such as water purification (e.g. potable water production from saline or non-saline resources, bioseparation, waste water treatment), gas separation and membrane contactors.<sup>63-65</sup>

The diameters of hollow fibres vary over a broad range, from 50 to 3000  $\mu\text{m}$ . Hollow fibres can either made as a homogenous dense structure or, more preferably, an asymmetric microporous structure. The latter has an ultrathin skin that forms the effective barrier to solute permeation. This skin can either be on the inside, or on the outside of the fibre depending on whether the feed flow is from the inside or the outside. Hollow fibres for UF and MF have the skin on the inside and also in the outside, whereas hollow-fine fibres for RO are smaller and have the skin on the outside. This is because of the high pressure required in



RO. Also, if the inside diameter is so small, the membrane would quickly block with retained species if the feed flow was from the inside out.

Hollow-fine-fibre RO membranes operate at high pressures and this is accomplished by engineering the membrane material into special modules. Essentially, hollow-fine-fibre membranes module consists of thousands or millions of individual fine fibres, depending on fibre dimensions, which are then are looped into a bundle around a perforated central feed tube. Both ends of the fibre bundle are sealed off by a potting resin creating a tube-sheet, open on one end and closed on the other end (See Figure 2-10).

The hollow-fine-fibre modules operate by pressurizing the feed water into the centre tube, in which it is distributed along the entire length of the permeator. The feed flows radially to the outside of the fibre shell. The pure water permeates through the fibre walls into the bore-side of the fibres and then exits through the tube-sheet into a permeate collector. The retentate flows between the outside of the fibre bundle and the inside wall of the vessel to the collector. The surface provided by fine fibres is ten times greater than that of spiral-wound membranes, about  $10^4 \text{ m}^2/\text{m}^3$ .

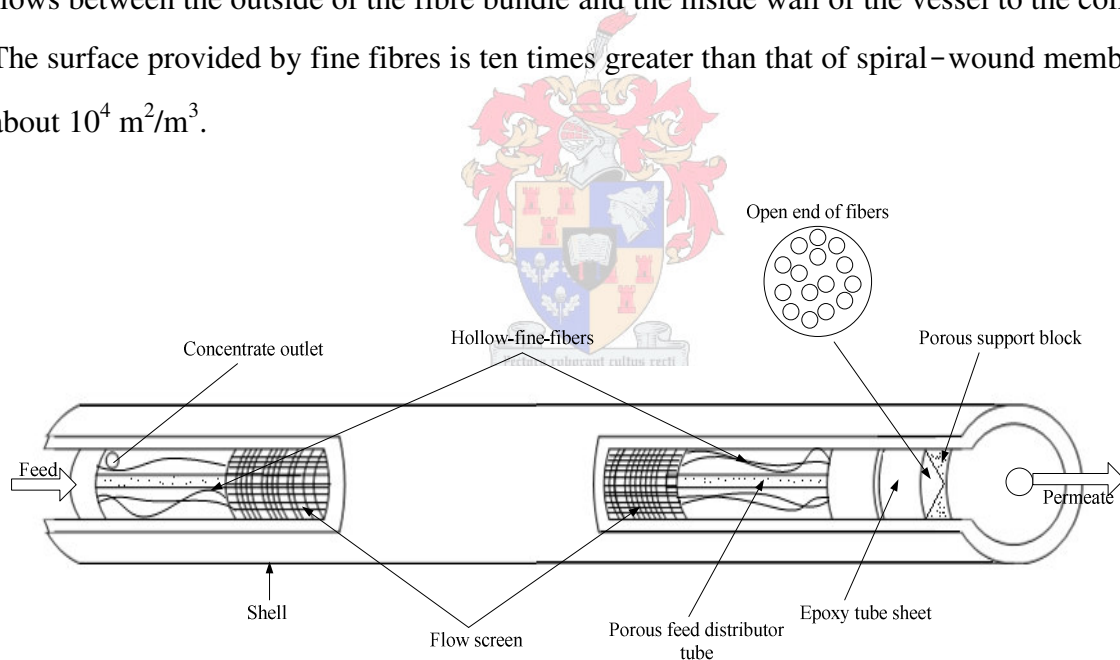


**Figure 2-10:** Schematic presentation of a hollow-fine-fibre module (Du Pont B9 Permeator).

Hollow fibres have key advantages over other membrane configurations, such as flat-sheets. Hollow fibres have extremely high membrane surface area to pressure-vessel volume, which gives high productivity per unit volume. It is for this reason that hollow fibres are commonly used in industry.<sup>66</sup> The other advantages of the hollow fibres that they are self-supporting, unlike the flat-sheet membranes that need a supporting material. In addition concentration polarization usually is smaller under most practical conditions in hollow fibres than in flat-sheet membrane systems.<sup>67</sup>



It is well known that it is very difficult to develop a hollow-fibre spinning process by adopting the process conditions developed for asymmetric flat-sheet membranes. This is because there are two coagulation processes occurring during the spinning of hollow-fibre (the interior and exterior surfaces), while there is only one coagulation process on the surface for an asymmetric flat-sheet membrane.

The spinning of asymmetric hollow-fibre membranes requires special handling procedures in order to achieve and maintain optimum permeation properties,<sup>68</sup> particularly in the following steps in the fabrication process:

- spinning of plasticized fibres;
- processing the fibres in a wet swollen state;
- replasticizing the fibres after the spinning operation; and
- physical modification of the fibres after the spinning operation.

### 2.8.1 The spinning process

There are three conventional methods for spinning hollow-fine fibres. The choice of the particular spinning method depends on the desired scheme for the fibre formation.<sup>69, 70</sup>

#### Melt spinning

In melt spinning the polymer is heated above its melting point in an inert atmosphere and then the liquid polymer is extruded through a spinneret.<sup>71</sup> By immediate cooling a phase transition occurs and the polymer solidifies. Hollow fibres made by this technique are usually denser and have lower flux than fibres prepared by wet spinning. This technique is more applicable for polymers which are not soluble in convenient solvents, such as cellulose triacetate, and polypropylene which therefore difficult to form by wet spinning. An example of hollow fibres prepared by melt spinning from a polymer/diluent system is polypropylene/soybean oil mixture.<sup>72</sup> Another example is fibres prepared from cellulose triacetate/sulfolane/Polyethylene glycol.<sup>73</sup>

#### Dry spinning

In the dry spinning technique the polymer is dissolved in a very volatile solvent. After extrusion the polymer solution is heated and because of evaporation of the solvent the polymer will solidify usually in the absence of a coagulation bath. This technique is known

to produce a more dense fibre structure than that obtained by wet spinning. Cellulose acetate/acetone is an example of a system used to prepare a fibre by dry spinning.<sup>74</sup>

### Wet spinning (dry-wet spinning)

In this process the polymer solution is extruded into a non-solvent bath where demixing occurs because of exchange of solvent and coagulant. Between the spinneret and coagulation bath there is an air gap where actually the membrane formation starts. This implies good control of this phase as a first requirement. Any type of membrane morphology can be obtained with this technique such as sponges and finger type-structures since many parameters involved can be varied. The majority of hollow fibres employed in technical membrane processes are spun by this technique. Hollow fibres made by this technique have the asymmetric structure of Loeb-Sourirajan membranes and subsequently improved membrane performance (high flux and high retention). The wet spinning technique is relatively simple to produce very-small-diameter membranes, as a fair amount of draw-down can occur at the point of extrusion. The nascent membrane is liquid when it leaves the spinneret, and as the bore-fluid (acetone/water in this study) does not have much coagulation power in the bore side, the final membrane diameter can easily be drawn down to smaller dimensions. In this study the dry-wet spinning technique will be used and the process is schematically illustrated by Figure 2-11.

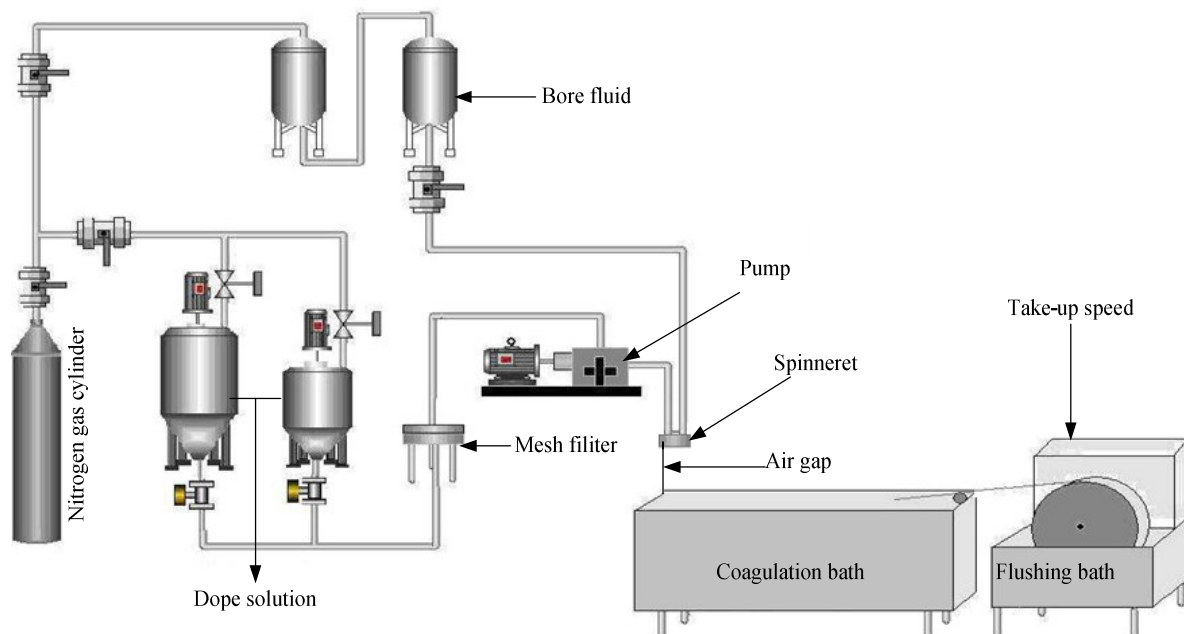


**Figure 2-11:** Schematic representation of typical hollow-fibre membrane spinning process.

## 2.8.2 Effect of spinning parameters on membrane morphology

There are several parameters involved in the spinning process of hollow-fibre membranes. The following have been investigated by others for their effects on both membrane morphology and separation performance:<sup>75</sup>

- polymer concentration;
- choice of solvents;
- choice of additives;
- length of air gap;
- take up speed;
- dope extrusion rate; and
- heat treatment.

### 2.8.2.1 Polymer concentration

The polymer concentration of the dope solution is a very important factor that influences the formation of the membrane structure during the phase inversion process. It is known that an increase in polymer concentrations will cause very high polymer concentrations at the film/bath interface, resulting in the formation of a less porous top layer. This will encourage the entanglement of polymer chains and hence reduce the formation of pores in the skin layer (reduced porosity). Thus a sponge-type structure will be obtained and, as a consequence, the separation potential of the membrane will be increased, but the permeability will be diminished. This structure also increases the mechanical strength of the hollow fibre, which is favourable for RO applications as it allows the fibres to withstand high operating pressures. A dope solution of low polymer concentration tends to higher precipitation rates and consequently increase the initiation of fingers in a finger-type structure.<sup>48, 76</sup>

Membranes cast from a dope solution with low CA content as follows 17% (m/m) CA, 68% (m/m) acetone, 1.5% (m/m) magnesium perchlorate, and 13.5% (m/m) water exhibits a higher water flux and lower retention than the original Loeb-Sourirajan membrane.<sup>77</sup> A 25% (m/m) CA, 30% (m/m) formamide and 45% (m/m) acetone casting solution was capable of producing membranes with good properties.<sup>78</sup> Flat-sheet CA membranes was produced by using two polymer concentration of 25 and 27.5% (m/m) and it was found that the later concentration gave high retention of up to 97%.<sup>79</sup> CA RO hollow fibres were spun by the

dry-wet spinning technique from a dope solution with polymer concentrations in the range of 25 and 28% (m/m) and the salt retention rates were 16 and 83.5% respectively.<sup>80</sup> A concentration of 30% CA was used to produce a hollow-fibre membranes and it gave a salt retention rate of 80%.<sup>81</sup> A dope-spinning solution consisting of 27% (m/m) CA in a mixture of 43.8 % (m/m) acetone and 29.2% (m/m) formamide was used to produce RO hollow-fibre membranes and it showed a salt retention of 94%.<sup>82</sup>

The complexity of the process of membrane preparation precludes a direct link or graph between concentrations of the polymer in the dope to the water flux or retention achieved. It has been shown however that higher concentration provides better retention.<sup>79</sup>

### 2.8.2.2 Choice of solvents

The choice of solvent is one of the most important parameters in the phase inversion process. Generally, the morphology of membranes can be controlled by the selection of solvents.<sup>62</sup> Dope solutions that contain aprotic solvents with high heat of mixing, such as (DMF), (NMP) and (DMAc) will precipitate rapidly when immersed in the coagulation bath. These solvents yield membranes with more open-porous structures (finger-like structure). On the other hand dope solutions with solvents with low heat of mixing such as acetone, dioxane and ethylformate will precipitate slowly, and yield relatively nonporous membranes (sponge like-structure).<sup>83</sup> Since the aim is to produce skinned membranes, the acetic solvent system is chosen. Figure 2-12 illustrates the apparent correlation between the solvent solubility parameter and membrane porosity.<sup>84</sup>

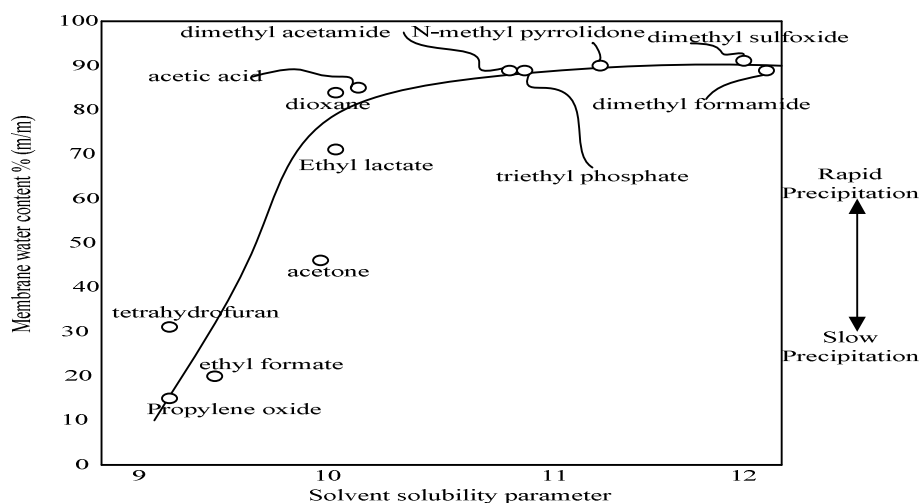


**Figure 2-12:** Effect of various solvents on the porosity of CA membranes cast from 15% (m/m).<sup>84</sup>

### 2.8.2.3 Choice of additives

A casting solution to be used for the preparation of a phase-inversion membrane usually consists of solvent, a polymer and an additive. The additives, such as salts and organic compounds, are less compatible with the polymer than the solvent. Even if the quantity of additive in a casting solution is small the effect of additives on the formation of membrane structure can be significant. Their characteristic as pore-forming agents improve permeation properties.<sup>85</sup> When a non-solvent is added to a casting solution, the non-solvent will lead the composition of the casting solution to thermodynamic conditions that lie close to the binodal demixing region, and result in instantaneous demixing and subsequently to a porous sub-structure with a thin top layer.<sup>86</sup>

Magnesium perchlorate and water were used as an additive in the development of the first asymmetric CA RO membrane by Loeb and Sourirajan.<sup>85</sup> Nowadays, formamide is found to be a good additive, since it acts as a swelling agent for CA rather than a solvating agent. Membranes manufactured with formamide included in the casting solution exhibit higher fluxes and retention,<sup>87</sup> exceeding the performance of the Loeb and Sourirajan type membrane, for which magnesium perchlorate was used as an additive.<sup>78</sup>

In conclusion, non-solvents have an opposite effect to solvents. Upon the addition of a non-solvent to the polymer solution, the polymer chains will shrink and coil between themselves, as they seek like sites in an unlike medium. The solution subsequently has no more solvating ability, and the polymer precipitates with little ingress of the coagulant.<sup>88</sup>

### 2.8.2.4 Bore fluid

It is known that the bore fluid composition has a significant influence on the formation of the inside structure of the hollow-fibre membranes and fibre dimensions. The bore fluid must necessarily provide a highly open circular lumen in the interior of the hollow fibre without affecting the dry/wet phase inversion process that takes place at the exterior surface. It has been demonstrated that using water as the bore fluid will produce a hollow-fibre membrane with a highly open circular lumen because of its strength as non-solvent for polymer.<sup>89</sup> However, it was found that reducing the activity of the water used as bore coagulant play an important role in determining the membrane performance. The activity of the water may be altered by the addition of solvents for the polymer. Two mixtures of DMAc/water and potassium acetate/water were previously used as bore fluids. The results revealed that the

selectivity of polysulfone hollow-fibre membranes increased with decreasing the water activity in both mixtures.<sup>90</sup> It was found that using a mixture of NMP and water as bore fluid in a CA hollow-fibre membrane for gas separation, improved the membrane separation.<sup>91</sup>

### 2.8.2.5 Air gap length

The air gap is the distance between the coagulation bath and spinneret from which the dope solution is extruded (Figure 2-11). Changing the air gap length during the spinning process affects the performance of the final fibre.<sup>92-95</sup> It was reported that an increase in the air gap distance leads to the formation of a hollow-fibre membrane with significantly lower permeation. This probably results from the higher gravity-induced elongation stress on the nascent fibres (still a flowable viscous solution), resulting in greater orientation and tighter molecular packing.<sup>92</sup> It was also found that the outer diameter or wall thickness decreased with an increasing air gap because of the enhanced elongation of the nascent fibre in the increased air gap. It was concluded that the water flux decreased while retention increased, which could be attributed to the enhanced gravity-induced elongational stress and orientation with increasing air gap leading to the formation of smaller elongation pores (Figure 2-13).<sup>92</sup>

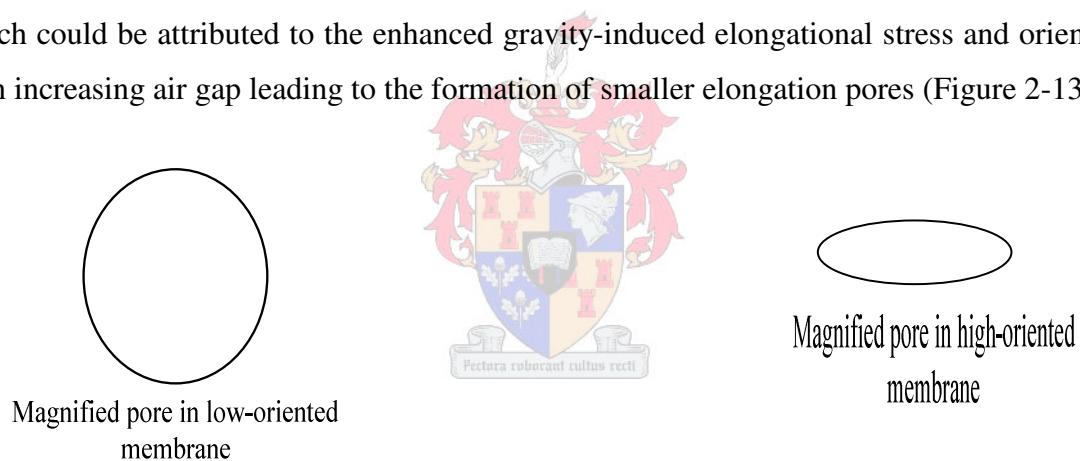


**Figure 2-13:** Schematic diagrams of two pores at low and high degree of orientation.

The fibre undergoes evaporation phase separation in the dry gap as solvent evaporates. The air gap is responsible for the formation of a thin dense skin on the outside of the fibre and the bulk of the fibre structure is formed in the coagulation bath.<sup>93, 94</sup> Pinnau et al were the first to incorporate a forced convection stage into their membrane production process.<sup>93, 95</sup> The membranes formed had a skin thickness of approximately 200 Å. They proposed that the aggressive nature of the evaporation step brought the composition of the outer layer of the fibre into a state of spinodal decomposition, a conclusion reached because of the turbidity of the fibre in the air gap. However, a spinodal outer layer should result in a micro-porous skin and a defect free skin on their membranes was reported.

There is a controversy whether an increase in the air gap distance will result in a fibre with lower permeability and higher selectivity.<sup>96, 97</sup> It was found that the average pore size on a membrane surface in the inside decreases with an increase in the length of the air gap. This is also because of the stretching and elongation state of the nascent fibres by their own weight and, as a result the polymer molecules stretch and therefore the aggregate move closer to each other and reorder themselves into a condition of greater stability.<sup>98</sup> Conversely, it was observed that an air gap length of 200 – 300 mm, produced fibres with very poor selectivity, whereas an air gap length of 100 – 150 mm yielded fibres with high selectivity for gas separation.<sup>99</sup> Higher orientation and tighter packing of the polymer molecules in the selective skin layer may occur as result of increasing the air gap length and where, therefore, hollow fibres with higher retention and lower flux will therefore be obtained.<sup>100</sup> It has been found that the air gap distance of 127 mm resulted in high flux hollow-fibre membranes made from CA.<sup>81</sup> This controversy remains as an air gap distance of 130 mm resulted in super selective hollow fibres for gas separation, while an air gap of 70 mm yielded fibres with an optimum gas separation.<sup>101, 102</sup>

#### 2.8.2.6 Dope extrusion rate

The effect of the dope extrusion rate has in many studies been linked with the effect of shear stress on the membrane structure, which is induced within the thin annulus of the spinneret.<sup>82-103, 104</sup> It was generally found that an increase in the dope extrusion rate results in an increase in the shear rate. The shear stress at the wall of the spinneret is then also increased. The increase in shear stress will affect the polymer orientation. The polymer molecular chains are inclined to line themselves up much better and, as a result of this orientation, the polymer molecules will pack closer to each other, leading to a dense skin layer. These hollow fibres with tighter skin on the lumen side will have a lower water flux and higher salt retention. Therefore the dope flow rate through the spinning processes plays an important role in determining the membrane performance. It was also shown that increasing the dope flow rate will result in higher selectivity of the hollow fibre membrane for gas separation.<sup>105</sup> UF membranes with a dense skin layer and smaller pore size was produced as result of higher polymer orientation at higher dope extrusion rate and resultant fibres have lower permeability and higher selectivity.<sup>106</sup> It was found that the orientation of polymer molecules increased on the skin layer of RO and gas separation hollow fibres with high dope extrusion rate and subsequently enhancing the gas selectivity and RO retention.<sup>101-104</sup>



### 2.8.2.7 Take-up speed

Hollow fibre membranes with small diameters (less than 300  $\mu\text{m}$ ) are favoured for RO, for two reasons. Firstly, they provide higher module productivity, and secondly they have a greater ability to withstand high operating pressures than larger diameters. These small fibre diameters are usually shaped using high take-up speed, which may also be associated with high tensile stress on the spin line. Sometimes a higher take-up speed can cause higher orientation, which is usually favourable for the desired membrane application.<sup>107</sup> Different take-up speeds were used in the preparation of hollow fibres by the dry-wet spinning and results showed that with higher take-up speeds the wall thickness and the outer and inner diameters are decreased.<sup>108</sup> It was also found that the water permeability increased while the retention decreased slightly, with an increase in take-up speed.

### 2.8.2.8 Heat treatment

The last step in membrane fabrication is the annealing by immersion in hot water. It was found that the freshly formed membranes for RO applications have very high water flux but almost no retention of sodium chloride (NaCl). The retention of these membranes was greatly improved from about 30% to more than 90% by heating in a bath of hot water. The flux of these membranes was also decreased as a result of the heat treatment.<sup>109, 110</sup> Annealing these membrane produces a decrease in void volume and permeability and, because pore size is generally decreased as well, an increase in permselectivity. The annealing procedure was used with all the CA membranes to modify the salt retention. The water flux decreases as the retention increases. The temperature of this annealing step determines the final properties of the membrane. Typical flux and retention curves for various annealed membranes are shown in Figure 2-14 A&B.<sup>111</sup>

In the annealing process the entire membrane shrinks somewhat and a densification of the skin layer takes places. The reason for this can be seen on the molecular level,<sup>31</sup> where the introduction of thermal energy causes translational motion of the macromolecules resulting in a closer approach of polar groups and neighbouring molecules so as to tend to coalesce with a decrease in free energy and void-spaces as the total surface area is decreased. With the proximity of neighbouring groups, virtual crosslinks are formed by strong dipole-dipole moments. These cross-links decrease chain mobility and, in a non-solvent medium, are irreversible; that is the non-solvent is not able to solvate the polar groups so enjoined.



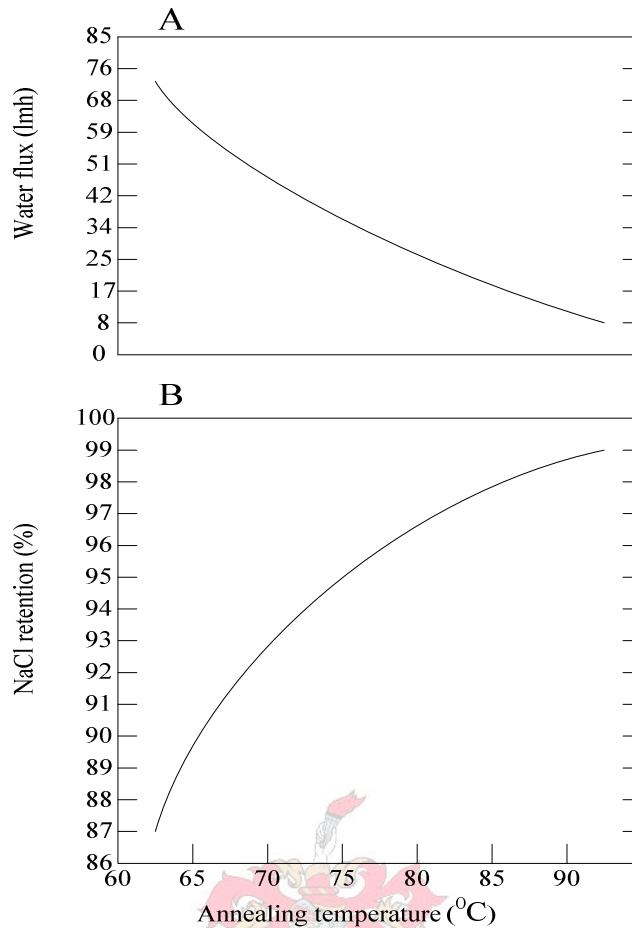


**Figure 2-14:** Typical flux and NaCl retention of asymmetric CA membranes.<sup>111</sup>

## 2.9 Conclusion

The literature review has highlighted key parameters affecting membrane performance and morphology. The remainder of this thesis investigates the effects of these parameters in order to produce hollow fine fibre membranes with performance superior to those discussed. The choice of polymer concentration and air gap length in this study was based on selected information from literature. The concentration of CA was fixed at 27% (m/m) and the length of the air gap was set to be at a maximum height of 120 mm. The other parameters of importance include the acetone/formamide ratio, the bore fluid ratio, dope extrusion rate and take-up speed rate and will be discussed in Chapter 5. The work to be developed in Chapter 3 is rather new in approach and hence there is little directly available in the literature.

### ***Chapter 3***

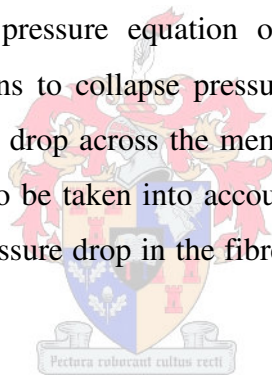
***The dimensional requirement for CA hollow-fine-fibre by means of  
Collapse and pressure drop calculations***



### 3.1 Resistance of hollow fibres to external pressure

#### 3.1.1 Introduction

In order for hollow-fine-fibre membrane to be useful in RO pressure applications, it must be able to withstand a considerable trans-membrane pressure difference. As the permeate flux is generally proportional to the trans-membrane pressure difference, use of higher applied pressures will lead to better productivity. However, there is a point above which the hollow-fibre cylindrical structure cannot withstand the pressure acting upon it and this is known as the collapse pressure. The ability of brackish water hollow-fine-fibre membranes to withstand its operating pressures without collapse, will be taken into account as an issue; firstly to produce highly resistant hollow-fine-fibre diameters, by using a suitable spinneret and secondly to provide a membrane module with high packing density (the smaller fibre dimensions, the higher resistance to brackish water operating pressures and subsequently the higher packing density). To determine the acceptable fibre dimension for RO, it was necessary to adopt the buckling pressure equation of cylindrical shells under external pressures to equate fibre dimensions to collapse pressure. Note that the smaller the fibre dimensions are, the higher pressure drop across the membrane, thus calculating the pressure drop across the fibre bore must also be taken into account to determine the acceptable fibre dimensions. This is because the pressure drop in the fibre bore plays an important role in the productivity of the fibre.<sup>112</sup>



#### 3.1.2 Elastic collapse pressure on cylindrical shells subjected to external pressure

Elastic collapsing pressure is the maximum pressure that can be applied to hollow cylindrical tubes for wall deformation to remain reversible. At higher pressures, the tubes collapse. When the external pressure applied on a cylindrical shell or tube exceeds certain values, the tube collapses, with longitudinal corrugations, according to the pressure increase.<sup>113</sup> This problem of finding the pressure required to bring about this collapse depends for its solution upon what is known in mathematical elasticity as the general theory of cylindrical shells under external pressure. For this reason, more rigid mathematical theory, which has been adopted by Southwell,<sup>113</sup> showed a good agreement with the theory of collapse pressure of bore tubes. This theory of elastic collapsing pressure will be used in this study and its formula is expressed by the following equation.

$$P = 2 \frac{E}{1 - \nu^2} \left( \frac{t}{OD} \right)^3 \quad (3.1)$$

where  $P$  is the collapse pressure,  $E$  is Young's modulus (GPa),  $\nu$  is the Poisson's ratio (dimensionless),  $OD$  is the outside diameter ( $\mu\text{m}$ ) and  $t$  is thickness of the hollow fibre ( $\mu\text{m}$ ) (outside radius - inside radius). The equation suggests that collapse pressure of hollow fibre is very high because  $OD$  is very small.

### 3.2 Pressure drop across the wall of a hollow-fine-fibre membranes

#### 3.2.1 Introduction

There is ample evidence in the literature suggesting that the pressure drop along the fibre bore varies considerably with the fibre diameter, the smaller the diameter, the higher the pressure drop.<sup>114</sup> It is therefore necessary to calculate the effect of pressure drop in the fibre bore and how much of this variation in the pressure drop will affect the chosen fibre dimensions determined by collapse pressure calculations. In this study, the steady laminar flow of incompressible fluid through the hollow-fine-fibre with a semipermeable wall and length will be expressed by the Hagen-Poiseuille equation for laminar flow,<sup>115</sup> in order to calculate the pressure drop across the fibre bore. The water flow through the fibre bore was considered to be laminar based on the smaller dimensions of hollow-fine-fibre membranes which are typically in the range of 50 – 500  $\mu\text{m}$ . Therefore the diameters of the fibres are small enough to keep the Reynolds number quite small.

#### 3.2.2 Pressure drop across the fibre wall of the hollow-fine-fibre membranes

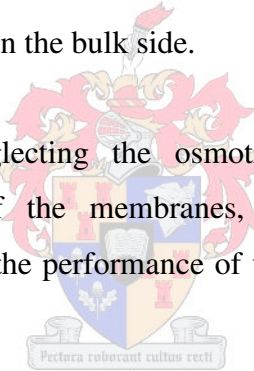
Hermans<sup>116, 117</sup> studied the effect of hydraulic flow characteristics of Berman's analysis in a permeable wall of a tubes on the flow mechanism of a hollow fibre and suggested that a Poiseuille's equation can be applied to the flow pattern inside the fibres. He therefore combined that equation with a membrane transport equation of pure water and proposed an initial model for complete water retention by hollow-fibre RO membranes. This model was taken as a basis by Orofino,<sup>27</sup> in the development of the hollow filament technology for a RO desalination system. He also analyzed the productivity of a module in the case of diluted feed solution, where the osmotic pressure was negligible.

The axial flow on the inside of a single hollow fibre was studied by Chen and Petty.<sup>118</sup> They studied the volumetric flow of an incompressible fluid undergoing RO in a hollow fibre with a semipermeable wall by applying Darcy's law for membrane transport. The fibre was sealed at one end with epoxy and open at the other end to atmospheric pressure. They used a diffusion model to describe the passage of salt through the membrane. However, Evangelista and Jonsson<sup>119</sup> proposed a model where the pressure drop inside a hollow fibre was considered with the concentration polarization on the shell side.

Sekino<sup>120</sup> used the Kimura-Sourirajan model to propose a friction-concentration-polarization model by employing the solution diffusion model and concentration polarization, and calculating the pressure drop in the hollow fibre bore using the Poiseuille equation and the pressure drop on the shell side by the Ergun equation.

Ohya et al.<sup>121</sup> studied the RO characteristics of a B-9 hollow-fibre membrane by neglecting the pressure drop on both the shell side and in the fibre bore. They took into account the effect of concentration polarization on the bulk side.

Other assumptions, including neglecting the osmotic pressure and the concentration polarization on the bulk side of the membranes, were made by Starov et al.<sup>122</sup> and Smart et al.<sup>123</sup> who optimized the performance of various hollow fibre geometries with their mathematical model.



### 3.3 Collapse pressure calculations

The purpose of this calculation is to determine an acceptable range of CA hollow-fibre dimensions for brackish water membranes, with sufficient strength to withstand high-operating pressures without collapse. This acceptable range of the fibre dimensions will also be used in addition to the pressure drop calculations, for selecting an appropriate spinneret orifice dimensions to prepare the required hollow-fibre membranes in this study.

Acceptable fibre dimension was obtained by using the elastic buckling (collapse) pressure equation for a cylindrical shell or tube under external pressures.<sup>88</sup> The collapse pressure of hollow-fibre membrane is given by equation (3.1) (Section 3.1.2). Therefore, to determine the acceptable fibre dimension from equation (3.1), the following parameters should be obtained.

1- Fibre wall thickness can be obtained by assuming the geometry of hollow-fine-fibre membrane as a thick-walled cylinder of nominal circular shape that has a ratio of outside to inside diameter of 2:1. This ratio was chosen arbitrarily.

Based on the above geometry and the object of producing hollow-fine-fibre in this study, the wall thickness  $t$  is assumed to be 50  $\mu\text{m}$ , which is the mean from the fibre's outside to its inside diameter.

$$t = (OD - ID)/2 \quad (3.2)$$

2- The overall osmotic pressure of sea water is considered to be 25 bar.

3- The Poisson ratio ( $\nu$ ) which is the ratio of transverse contraction strain to longitudinal extension strain in the direction of stretching force.

Poisson's Ratio ( $\nu$ ) can be expressed as

$$\nu = \varepsilon_t / \varepsilon_l \quad (3.3)$$

Where ( $\nu$ ) is the Poisson's ratio,  $\varepsilon_t$  is the transverse strain and  $\varepsilon_l$  is the longitudinal or axial strain of the hollow fibre.

4- Young's modulus which is ( $E$ ) is a measure of the stiffness of an isotropic elastic material to elastic deformation. It is defined as the ratio of the tensile stress to the tensile strain.

Young's modulus ( $E$ ) can be expressed as

$$E = \sigma / \varepsilon \quad (3.4)$$

Stress and strain for Poisson's ratio and Young's modulus can be expressed as

$$\sigma = F/A \quad (3.5)$$

$$\varepsilon = dl/l \quad (3.6)$$

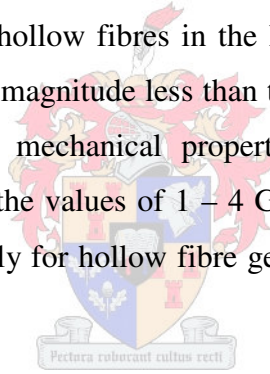
where  $F$  is the force applied,  $A$  is the cross-sectional area through which the force is applied,  $dl$  is change in length and  $L$  is initial length of the hollow fibre.

For isotropic materials the bulk and shear modulus are linked to Young's modulus ( $E$ ) and Poisson's ratio ( $\nu$ ) by:<sup>124</sup>

$$E = 2G(1 + \nu) \quad E = 6K(0.5 - \nu) \quad (3.7)$$

where ( $G$ ) is shear modulus, which is the ratio of shear stress to the shear strain, ( $K$ ) is the bulk modulus, which is the substance's resistance to uniform compression.

The Poisson's ratio of a stable, isotropic, elastic material cannot be less than -1.0 nor greater than 0.5 due to the requirement that the elastic modulus, the shear modulus and bulk modulus have positive values.<sup>125</sup> Most materials have Poisson's ratio values ranging between 0.0 and 0.5. Rubber has a Poisson ratio of nearly 0.5. Cork's Poisson ratio is close to 0. CA Poisson ratio is 0.4.<sup>126</sup> Typical Young's modulus (modulus of elasticity) values found in the literature for CA hollow fibres was as high as 0.114 GPa and as low as 0.094 GPa.<sup>127</sup> The first value was for a CA hollow fibre prepared by the wet spinning process for microfiltration from a dope solution containing 27% CA and 73% formic acid. The second value was also for CA prepared by wet spinning from a dope solution containing 26.5% CA, 0.5% chitosan and 73% formic acid.<sup>127</sup> The Young's modulus values of the CA hollow fibres are generally comparable with that of other CA hollow fibres in the literature. These values of Young's modulus were typically an order of magnitude less than the value of the Young's modulus of CA as raw material (1– 4 GPa, mechanical properties of CA powder from Eastman Company). This is likely because the values of 1 – 4 GPa are general characteristics of the polymer material and not specifically for hollow fibre geometries which have an asymmetric porous structure.



The acceptable fibre dimension can then be obtained by deriving the outside diameter from equation (3.1), giving equation (3.8). The parameters used in equation (3.8) were chosen from polymer characteristics taken from literature, allowing the outside diameter to be predicted. Therefore equation (3.1) becomes:

$$OD = \sqrt[3]{\frac{2Et^3}{P(1-\nu^2)}} \quad (3.8)$$

$$OD \cong 237 \mu\text{m}$$

Determining the effect of changing fibre dimensions on the collapse pressure can also be calculated using equation (3.1) with changing the fibre dimensions of the obtained fibre diameter (237  $\mu\text{m}$ ), while maintaining a constant wall thickness. These calculations are presented in Tables 3-1 and 3-2 respectively. Figure 3-1 shows the effect on the collapse

pressure of a hollow-fine fibre, calculated using both values of Young's modulus (0.114 and 0.094 GPa). Tables 3-1 and 3-2 show the influence of varying the outside fibre diameter of 237  $\mu\text{m}$  on the collapse pressure values at two different Young's modulus values. The variation of outside fibre diameter was done by keeping a constant wall thickness, while increasing and decreasing the inside and outside fibre diameter, respectively at constant value of 5  $\mu\text{m}$ . The inside diameter was calculated by substituting the value of 237  $\mu\text{m}$  and wall thickness of 50  $\mu\text{m}$  in equation (3.2).

**Table 3-1:** Hollow-fine-fibre collapse pressure (Young's modulus 0.114 GPa, wall thickness 50  $\mu\text{m}$ )

Inside diameter ID ( $\mu\text{m}$ )	Outside diameter OD ( $\mu\text{m}$ )	Collapse pressure P (GPa)	Collapse pressure (bar)
62	162	0.00798	79.80
67	167	0.007285	72.84
72	172	0.006668	66.67
77	177	0.006119	61.18
82	182	0.005628	56.27
87	187	0.005188	51.88
92	192	0.004794	47.93
97	197	0.004438	44.37
102	202	0.004116	41.16
107	207	0.003825	38.25
112	212	0.003561	35.60
117	217	0.00332	33.20
122	222	0.003101	31.01
127	227	0.002901	29.00
132	232	0.002717	27.17
137	237	0.002549	25.48
142	242	0.002394	23.93
147	247	0.002252	22.51



**Table 3-2:** Hollow-fine-fibre collapse pressure (Young's modulus 0.094 GPa, wall thickness 50  $\mu\text{m}$ )

Inside diameter ID ( $\mu\text{m}$ )	Outside diameter OD ( $\mu\text{m}$ )	Collapse pressure P (GPa)	Collapse pressure (bar)
62	162	0.00654	65.45
67	167	0.00597	59.74
72	172	0.00546	54.68
77	177	0.00501	50.18
82	182	0.00461	46.15
87	187	0.00425	42.55
92	192	0.00393	39.31
97	197	0.00363	36.39
102	202	0.00337	33.76
107	207	0.00313	31.37
112	212	0.00292	29.20
117	217	0.00272	27.23
122	222	0.00254	25.43
127	227	0.00237	23.79
132	232	0.00222	22.28
137	237	0.00209	20.90
142	242	0.00196	19.63
147	247	0.00184	18.46



The results show that the collapse pressure decreases gradually with increasing outside diameters and decreasing Young's modulus. Therefore, the collapse pressure is directly dependent on the Young's modulus and inversely to the outside diameter. From Figure 3-1 there is a clear indication that the Young's modulus and the fibre dimensions have a significant effect on the collapse pressure and subsequently give the hollow-fine fibre enough mechanical strength to withstand high operating pressures encountered in RO without collapse. From our calculations it can be seen that for high operating pressures required for RO, it is recommended to keep the internal diameter of the fibres in the order of magnitude of the fibre wall thickness.

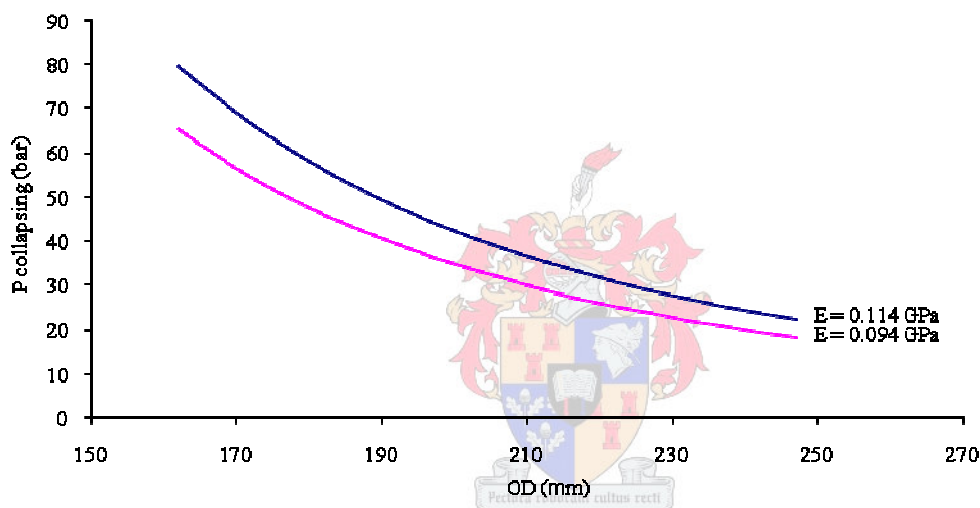


**Figure 3-1:** Collapse pressure of hollow fibre, calculated using both values of Young's modulus (0.114 and 0.094 GPa).

It can be seen from Figure 3-1 that there is an acceptable range of fibre dimensions (222 – 247  $\mu\text{m}$ ) that showed an ability to withstand the operating pressure for brackish water applications. Typically the operating pressure used for brackish water desalination would be in the range of 20 – 25 bar as the lower salt concentration creates a lower osmotic pressure and therefore the lower RO pressure is possible. Therefore a 50  $\mu\text{m}$  wall thickness and outside fibre diameters within the range of 222 – 247  $\mu\text{m}$  would be acceptable for brackish water RO applications. At this particular range of outside diameters and 50  $\mu\text{m}$  wall thickness, the hollow-fine fibre should not be operated at pressures greater than 25 bar to avoid any collapse. The next step is to acquire an appropriate spinneret at which the orifice dimensions will yield a membrane with dimensions within the specified range.

### 3.4 Pressure drop across the wall of a hollow-fine-fibre membrane

Pressure drop along the fibre bore is greatly affected by the size of internal diameter.<sup>114</sup> Therefore the pressure drop calculation is necessary for the specified range of the fibre dimensions determined above (Section 3.3).

The pressure drop along the fibre bore is calculated by the Hagen-Poiseuille equation. Numerical analysis by a computer program (FORTRAN) is used to solve the equation and the software codes are shown in (Appendix B). The governing equations in this calculation are fluid pressure drop, material balance and membrane transport equations.

The assumptions made in this calculation are as follows:

- The flux in the fibre bore is from the left to the right, where there is no pressure drop at the sealed end from the left, but there is a pressure drop along the length of the fibre towards the right. The fibre is assumed to be 1 m long. At one end, the fibre is sealed and other end, it is open to the atmospheric pressure (Figure 3-2).
- The pressure drop in the shell is small, and the pressure in the shell is nearly equal to the feed pressure.

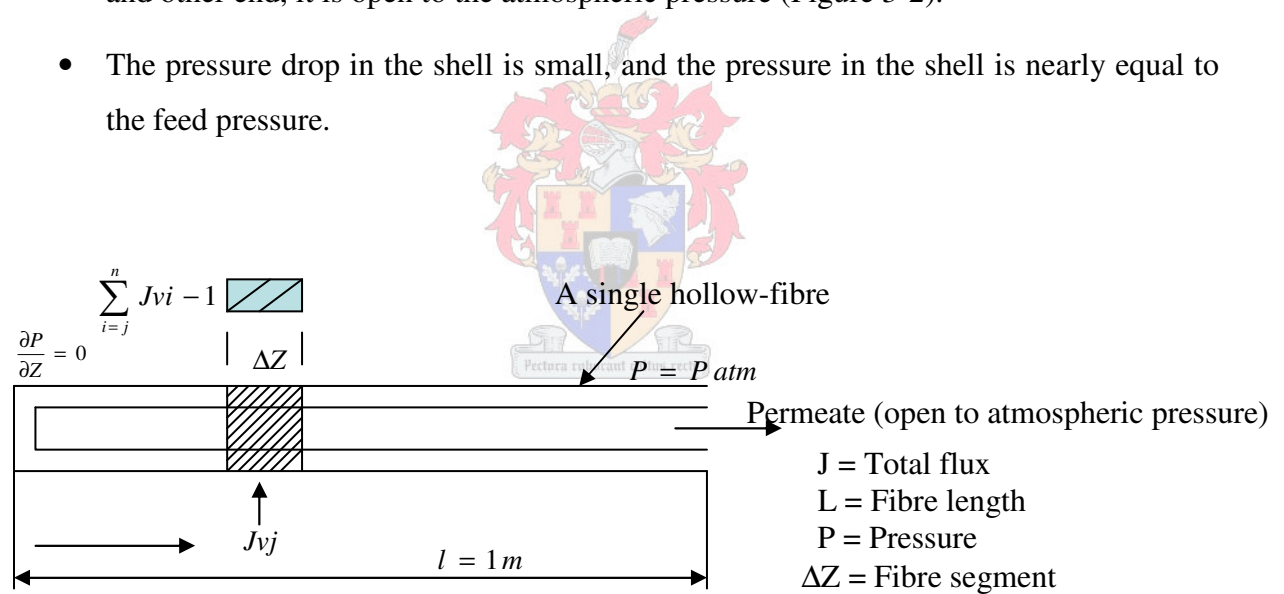


**Figure 3-2:** Schematic diagram of single hollow-fine fibre.

#### 3.4.1 Fluid pressure drop equations

The axial pressure drop inside the fibres is expressed by the Hagen-Poiseuille equation:

$$\Delta P = \frac{128 \mu Z Q_p}{\pi d_f^4} \quad (3.9)$$

Differentiating this equation with respect to the length of the fibre, we get:

$$\frac{dP}{dZ} = \frac{128 \mu Q_p}{\pi d_i^4} \quad (3.10)$$

where  $P$  is the pressure inside the fibre (Pa),  $Z$  is the axial direction of the fibre (m),  $d_i$  is the inside fibre radius (m),  $\mu$  is the dynamic viscosity of water =  $0.798 \times 10^{-3}$  (Pa.s) and  $Q$  is the flow rate ( $\text{m}^3/\text{sec}$ ).

### 3.4.2 Material balance equation

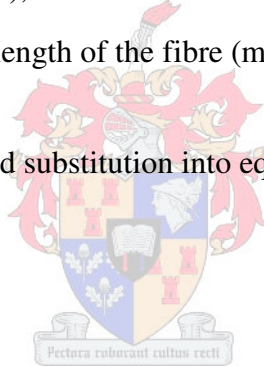
The material balance within the fibre bore is given by the following equation:

$$\frac{dQ}{dZ} = \pi d_o J_v \quad 0 \leq Z \leq L \quad (3.11)$$

where  $d_o$  is the outside radius (m),  $J_v$  is the total flux or the solution flux across the membrane ( $\text{m}^3/\text{m}^2 \cdot \text{sec}$ ) and  $L$  is the length of the fibre (m).

Differentiation of equation (3.10) and substitution into equation (3.11) yields:

$$\frac{d^2 P}{d^2 Z} = \frac{128 \mu}{d_i^4} d_o J_v \quad (3.12)$$



Equation (3.12) has the following boundary conditions:

$$\text{at } Z = 0 \quad p = p_{\text{atm}} = 101\,325 \text{ Pa}$$

$$\text{at } Z = L \quad \frac{dP}{dz} = 0$$

In order to determine the pressure drop along the fibre, the axial direction of the fibre ( $Z$ -coordinate) is divided into  $m = 100$  segments each segment is 1 cm in length. Regarding the pressure drop in the fibre bore, however, the axial direction is defined as the length of the fibre.

Integrating of equation (3.12) to obtain the permeate pressure ( $P_{PJ}$ ) in the fibre segment  $\Delta Z$  with respect to  $Z_1$  and  $Z_2$  yields:

$$\int_{z_1}^{z_2} \frac{dP}{dZ} = \int_{z_1}^{z_2} \frac{128 \mu}{d_I^4} d_o J_v Z \quad (3.13)$$

Discretisation of equation (3.13) by changing it to a linear equation yields equation (3.14). This equation will be solved numerically by FORTRAN.

$$P_{pj} - P_{pj-1} = \frac{128 \mu \Delta Z^2}{d_I^4} d \sum_{i=j}^n J_{vi} \quad (3.14)$$

where  $P_{pj}$  is the pressure inside the fibre (Pa),  $\Delta Z$  is the distance between two segments (length of fibre divided by number of segments) (m),  $d_I$  is the inside fibre radius (m),  $\mu$  is the dynamic viscosity of water (Pa.s) =  $0.798 \times 10^{-3}$ ,  $J_v$  is the total flux or the solution flux across the membrane segment ( $\text{m}^3/\text{m}^2 \text{ sec}$ ) and  $j$  subscript at axial coordinates.

### 3.4.3 Membrane transport equations

The solution–diffusion model is a practical model for explaining membrane permeation, and is described as follows:

Water flux  $J_w = A (\Delta P - \Delta \pi)$   $\text{kg}/\text{m}^2 \cdot \text{s}$

$$J_w = A (P_B - P_p) - (\pi_M - \pi_p)$$

$$\pi = \alpha C$$

where  $\pi$  is the osmotic pressure,  $C$  is the solute concentration,  $\alpha$  is osmotic pressure proportionary constant

then  $J_w = A (P_B - P_p) - \alpha (C_M - C_p)$

Solute flux  $J_s = B \Delta C$   $\text{kg}/\text{m}^2 \cdot \text{s}$

$$J_s = B (C_M - C_p)$$

where  $J_w$  is the water flux through the membrane,  $J_s$  is the solute flux through the membrane,  $A$  is the water permeability constant,  $B$  is the solute permeability constant,  $P_B$  is bulk pressure

$P_p$  is the permeate pressure,  $\pi_M$  is osmotic pressure on membrane surface,  $\pi_p$  is osmotic pressure on the bore side and  $C_p$  is permeate concentration.

The effect of concentration polarization is usually very small in hollow-fibre RO systems because of relatively low product flux, which is sufficient to reduce the effect of concentration polarization.<sup>128</sup> Where high membrane flux leads to a rapid build-up of retained solutes on the membrane surface and results in concentration polarization.<sup>129</sup> The interface concentration  $C_M$  at the membrane surface can be replaced by the local brine concentration  $C_B$ .

then:

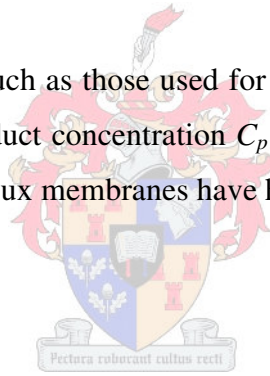
$$J_w = A [\Delta P - \alpha(C_B - C_p)]$$

$$J_s = B(C_B - C_p)$$

With a tight membrane structure, such as those used for RO desalination processes, a further assumption can be made. The product concentration  $C_p$  can be neglected because the flux is so low in these membranes. High-flux membranes have high  $C_p$ .

$$J_w = A(\Delta P - \alpha C_B)$$

$$J_s = BC_B$$



The total flux or solution flux ( $J_v$ ) in the equations above is given by the sum of the water flux and the solute flux, ( $J_s$ ). With highly selective membranes the solute flux can be also neglected.

$$J_v = J_w + J_s/\rho \approx J_w/\rho$$

$$J_v = J_w/\rho$$

In addition, our assumptions will include the use of pure water as feed solution. Thus, the local brine concentration (feed concentration)  $C_B$  can be neglected and the solution flux equation becomes:

$$J_v = J_w = A(\Delta P) = A(P_B - P_p)/\rho \quad (3.15)$$

### 3.4.4 Numerical analysis to determine the pressure drop

The solution flux is calculated according to equation (3.15) which assumes that permeate pressure ( $P_p$ ) is equal to atmospheric pressure 101 325 Pa. The bulk pressure  $P_B$  is assumed to be equal to the feed pressure. For brackish water desalination at lower salt concentration, lower feed pressure, as low as 20 bar, are used. At slightly higher salt concentration, the higher feed pressure of around 25 bar can be used. Equation 3.15 requires a water permeability constant for CA. This was found in the literature as  $4.294 \times 10^{-10} \text{ Kg/m}^2 \cdot \text{s} \cdot \text{Pa}$ .<sup>130</sup> This water permeability constant is used in the solution-diffusion model and, when using pure water, is equal to

$$A_w = D_w c_w v_w / RTl \quad (3.16)$$

where  $D$  is the diffusion coefficient  $\text{m}^2/\text{s}$ ,  $c$  is the molar concentration  $\text{kg}\cdot\text{mol}/\text{m}^3$ ,  $v$  is the molar volume  $\text{m}^3/\text{mol}$ ,  $R$  is the gas constant  $8.314 \text{ J/mol}\cdot\text{K}$ ,  $T$  is the absolute temperature  $\text{K}$ ,  $l$  is the membrane thickness (mm) and the subscript  $w$  indicating the solvent (water). According to the Kimura and Sourirajan approach of transport phenomena across RO membranes, the solvent and solute fluxes through the membrane are mainly characterized by two phenomena: solvent transport in terms of the pure water permeability constant  $A$ , and solute transport in terms of the solute permeability constant  $B$ .<sup>131</sup> The solute permeability constant was neglected in this calculation as the feed concentration was assumed to be pure water flux. Therefore, the solution flux for a single hollow-fine fibre will be calculated as follows.

$$(J_v) = 4.294 \times 10^{-10} (25 \times 10^5 - 101325) / 1000 = 1.03 \times 10^{-6} \text{ m}^3/\text{m}^2 \cdot \text{sec}.$$

The pressure drop can be obtained using equation (3.14), and the finite difference method is applied to numerically solve it. Figure 3-3 shows the pressure drop across the fibre wall of assumed diameter above (Section 3.3) for hollow-fine-fibre membranes at wall thickness of  $50 \mu\text{m}$ .

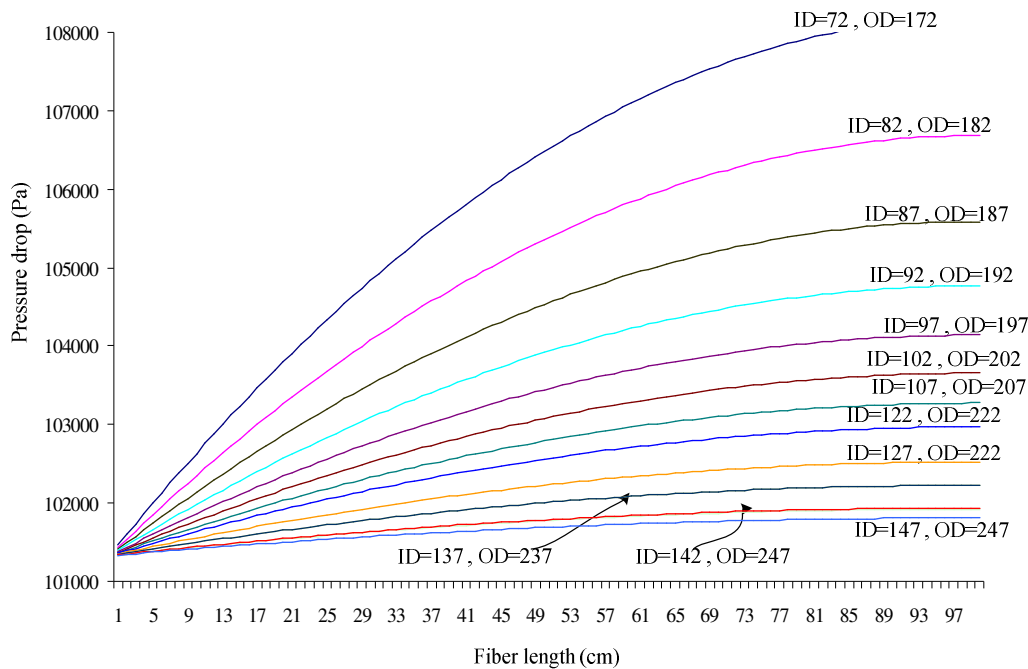


**Figure 3-3:** Pressure drop across the fibre wall of hollow-fine-fibre membranes.

Figure 3-3 shows that the pressure drop along the fibre length decreases significantly as the diameter of the hollow fibre increases. This is because pressure drop is inversely proportional to the diameter to the power four which is in agreement with Hagen-Poiseuille equation. Pressure drop in the fibre bore plays an important role in the productivity of the fibre. The smaller the fibre dimensions, the higher the pressure drop and subsequently lower water flux (less product). Therefore the workable fibre dimensions should have a smaller pressure drop and also a high collapse pressure resistance, within the operating conditions for a brackish water membrane. It can be seen from Figure 3-3 that, as the fibre diameter increases while maintaining a constant wall thickness, the pressure drop in the fibre bore decreases. The number of fibres that can be accommodated in the module of a given size also decreases. As a result, for a given operating condition there exists a region of acceptable fibre diameters which shows a reasonable pressure drop at the given operating pressures. It can be seen from Figure 3-3 that the range of fibre dimensions of 222 – 247  $\mu\text{m}$  obtained by the collapse pressure calculations have reasonable values of pressure drops compared to smaller fibre dimensions where the pressure drop is high. Hence, the pressure drop calculations will also limit the selection of fibre diameters for brackish water desalination. Therefore, the range of 222 – 247  $\mu\text{m}$  would be acceptable for making CA hollow-fine-fibre membrane for brackish water desalination in terms of collapse pressure and pressure drop. Note, operating conditions for brackish water membranes range from 20 – 25 bar and relies on feed concentration.<sup>13</sup>

### 3.5 Conclusion

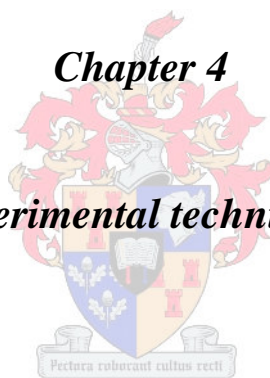
An acceptable range of dimensions were determined for hollow-fine-fibre membranes to allow the membrane to exhibit high collapse pressures, i.e., the hollow-fine-fibre membranes will withstand large external pressure differences. Thus, the hollow-fine-fibre membranes can have a relatively low ratio of wall thickness to outside diameter and thereby provide an advantageously large bore diameter to minimize the pressure drop to flux passing within the bore. The dimensional requirement for preparing brackish water CA hollow-fine-fibre membrane is in the range of 222 to 247  $\mu\text{m}$  outside diameter, within the operating conditions of brackish water. Based on the above calculations and the assumed fibre geometry, the appropriate spinneret dimensions will be in the ratio of 2:1 outside to inside diameter. The selected spinneret was obtained in the ratio of 600  $\mu\text{m}$  outside diameter to 400  $\mu\text{m}$  inside diameter.





## ***Chapter 4***

### ***Experimental techniques***



## 4.1 Introduction

During the current study on fabrication technique of CA hollow-fine-fibre membranes for brackish water desalination, various equipment and methods were used, which will be discussed in the following chapter. The procedures described in this chapter are classified into two sections; preparative techniques, used in the fabrication of the hollow-fine-fibres membranes (including solution preparation, fibre spinning etc.), and the characterization methods used to characterize the fibres (including fibre analysis, evaluation of hollow fibres etc.).

## 4.2 Materials

The following materials were used to prepare the spinning solutions, and later mounting the fibres in bundles. CA powder (number average molecular mass 40 000 with acetyl content 39.8% (m/m)) was purchased from (Eastman, United States) and used as the membrane forming polymer. Analytical grade acetone was purchased from (Kimix, South Africa) and used as solvent for the polymer. Formamide was purchased from (Labchem, South Africa) and used as non-solvent. Polyurethane was purchase from (Pach-Chem, South Africa) and used as an adhesive for potting the hollow fibres.

### 4.2.1 Polymer

The polymer of choice for this study was cellulose acetate (CA). It is one of the most commonly used polymers in the membrane manufacturing industry. The molecular structure is shown in Figure 4-1. The importance of this polymer was discussed in (Section 2.6.1).

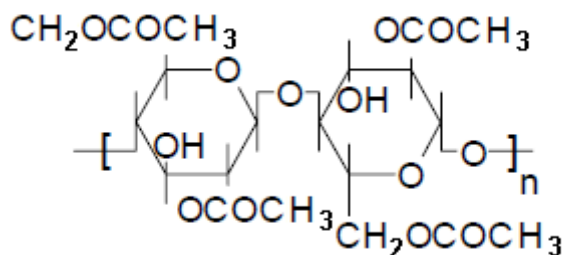


**Figure 4-1:** Molecular structure of CA.

CA is prepared by the acetylation of cellulose. Acetylations of cellulose are usually carried out with sulfuric acid as catalyst. Then CA is prepared by treating cellulose with acetic acid and then with acetic anhydride in the presence of the sulfuric acid catalyst. The repeating anhydroglucose unit in the cellulose backbone contains three hydroxyl groups. These hydroxyl groups can react readily with acetic acid to form CA.<sup>132</sup> Cellulose is considered to be a hydrophilic polymer due of the three hydroxyl groups on each repeating unit which form hydrogen bonds with water. CA is less hydrophilic than cellulose. This hydrophilic/hydrophobic character makes CA a desirable membrane material for RO and the choice of CA was based on its high permeability rates for water. Since the CA membrane is an organic ester, it is very sensitive to hydrolysis in alkaline and acidic conditions and high temperature in water. The hydrolysis rate is lowest at a pH of about 6 and CA membranes are typically operated at pH of 5.8.<sup>48</sup> The properties of the CA used in this study are tabulated in Table 4-1

**Table 4-1:** Properties of CA used in this study

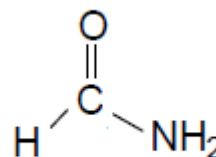
Property	CA (Cellulose Acetate)
Grade	398 – 10
Manufacturer	Eastman Kodak (USA)
Acetyl content (degree of substitution 2.45)	39.8% (m/m)
Hydroxyl content	3.5% (m/m)
Glass transition temperature	185 °C
Ash content	< 0.05 %

#### 4.2.2 Low molecular mass components

Two low molecular mass components were used for preparing the dope solution: acetone was used as the solvent and formamide as the non-solvent. Their properties are given in Table 4-2. Their molecular structures are shown in Figure 4-2.



**Figure 4-2:** Acetone.



Formamide.

**Table 4-2: Properties of acetone and formamide used in this study**

	Formamide	Acetone
Supplier	Labchem (USA)	Kimix (SA)
Grade	AR	AR
Molecular mass	45.04	58.08
Melting point	2 – 3 °C	-94 °C
Boiling point	210 °C	56 °C
Viscosity	3.764 cP at 20 °C	0.32 cP at 20 °C
Solubility in water	Miscible	Miscible

### 4.2.3 Fibre mounting adhesive

The adhesive used for mounting hollow fibres in a test cell was two-component resins (comprising a resin and a hardener), which was purchased from (Pac-Chem cc, South Africa).

## 4.3 Hollow-fibre spinning

### 4.3.1 Preparation of the spinning solution

Polymer to be used was first dried overnight in a vacuum oven to remove any water present, the solvent and non-solvent were used without further purification. The dope solution required for spinning was prepared by dissolving the polymer powder in a solvent and non-solvent mixture stirred mechanically for 24 h at room temperature.

### 4.3.2 Description of the spinning apparatus

A schematic diagram of the spinning apparatus is shown in Figure 4-3. The polymer, solvent and non-solvent were placed in a jacketed stainless steel vessel (3l) and mixed until a homogeneous solution was obtained. The jacketed part of the vessel was filled with glycerine, and the vessel was wrapped with electrical heating tape (to heat the glycerine and hence the polymer mixture). A thermocouple was immersed in the glycerine to monitor the temperature of the vessel. Heating of the tape was controlled with a voltage controller. A stirring blade, connected to a motor, was immersed in the vessel to mix the polymer solution. The valve underneath the vessel was closed while the solution was being mixed and was opened when the solution was to be drained from the vessel during the spinning. The valve and the vessel were connected by plastic tubing to the gear pump.

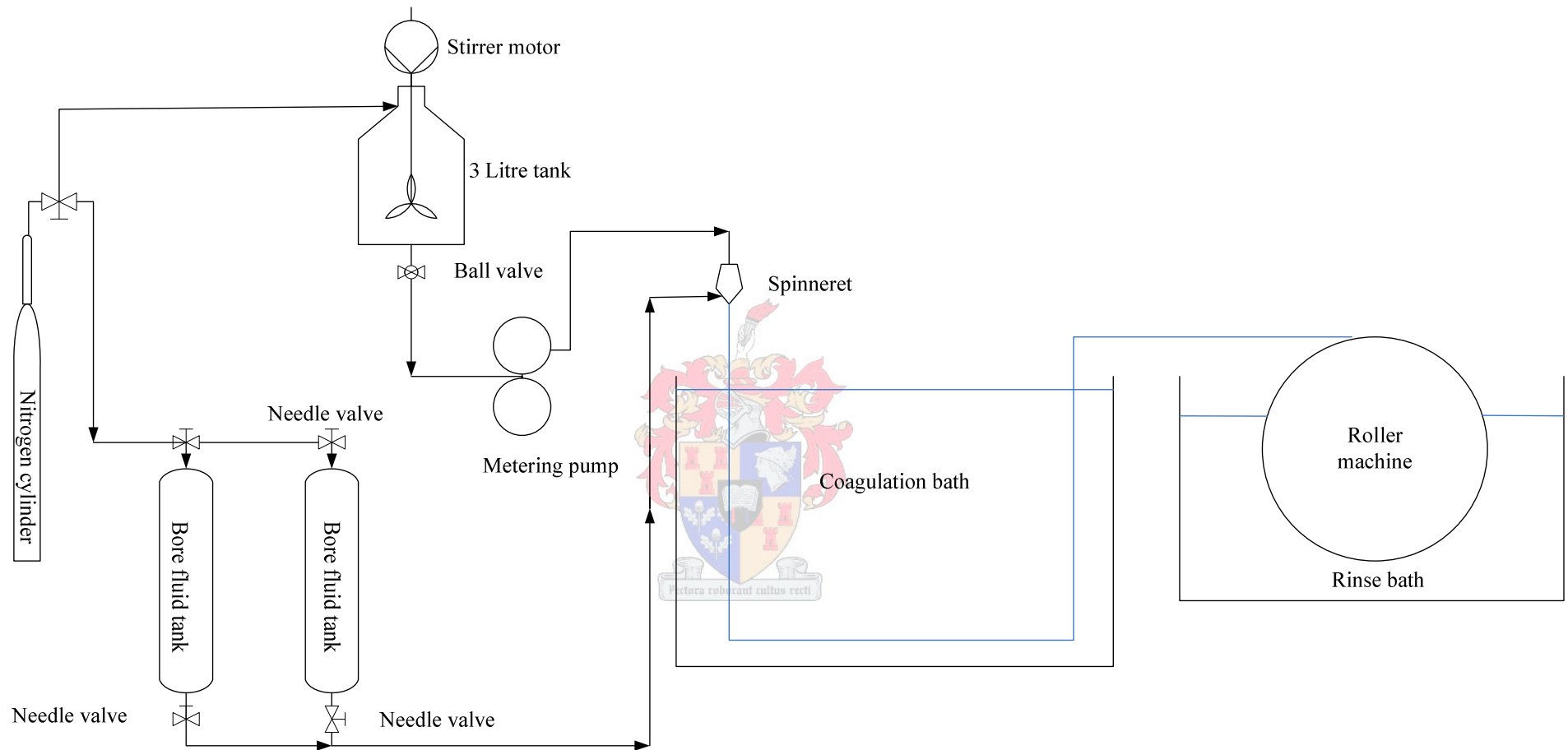


**Figure 4-3:** Schematic diagram of the dry-wet solution spinning apparatus.

The stainless steel vessel was sealed, except for an inlet in the lid to allow nitrogen gas to be delivered to the vessel. The nitrogen was used to force the dope solution into the pump during spinning. The positive displacement gear pump was designed to be used at different viscosities. The delivery rate of the gear pump was 1.2 ml/revolution. The pump outlet was connected to a mesh filter (5  $\mu\text{m}$ ).

The tube-in-orifice spinneret used is shown in Figure 4-4 and in Figure 4-5. It is a spinneret. The dimensions of the spinneret were as follows: outer diameter of the orifice is 600  $\mu\text{m}$  and the diameter of the inner orifice 400  $\mu\text{m}$ . The spinning solution is entered through the annulus formed by these two orifices. The spinneret was attached to the pump outlet with a short length of flexible nylon pressure tubing. The bore fluid was delivered to the fibre through a needle in the centre of the spinneret. The needle was held in place by set screws on either side of the top of the spinneret. The needle must be adjusted so that it is flush with the base of the spinneret, not retracted into the spinneret, or sticking out into the nascent fibre.

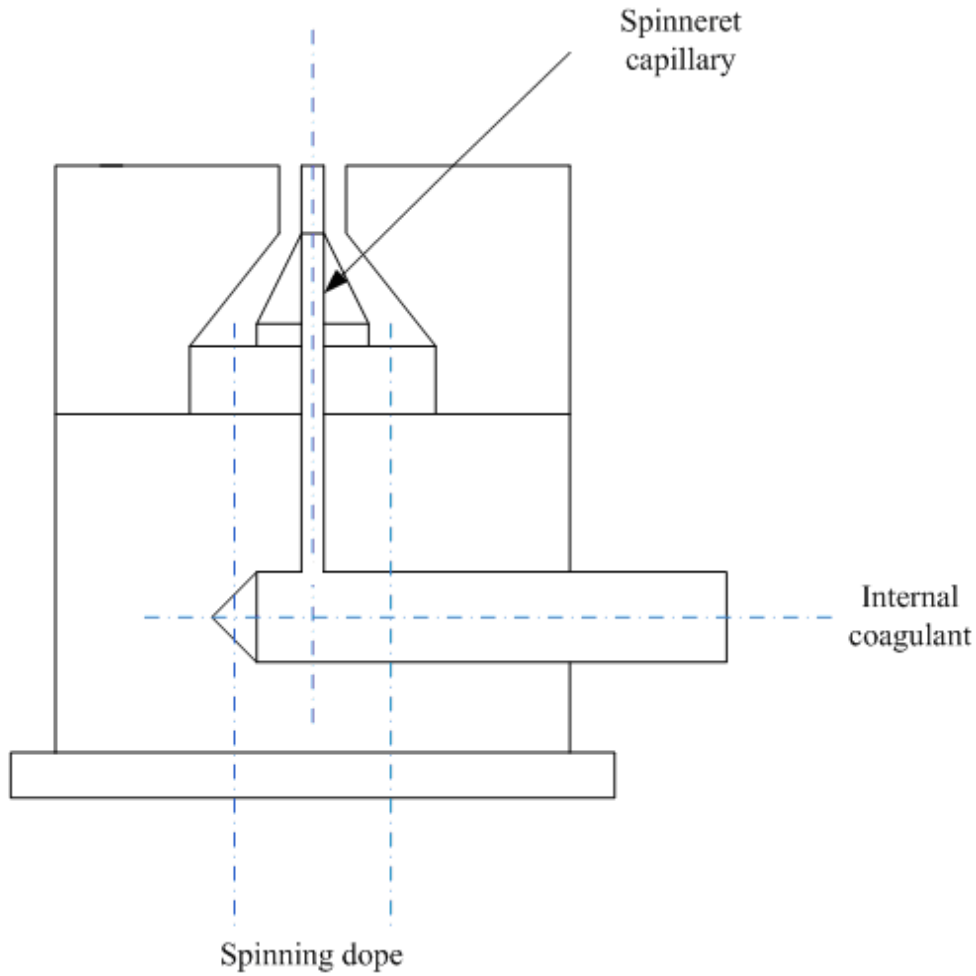
Water and acetone was used as the bore fluid. The bore fluid was drawn from the bore fluid cylinder, and the flow was controlled with a needle valve.

The coagulation bath dimensions were 2400×1000 mm. The bath temperature was controlled from room temperature to 5 °C. The take-up winder was immersed in a small bath and the immersion depth can be adjusted to different levels to ensure that the hollow fibres were held under water for leaching and solidifying evenly. The winder was adjusted with a controller that can be varied between 0 and 120 r/min.

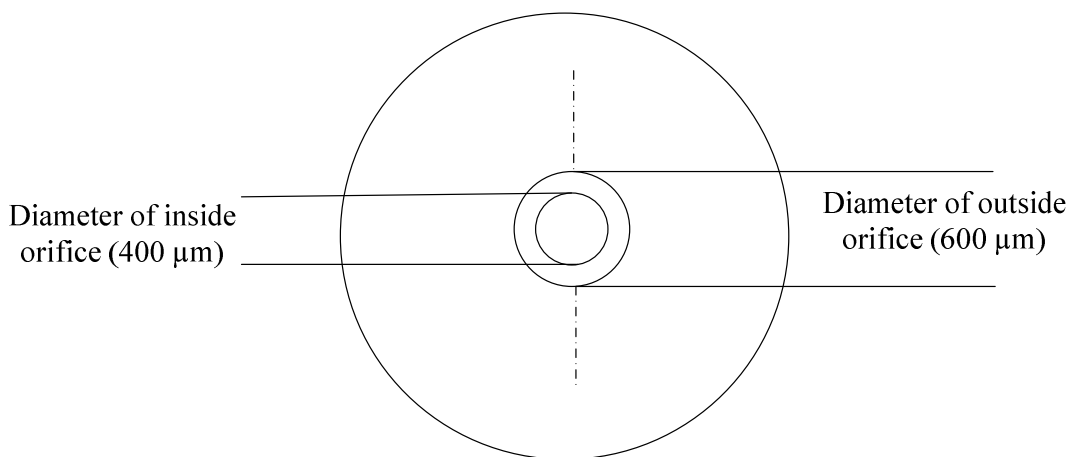
A cylindrical chimney was placed in the air gap. The chimney was made of clear glass so that the fibres can be observed during spinning. The air gap, which is the space from the spinning die to the coagulation bath, is adjustable from 10 to 120 mm. The hollow fibre was spun through the central cylinder and then passed through the bath. It is important not to let the fibres touch the inside of the central cylinder because the fibre is still in liquid form. Nitrogen gas was fed to the lower section of the chimney at a flow rate of 1 l/min at 20 °C, where it flows around the cylinder and out of the top.

### 4.3.3 The spinning process

To prepare of casting solution, the solvent and non-solvent were first added to the vessel, followed by the polymer. The stirrer was set to stir the polymer solution for 24 h to ensure



Side view



Bottom View

**Figure 4-4:** Tube-in-orifice spinneret used in the production of hollow-fine fibres.

that all components are dissolved completely. As the dissolution proceeded, the polymer dope viscosity increased and hence the stirrer was set at its higher torque level to maintain the stirring speed. After about 24 h of stirring, a clear homogeneous polymer solution was obtained. The solution was typically full of air bubbles and dissolved gases after 24 h of stirring; hence it had to be kept under vacuum for 6 hours. The preparation of a homogenous solution generally takes two days to complete.

A solution containing air bubbles cannot be spun into fibres and therefore this procedure of degassing was important to prevent the formation of hollow-fibre membranes with defects that could subsequently reduce the salt retention.

The first task was to ensure that the spinning apparatus is correctly assembled. The second was to ensure a homogeneous, bubble-free spinning solution.

The quench bath was filled with water (Figure 4-5) to ensure that the fibres were adequately immersed in the water. The fibres were removed from the coagulation bath during take-up; the fuller bath also gave a slightly longer solidification period. During take-up, the solidification of the polymer continued as the take-up roller was immersed in the coagulation bath. This is essential as the bore fluid must also be removed from the membranes.

The bore fluid metering was started before the polymer solution pump was pumped to the orifice to prevent polymer from plugging the needle in the middle of the spinneret that delivers the water/acetone to the bore.

To begin the flow of the spinning solution, the valve under the stirring vessels was opened. Spinning solution was delivered to the pump by the nitrogen pressure in the vessel. This pressure was set between 100 to 200 kPa to ensure that the suction side of the pump was flooded before the pump was switched on and the desired pump speed set. Guide rollers were used to hold the fibres underneath the water in the quench bath and the fibres were pulled across the surface of the water by hand, passing it under the roller and subsequently onto the take-up wheel. The fibres were pulled smoothly through the bath. A refrigeration unit was connected to the coagulation bath to control the temperature of water between 5 to 7 °C to allow for rapid solidification of the hollow fibre filament as it in contact with water in the coagulation bath.



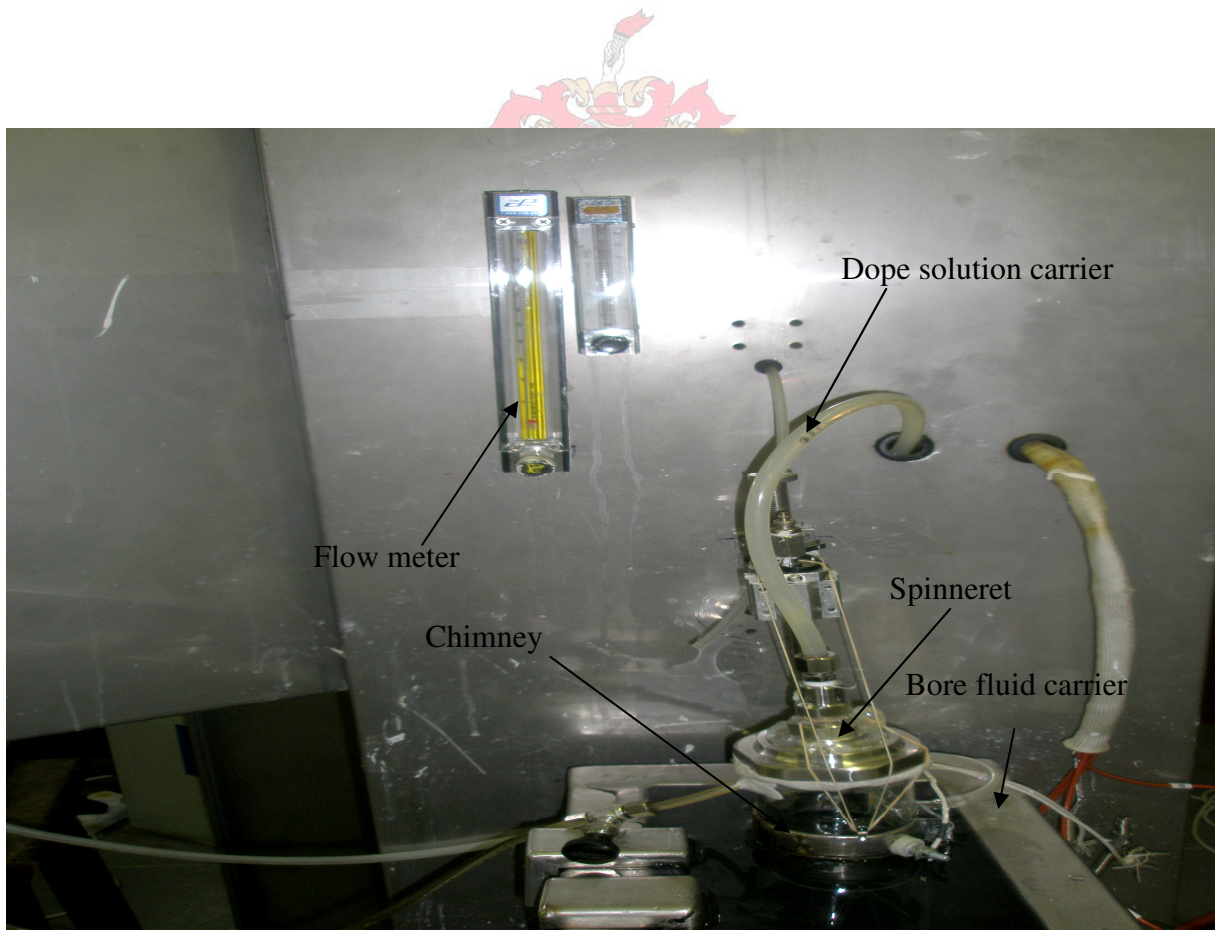
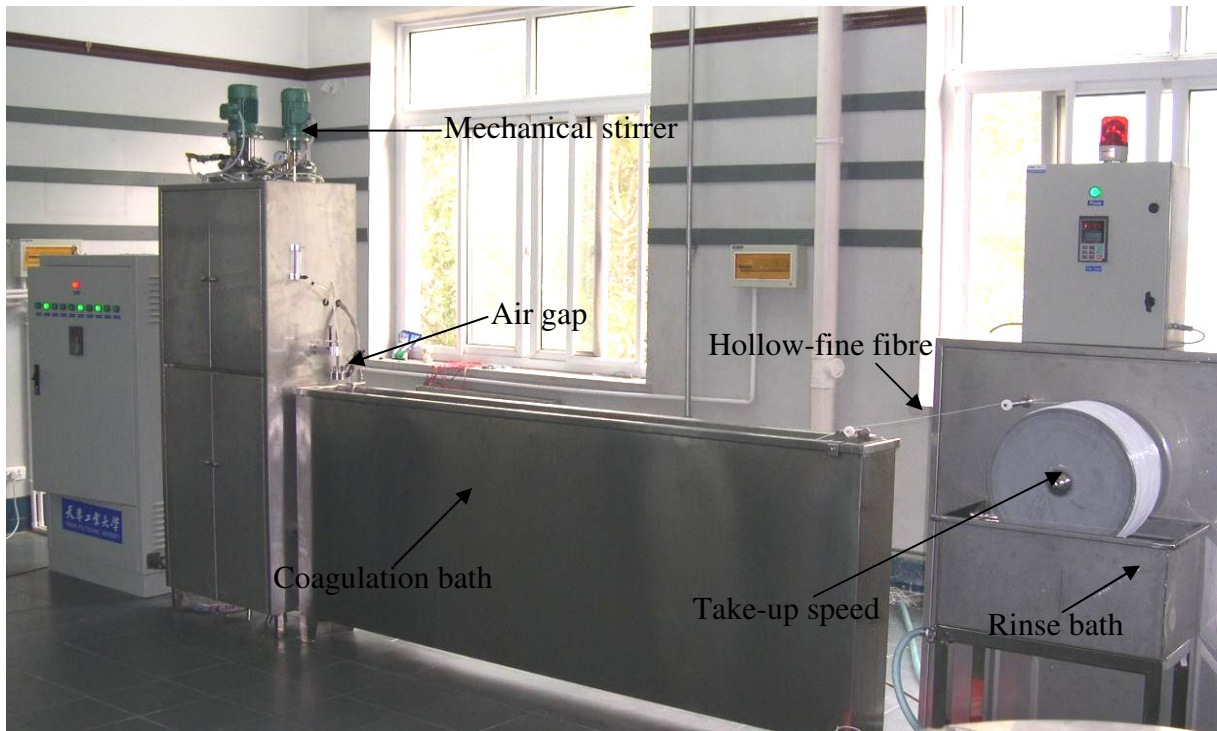


**Figure 4-5:** Photographs showing apparatus used during the dry-wet spinning process.

Having set the spinning parameters and commencing spinning, sufficient fibres were spun to afford samples for analysis. The fibres were labelled and placed in a washing tank, the washing water was changed daily over two to three days.

A trough of water was positioned underneath the collecting wheel (take-up) to ensure that the fibres were always wet. The water in the trough ensured that the all residual solvent was released from the fibres (by diffusion). A large amount of residual solvent remains in the fibres directly after spinning and if it is not removed, the fibres may become dense because of the plasticising effect of the solvents. The fibres were then cut on the collecting drum, using a scalpel.

The system was cleaned after each run, using the same solvent as used to prepare the spinning solution. The typical spinning conditions for preparing CA hollow-fine-fibre membranes are tabulated in Table 4-3.

#### 4.4 Storage of hollow fibres

The cut fibres were immersed in water tanks for at least 24 h (see Figure 4-6) to remove any residual traces of solvent trapped in the fibres and to keep the fibres wet, to prevent any damage upon drying out. As water evaporates from small pores high surface tension forces can be generated, which can damage the membrane active layer.

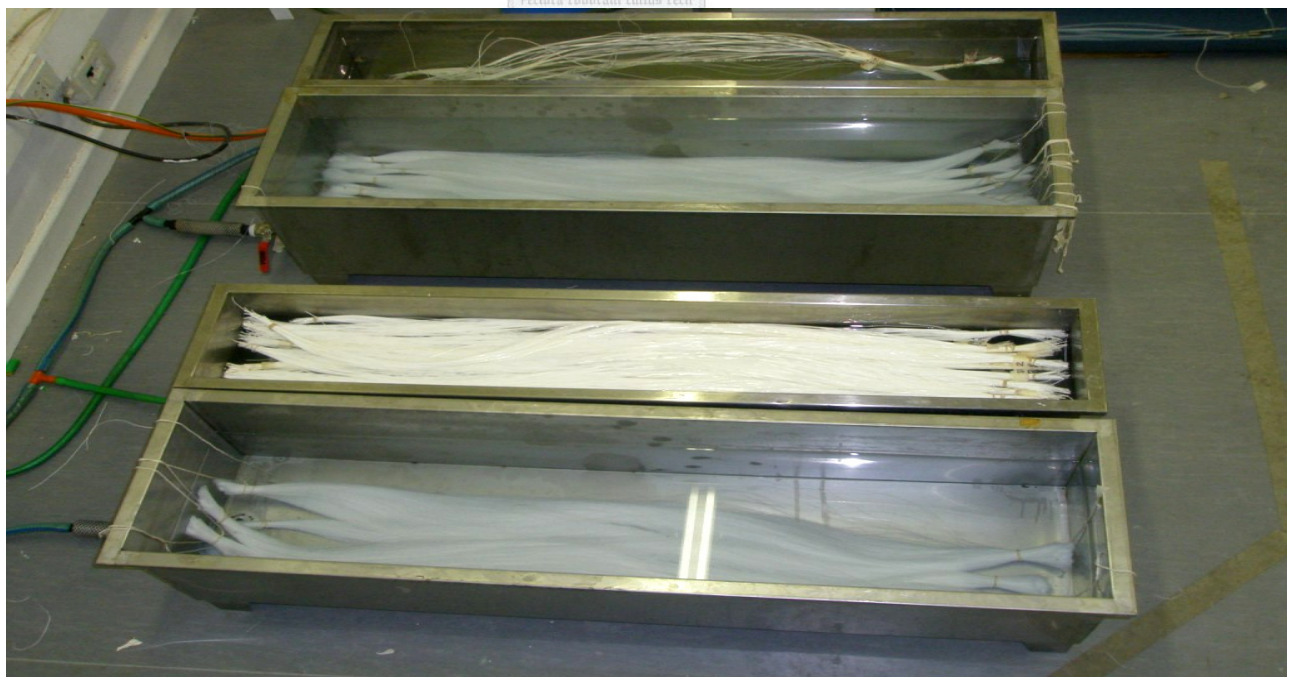
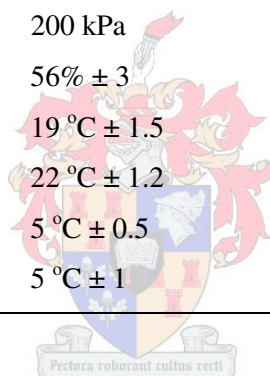


**Figure 4-6:** Photographs of the preservation tanks containing fibres.

The typical spinning conditions used to prepare CA hollow-fine-fibre membrane for brackish water desalination have been discussed in Chapter 2, 3 and 5 are summarised in Table 4-3.

**Table 4-3:** Typical spinning conditions used to prepare CA hollow-fine-fibre membranes by statistical analysis

Polymer content (m/m)	27% CA	(from chapter 2)
Acetone/formamide ratio (m/m)	0.847 – 1.1471 – 1.447	(from chapter 5)
Coagulation bath	Water	(from chapter 2)
Bore fluid (acetone/water ratio)	1 – 1.5 – 2.3 (m/m)	(from chapter 5)
Bore fluid rate	3 ml/min	(experimental trials)
Air gap distance (mm)	40 – 80 – 120	(from chapter 2)
Spinneret dimensions ( $\mu\text{m}$ )	400 $\mu\text{m}$ OD/600 $\mu\text{m}$ ID	(from chapter 3)
Take-up speed rate	96 r/min	(from chapter 5)
Dope extrusion rate	10 ml/min	(from chapter 5)
Bore fluid tank pressure	45 kPa	(Machine operating conditions)
Dope solution tank pressure	200 kPa	(Machine operating conditions)
Room humidity	56% $\pm$ 3	(Lab conditions)
Room (wet bulb)	19 °C $\pm$ 1.5	(Lab conditions)
Room (dry bulb)	22 °C $\pm$ 1.2	(Lab conditions)
Coagulation bath temperature	5 °C $\pm$ 0.5	(from chapter 2)
Take-up bath temperature	5 °C $\pm$ 1	(from chapter 2)



## 4.5 Hollow-fine-fibre analysis

### 4.5.1 Determination of membrane morphology by scanning electron microscopy

It is important to study the membrane morphology by SEM, as it shows what membrane structure was obtained in terms of porosity distribution, whether from inside or the outside. A small bundle of the spun fibres was taken from the preservation tank and immersed in ethanol for 2 h and hexane for another 2 h. The fibres were removed from the low surface tension hexane solution and dried in air for one day. This step was done to prevent the overall fibre structure from collapsing due to capillary forces. Vertical glass tubes were used to hold the fibres in the ethanol and hexane solutions.

The dried fibres were immersed in liquid nitrogen for 30 to 45 sec to reduce the polymer's temperature to below its brittle point and then fractured to give a clean cross-section. Three



or four fibres from each experiment were broken into small pieces (about 2 to 3 mm) and mounted on the microscope stubs with double-sided tape for analysis (Figure 4-7).

The samples were coated with gold, using a sputter-coater, and then images recorded using SEM (FEI Company, Netherlands). Pictures were taken at  $\times 2000$  magnification all the way across the section of the wall. Pictures at  $\times 4000$  magnification were also taken near the outside wall of the fibre so that the region of the fibre where the pores are smaller could be seen more closely.



**Figure 4-5:** Photograph of hollow-fine fibres mounted on stubs for SEM analysis.

#### 4.5.2 Measurement of hollow-fine-fibre dimensions

Accurate measurements of the inside and outside diameters of the fibres were made by SEM. For a perfect cylindrical fibre  $d_o = d_i + 2(t)$  where  $d_o$  is the outside diameter,  $d_i$  the inside diameter and  $t$  the wall thickness.

#### 4.5.3 Determination of mechanical properties of hollow-fine fibres

The strength of fibres is important as the fibres must withstand high operating pressures without collapse. The main parameters of interest are the breaking tensile strength, breaking tensile elongation and Young's modulus, which is the slope of stress-strain curve before yield point. The mechanical properties of the hollow fibres were measured using an INSTRON

4444 with an INSTRON Max 50N load cell. Flat pneumatic actions grips, with a 2.5 cm grip width, were used to clamp the yarns in place. The accompanying INSTRON series LX software for windows (Merlin Version) processed the instrument data automatically. The initial length of the fibre specimen was 220 mm (120 mm test length plus 100 mm for grips). Standard test method ISO 2062:1995 for determining the single-end breaking force and elongation at break of fibres was used. The cross-sectional area of the hollow-fine fibre was calculated from the SEM images. Each data point for a single fibre was obtained from the average value of five fibres for each membrane test cell. The test were carried out at 20 °C and 65% humidity. The mechanical properties data were used to calculate Young's modulus in order to validate, the collapse pressure calculations of the produced fibre with different dimensions for brackish water desalination (Section 5.7). Elongation and tensile strength at break were automatically calculated by the computerized INSTRON for each of the samples according to the following equations.

- Tensile strength was calculated by dividing the maximum force (breaking load) by the cross-sectional area of the hollow-fine fibre.

$$\text{Tensile strength} = \frac{F}{A}$$

- Hollow-fibre elongation was calculated at the position of rupture:

$$\text{Elongation} = \frac{\Delta L}{L}$$

- Young's modulus was calculated from the initial slope of the tensile curve according to the following equation:

$$E = \frac{\text{tensile stress}}{\text{tensile strain}} = \frac{F/A}{\Delta L/L}$$

Where  $E$  is Young's modulus,  $F$  is the force applied to the fibre,  $A$  is the original cross-sectional area of the fibre,  $\Delta L$  is the displacement at maximum load and  $L$  is the original length of the fibre test specimen.

#### 4.6 Preparation of a membrane bundle

A fibre bundle was prepared to allow easy handling of the hollow fibres once the spinning was complete. Such a membrane bundle, shown in Figure 4-8, was specifically designed for fitting into the test cell of the existing laboratory scale membrane test rig. The bundle is an assembly of 30 wet hollow-fine-fibre membranes fitted at two ends into stainless steel tubing. The detailed assembly procedure is given below.

- Two stainless steel tubes were made in the following way. A 5 cm length of 3/8 inch outer diameter stainless steel tubing was cut and reamed.
- Thirty fibres were cut to a length of 60 cm and threaded through the 5 cm stainless steel tubing until a 5 cm length protruded from the top. The fibres were then glued by injecting the epoxy resin over 12 cm length of the fibres from the top, and then thread a 5 cm of the glued fibres inside the tube.
- When the epoxy was firm (not hard) the excess epoxy of 2 cm was cut cleanly, using a scalpel blade. This revealed the open bores of the hollow-fibre membranes. The membrane bundle was then inserted into the test cell of 50 cm length, using back and front ferrules to complete the sealing. This test cell was made of two connectors welded to 1/2 inch stainless steel tubing. The cell has inlet and outlet valves, one for the feed and other for retentate.

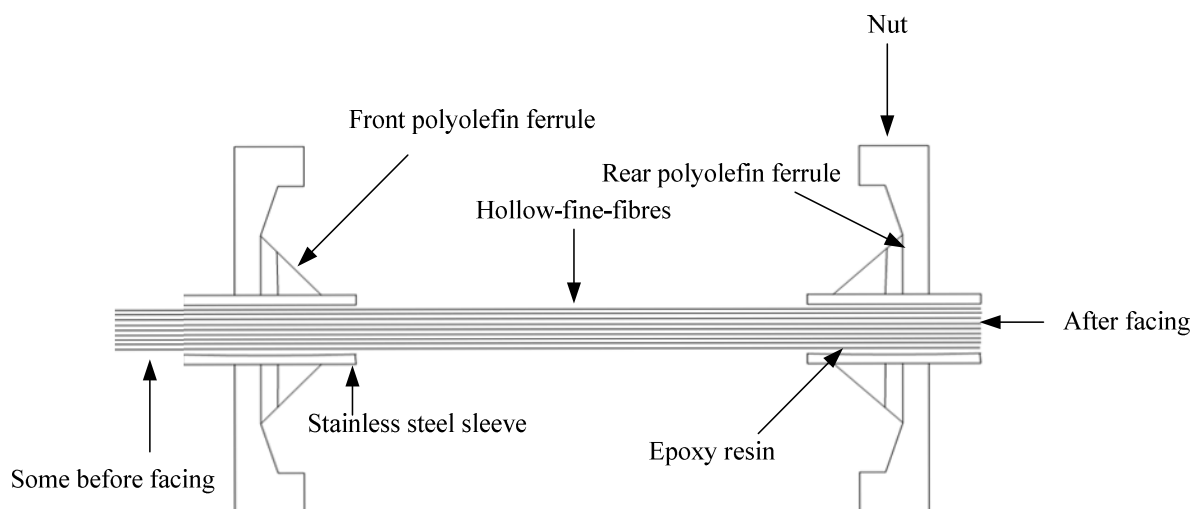


**Figure 4-6:** Schematic diagram of a hollow-fine-fibre membrane bundle.

#### **4.7 Post-treatment of hollow-fine fibres**

The heat treatment of CA hollow-fine-fibre membrane plays an important role in RO performance. By heat treatment of CA membranes, the less porous skin section of the membrane is densified further due to segmental chain motion and intermolecular bonding.<sup>31</sup> The annealing step was made in a stainless steel tank, with pH adjusted (pH 5.76 – 6.21) RO water. The water was heated by electrical heater and the temperature was controlled by mean of a temperature controller. The fibres were subjected to hot water treatment twice, after spinning and while in the membrane bundle form. The temperature used was 86 °C, and the period of immersion was 30 min in both instances (Section 5.7).

#### **4.8 Evaluation of hollow-fine fibres**

The analytical techniques, used to determine the resistance of the hollow fibres to collapse pressure and their RO performance (i.e. suitability as RO membranes) in terms of flux and salt retention is described in the following paragraphs.

##### **4.8.1 Determination of RO performance (flux and salt retention)**

Tests to determine the flux and salt retention of the fibres were carried out on the cross-flow filtration rig assembly, shown in Figure 4-9. The rig was constructed from stainless steel piping and fittings. It contains two test cells into which the membrane bundles can be fitted and are connected to a Hydra-Cell high-pressure pump. The feed solution for these cells was contained in a 50 L tank. The feed tank temperature was kept constant at 24 °C by a refrigerator unit. The volumetric flow rate was measured using a rotameter, whilst the inlet and outlet pressures were recorded on the pressure gauges P1 and P2, respectively. A by-pass loop allows the operator to control the pressure and flow rate in the rig.

A feed solution of 2 000 ppm (2 g/l) NaCl in RO water was prepared. As the outer surface of the hollow fibre is the selective layer, the feed solution was pumped into the shell side of the fibre bundle while the permeate (flux) was discharged from the permeate outlet, which is open to the atmosphere (Higher pressures can be used for higher feed concentrations). The permeate flow rate was determined volumetrically using a stop watch and 25 ml measuring cylinder. The salt concentrations in the feed and in the permeate were determined by using a conductivity meter (CyberScan Con 500 Bench). Three test cells were used for each membrane bundle and the data presented are the average of these measurements. The percentage salt retention (R) was calculated according to the following equation:

$$R = \left(1 - \frac{C_p}{C_f}\right) \times 100 \%$$

where  $C_f$  is the salt concentration of the feed ( $\mu\text{S}$ ),  $C_p$  is the salt concentration of the permeate ( $\mu\text{S}$ )

The permeation water flux was calculated according to the following equation:

$$J = \frac{V}{A \times t}$$

where  $V$  is the volume of the permeate (l),  $A$  is the surface area of the hollow-fine fibre ( $\text{m}^2$ ),  $t$  is the collection time of permeate (d),  $J$  is the water flux ( $\text{l}/\text{m}^2\text{d}$ )

#### 4.8.2 Determination of collapse pressure

Determination of collapse pressure was made using the test rig described below. It is the same test that was used to determine the RO performance. In the collapse pressure test, the permeate flow rate was collected over a range of different applied pressures. The permeate flux was then calculated and plotted as function of different applied pressures for different fibre dimensions. The plot (Section 5.6) will be used to illustrate at which pressure the CA hollow-fine-fibre membranes show a sudden decline in the permeate flux as a result of pressure failure (collapse pressure).

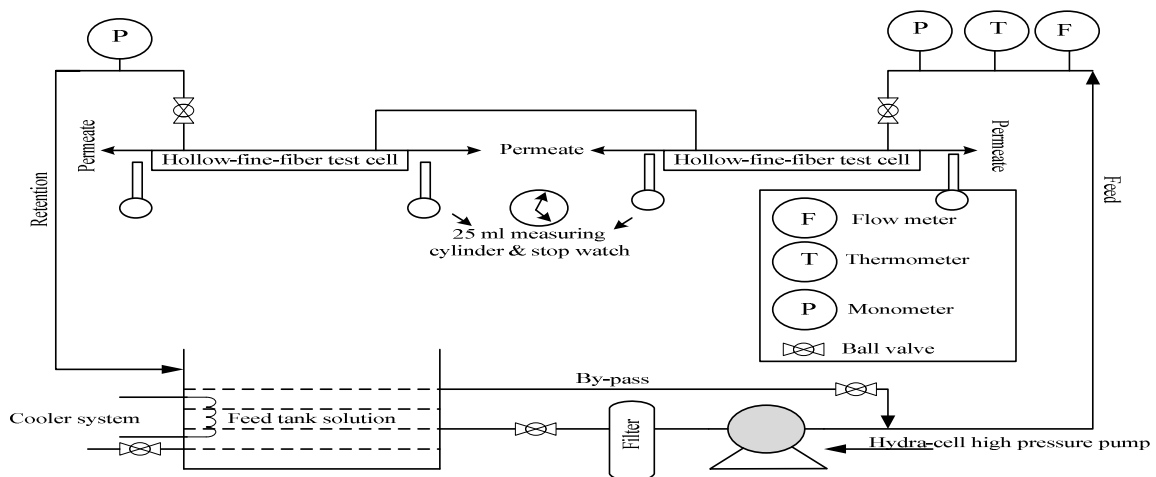
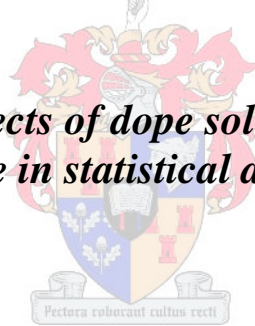


**Figure 4-7:** Schematic of hollow-fine-fibre membrane test rig plant.



## ***Chapter 5***

***Investigations into the effects of dope solution and spinning process  
for use in statistical analysis***



## 5.1 Introduction

The current investigation was intended to determine the possible effects of various factors of the dope solution formulation and the spinning process on the performance of CA hollow-fine-fibre membranes used for brackish water desalination. The factors investigated included the solvent to non-solvent ratio in the spinning dope, bore fluid ratio, take-up speed, dope extrusion rate, heat treatment and collapse pressure. These factors will be discussed in the statistical analysis (Chapter 6).

## 5.2 Solvent to non-solvent ratio

The selection of acetone as a solvent for the polymer was predicated on the fact that a dope solution with acetone precipitates slowly and yields a relatively non-porous membrane. In order to understand the mechanism of precipitation rate connected to the choice of solvent in terms of high and low heat of mixing, the temperature change on mixing 25 ml volume of water at 20 °C with 25 ml of different solvents at 20 °C was measured. The results are tabulated in Table 5-1.

**Table 5-1:** Temperature changes associated with heat of mixing

Solvent 25 ml	Non-solvent 25 ml	Temperature change °C	Temperature increase °C
DMAc	Water	37.5 °C	17.5
NMP	Water	35.4 °C	15.4
DMF	Water	34.4 °C	14.4
Acetone	Water	26.5 °C	6.5

The results showed that the most exothermic process occurred with the mixing of DMAc with water. It was clear from Table 5-1 that acetone showed lower heat of mixing compared to the other solvents which exhibited higher heats of mixing. Therefore acetone was subsequently chosen due to its relatively low heat of mixing.

Formamide was chosen as an additive in this study because of its good property as pore-forming agent in CA RO membranes.<sup>28</sup> Hence various ratios of solvent to non-solvent were used to determine the desirable structure and the performance of CA hollow-fine-fibre membrane. SEM images of CA acetate hollow-fine fibre spun from a dope composition with a solvent to non-solvent ratio of about 2.04 and bore fluid of 70 % acetone and 30% water are presented in (Figure 5-1). Conical voids, called macrovoids, are observed in the interior structure of the porous sublayer of the hollow fibre. Macrovoids are hollow defects found

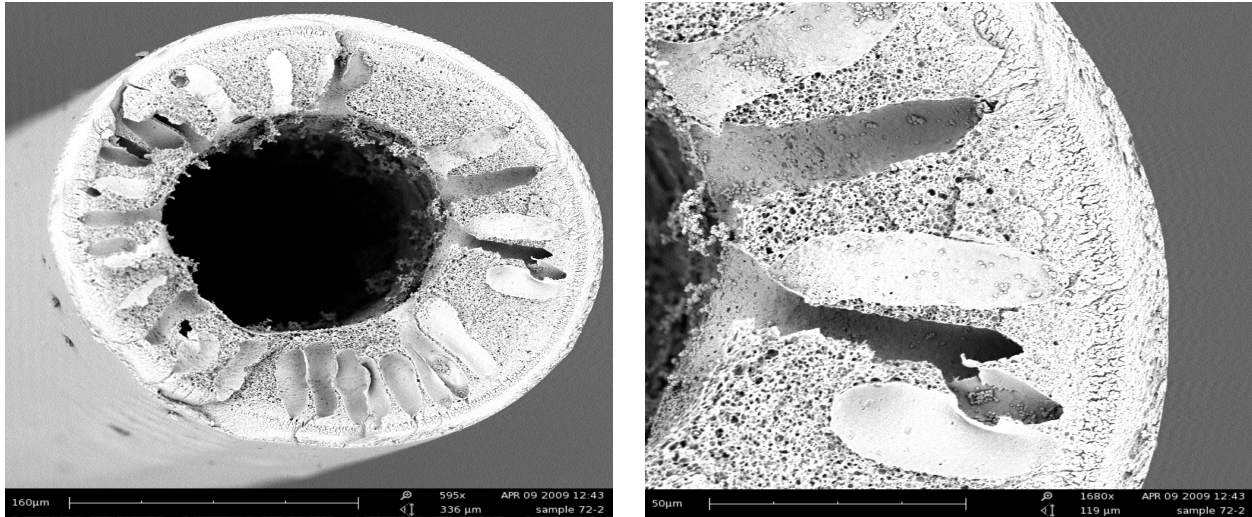


**Figure 5-1:** SEM images of hollow-fine fibre spun from dope containing 27% CA, 49% acetone and 24% formamide. (acetone: formamide ratio 2.04).

beneath the surface of the membrane and are often described as tear-drop or finger-like. It was suggested that the formation of macrovoids is a result of an excessively fast precipitation rate.<sup>133</sup> It was explained that, under the top layer, nuclei could be created, which contains a high solvent concentration. This may induce local delay of demixing, which keeps the polymer solution around the nucleus stable while the nucleus is growing. As long as the solution remains stable no new nuclei deeper in the membrane are formed and the nucleus can grow to form a macrovoid.<sup>134</sup> Two different techniques were described to prevent macrovoid formation by reducing the precipitation rate.<sup>135</sup>

- Reducing the propensity of the precipitant to diffuse into the cast solution. This can be achieved in two ways: firstly, by reducing the temperature of the precipitant, resulting in reduced diffusivity of the non-solvent; secondly, by choosing a solvent and non-solvent combination with a low heat of mixing. When the heat of mixing is high, the high affinity between the solvent and non-solvent causes an increase in the rate of precipitation.<sup>135</sup>
- Increasing the viscosity of the dope solution to reduce the rates of diffusion in and out of the nascent membrane. This may be achieved in two ways. Firstly, by reducing the temperature of the casting solution to increase its viscosity; secondly, the viscosity can be increased by increasing the concentration of the polymer in the casting solution.<sup>135</sup>

Particularly macrovoids, when present in such large numbers, can lead to weak spots in the fibres, which will reduce the fibres ability to withstand high pressure during RO applications, and hence must be avoided. Therefore macrovoids can be avoided by decreasing the rate of precipitation with increasing the formamide ratio as was suggest by Kesting.<sup>28</sup> In an attempt to understand the mechanism by which the formamide affected the rate of precipitation,

experiments were carried out to examine the heat of mixing when adding formamide to the dope solution. The change in temperature on mixing a 25 ml volume of water at 20 °C with 25 ml of acetone at 20 °C was measured and then measuring the temperature change by adding different concentrations of formamide to the water/acetone mixture.

**Table 5-2:** Temperature changes associated with heat of mixing

Acetone	Water	Temperature change	Formamide	Temperature change after adding formamide
25 ml	25 ml	26.5 °C	-	-
25 ml	25 ml	26.5 °C	5 ml	24.4 °C
25 ml	25 ml	26.5 °C	10 ml	22.2 °C
25 ml	25 ml	26.5 °C	15 ml	20.7 °C

The results (Table 5-2) showed that there is a gradual decrease in temperature with increasing formamide concentration in acetone/water mixture. It is evident that the higher formamide concentration in water, the lower the heat of mixing. Figure 5-2 shows SEM images of CA acetate hollow-fine fibre spun from a dope composition with solvent to non-solvent ratio of 1.447 and a bore fluid of 70% acetone and 30% water. Figure 5-2 showed that there was a definite advantage in increasing the formamide ratio into the dope solution and raises the question of how the formamide alters the phase inversion process such that the sponge-like structures are obtained. There are two possible explanations for this. The first explanation suggests that the dopes containing a higher formamide ratio have higher a viscosity, which reduces the rates of diffusion of the non-solvent and solvent.<sup>133</sup> Table 5-3 shows the viscosities of the various types of spinning dope. The data represent values estimated at zero shear rates at 23.4 °C. On the basis of the data in Table 5-3 a prediction could be made to suggest that the dope with high formamide content would have the best morphology (i.e. complete absence of macrovoids).

**Table 5-3:** The viscosities of 27% (m/m) CA polymer spinning solution with different solvent/non-solvent ratio (Zero shear rate at 23.4 °C)

Solvent/Non-solvent ratio	Viscosity (cP)
2.04	32 933
1.447	43 071
1.147	49 849

The second explanation suggests that the rates of polymer precipitation from solutions with high formamide ratio (lower heat of mixing) were slower than those of polymer solutions with low formamide addition (high heat of mixing) (Table 5-2). From these results it was argued that increasing the formamide concentration in the dope solution will slow down the rate of precipitation by decreasing the heat of mixing. This is possibly because formamide can



associate with water (the main precipitant) by hydrogen bonding, and this association reduces the activity of the water as a non-solvent, and consequently reduces the rate of precipitation.<sup>28</sup> The CA hollow-fine-fibre membrane as shown in Figure 5.2 had the following RO performance: retention of 94.5% and flux of 45 L/m<sup>2</sup>.d (2 000 ppm NaCl and 20 bar).

As the ratio of solvent to non-solvent decreased in the dope solution to 1.147, a membrane with uniform structure was formed, as seen in Figure 5-3. This membrane had salt retention of 95% and water flux of 53 L/m<sup>2</sup>.d (2 000 ppm NaCl and 20 bar).

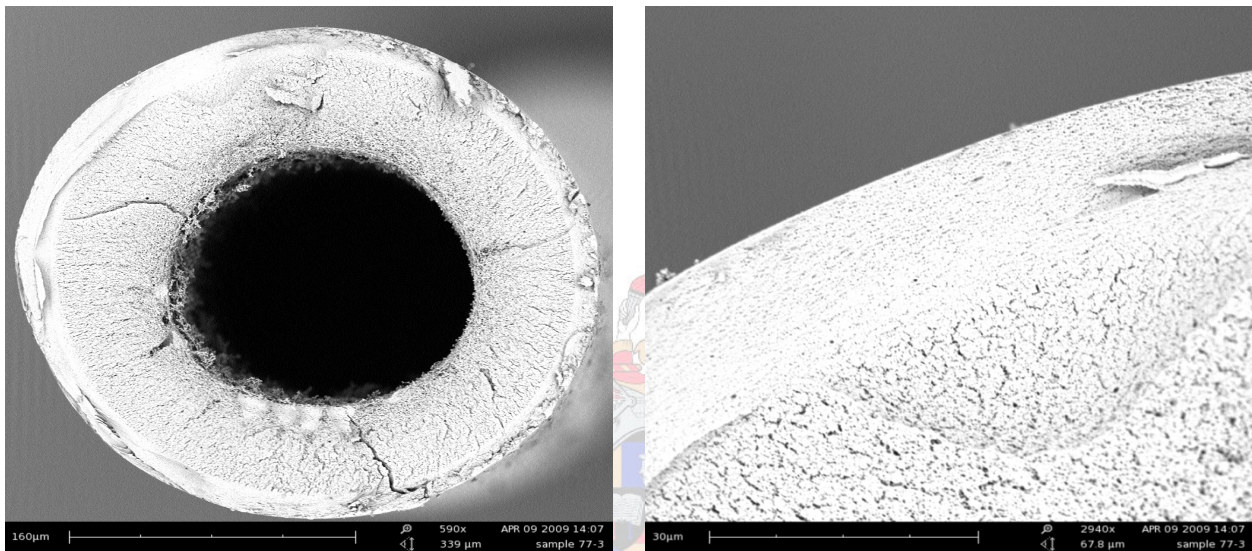


**Figure 5-2:** SEM images of hollow-fine fibre spun from dope containing 27% CA, 43.2% acetone and 29.8 % formamide. (acetone: formamide ratio 1.447).

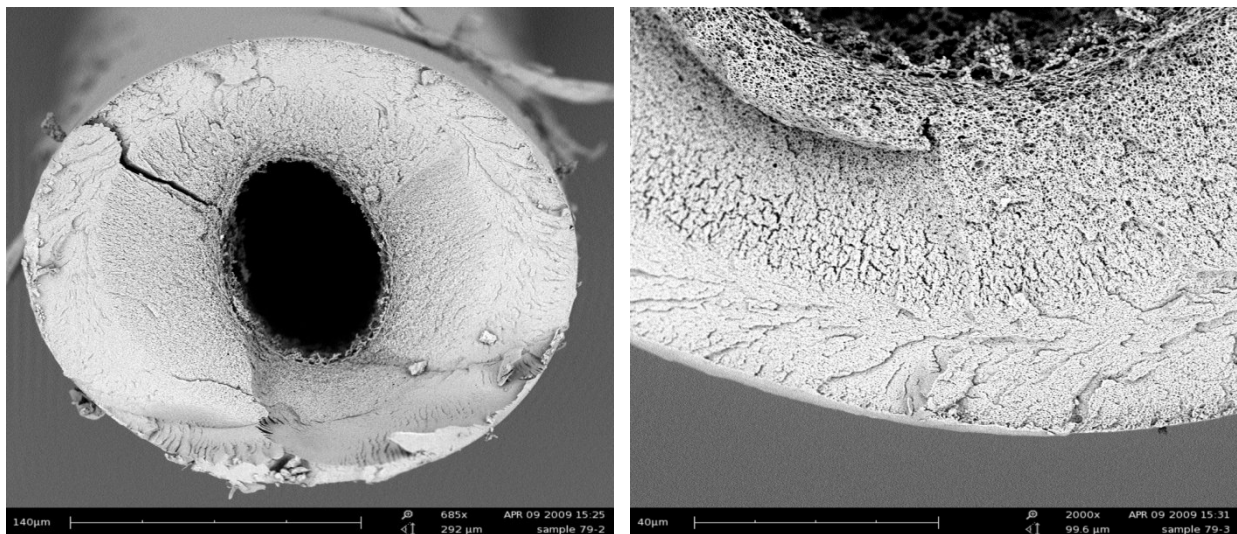


**Figure 5-3:** SEM images of hollow-fine fibre spun from dope solution containing 27% CA, 39% acetone and 34% formamide. (acetone: formamide ratio 1.147).

Formamide acts as pore-forming agent and, with a slow precipitation rate which a high formamide to acetone ratio causes in the dope solution, more pores will be presented in the membrane structures compared to membranes prepared from a dope solution with a lower formamide ratio. Furthermore, the choice of the mid-level of solvent to non-solvent ratio of 1.147 in the statistical analysis will be based on the above findings.

In the present study, it was found that the use of acetone as solvent resulted in a high tendency to form a dense structure due to a very slow precipitation process. Adding non-solvent (additive) to the dope solution will shift the composition path of the dope solution in the direction of the liquid-liquid demixing gap and a porous membrane can be produced with high permeability. When no non-solvent is added to the dope solutions, a nonporous (dense) membrane will be obtained.

### 5.3 Bore fluid

In this study the effect of different bore fluids on the fibre morphology was first examined by observations from SEM images (as described in this section) and later by RO performance of the hollow-fine fibres (as described in the following chapter).

When water is used as the bore fluid, coagulation of the polymer solution takes place at the point of extrusion and causes the nascent fibre to solidify from the inside while still in the air gap. Figure 5-4 shows SEM images of hollow-fine fibres spun when using water as the bore fluid. Those hollow-fibre membranes tend to have a much denser structure with many long finger-like macrovoids at the inner diameter. Typically, water is a powerful coagulant with high activity and has a strong nonsolvent strength for polymers. As a result when using water as bore fluid, there is instantaneous liquid-liquid demixing, thus the resultant fibres will have macrovoids on the inner surface beneath the skin layer.<sup>136</sup> Ideally, the activity of the bore fluid should be chosen to minimize interaction with the nascent membrane. It has been suggested that reducing the water activity will slow down the mass transfer during the wet phase inversion that occurs at the inner surface and subsequently the resultant fibres will have a sponge-like structure.<sup>90, 101</sup> It was recommended that the ideal bore fluid should have moderate coagulation strength for the polymer and high miscibility with the solvent or the solvent mixture, and be relatively inexpensive and non-toxic.<sup>137</sup> Hence a mixture of acetone and water was chosen for the bore fluid in this study.

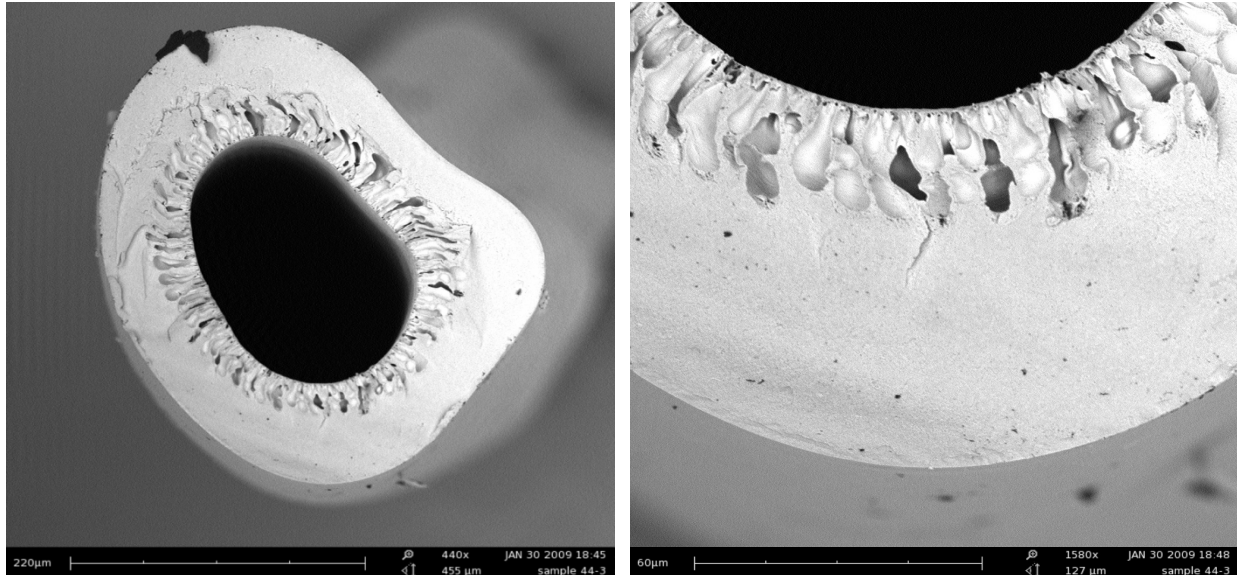


**Figure 5-4:** SEM images of hollow-fine fibre spun from dope solution containing 27% CA, 44% acetone and 29 % formamide, with water as bore fluid.

Fibres spun with 90% acetone and 10% water cannot be formed because the bore fluid contains too much solvent and will begin dissolving the nascent fibre in the air gap. Fibres spun with 80% acetone and 20% water tended to have a weak structure on the inside, with a pronounced interface between the inner and outer structure of the fibre as can be seen in Figure 5-5. Using 20% acetone with 80% water resulted in fibres as shown in Figure 5-6. The finger-like structures at the inner edge is suppressed by reducing the inner coagulant activity but the fibres have complete dense structures from both sides. When 70% acetone and 30% water was used as bore fluid the spun fibres tended to have porous substructure at the bore surface see Figure 5-7.

Since a mixture of 70% acetone and 30% water has a lower coagulation power than that of water, delayed liquid-liquid demixing takes place at the interior structure of the nascent fibre. As a result, a sponge-type structure is obtained with a more open porous structure that seems to be uniformly distributed. It was found from the above observations that a bore fluid of 70% acetone and 30% water gave a virtually open bore structure. The high level of the bore fluid was set at this value and the mid-level and low level were 60% and 50% acetone respectively for use in later studies (Chapter 6). Moreover, the hollow fibres obtained using acetone/water as bore fluid showed a good resistance to higher take-up speeds without breakages. This is because that the nascent fibre does not completely solidify while still in the air gap



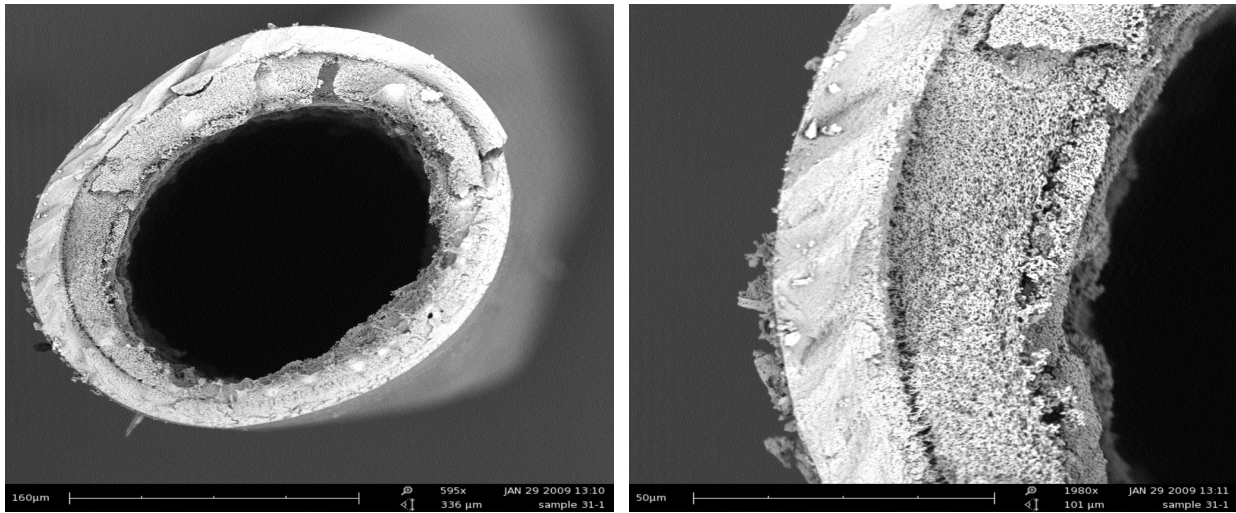


**Figure 5-5:** SEM images of hollow-fibre fibre spun from dope solution containing 27% CA, 44% acetone and 29 % formamide, with 80 % acetone and 20% water as bore fluid.

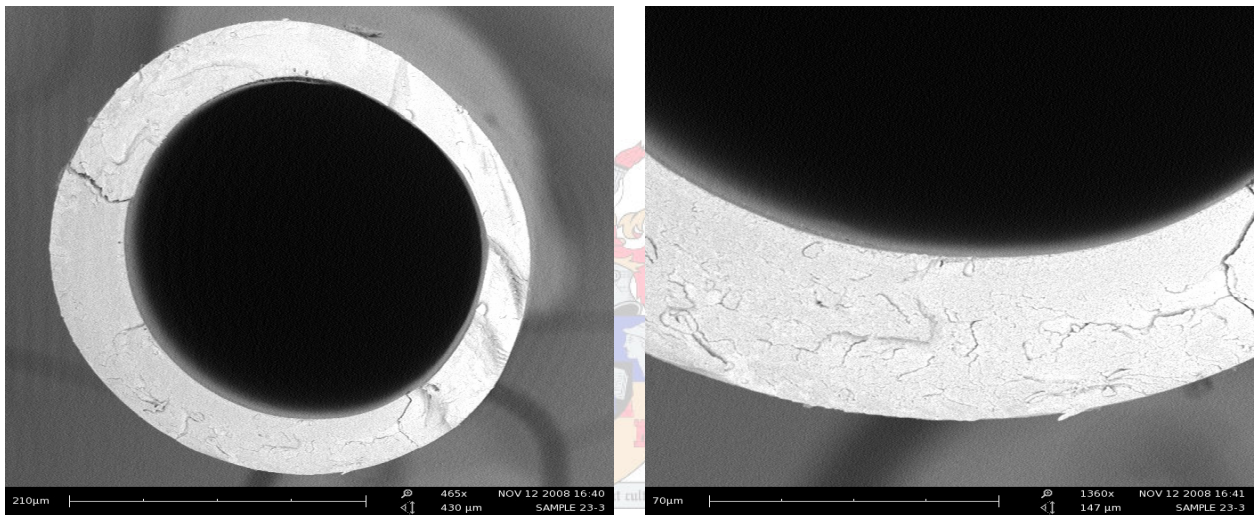


**Figure 5-6:** SEM images of hollow-fine fibre spun from dope solution containing 27% CA, 44% acetone and 29% formamide with 20% acetone and 80% water as bore fluid.

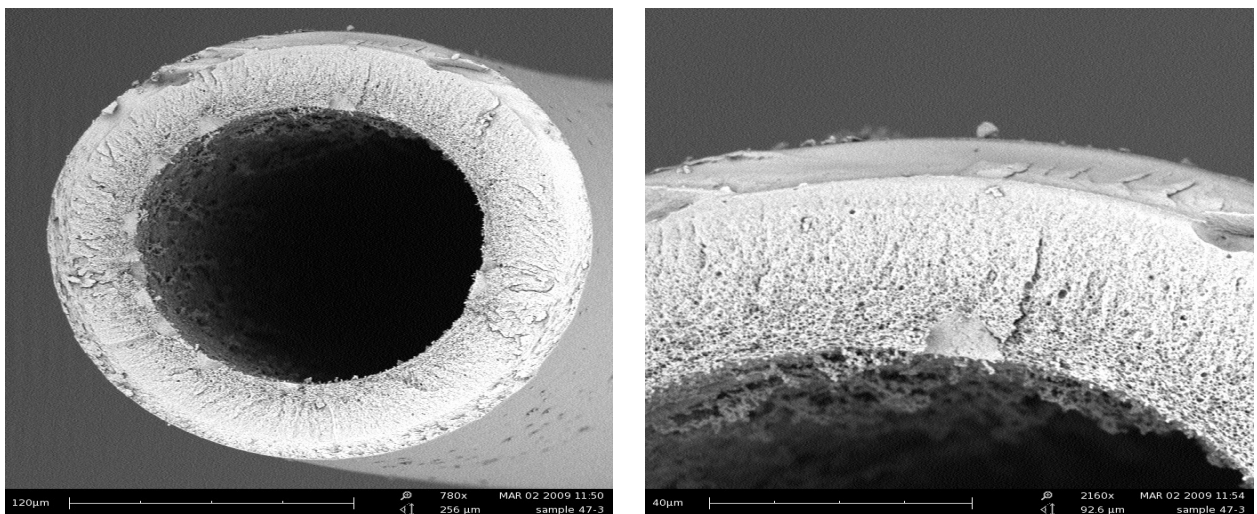


**Figure 5-7:** SEM images of hollow-fine fibre spun from dope solution containing 27% CA, 44% acetone and 29% formamide with 70% acetone and 30% water as bore fluid.



## 5.4 Dope extrusion rate

In order to get an optimum spinning dope extrusion rate (DER), various rates (ranging from 8 – 12 ml/min) were used to spin the CA hollow-fine-fibre membranes. The spinning conditions were as follows: the bore fluid rate and take-up speed were set at 3 ml/min and 88 r/min respectively, the bore fluid ratio was 70% acetone and 30% water (m/m). The results from using different DER are tabulated in Table 5-4.

**Table 5-4:** Effect of dope extrusion rate on retention and flux of CA hollow-fine-fibre membranes for brackish water desalination

Dope extrusion rate (ml/min)	Solvent/non-solvent ratio (m/m)	Bore fluid rate (ml/min)	Retention (%)	Flux (L/m <sup>2</sup> .d)
8	1.447	4	92.6 ± 0.32	55 ± 2
10	1.447	4	94.5 ± 0.14	45 ± 1
12	1.447	4	94.2 ± 0.43	41 ± 3

Test conditions: (2 000 ppm NaCl and 20 bar)

The results showed that there is a fairly strong correlation between the DER, the retention and the flux rate of the CA hollow-fine-fibre membranes. The results in Table 5-4 showed that the retention rate increased while the flux decreased with increasing DER. It can also be seen that there is value, beyond which the flux started to decrease again with an increase in the DER due to an increase in the shear stress in the spinneret. The increase in shear stress will affect the polymer orientation. Therefore, the polymer molecules will pack closer to each other as result of this orientation that is induced by shear stress in the spinneret.<sup>82-103, 104</sup> Based on these findings, the DER was fixed at 10 ml/min throughout the study.

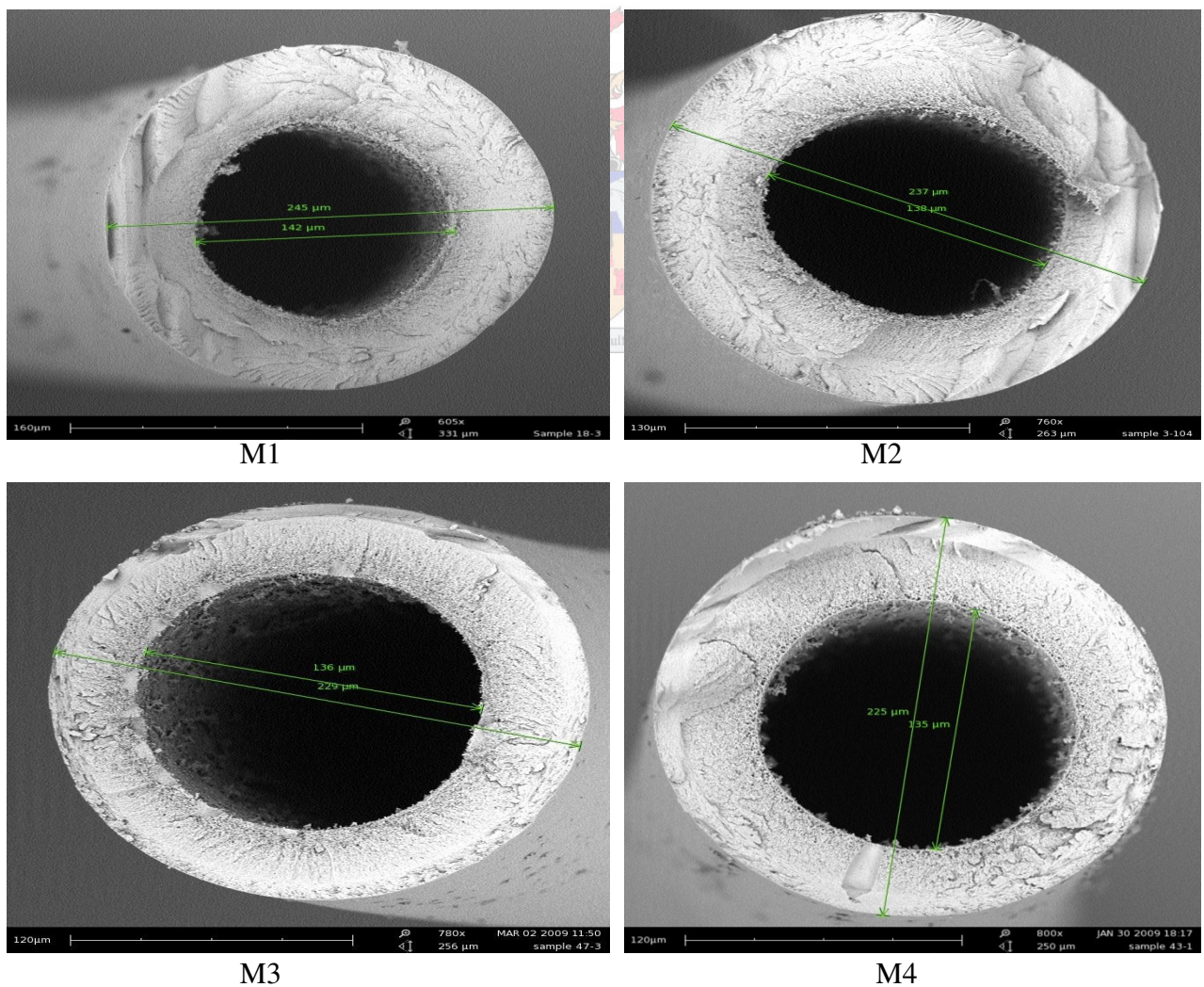
## 5.5 Take-up speed

Take-up speed can be used effectively to draw-down the size of the fibres to within the range established earlier (Section 3.3). In order to produce CA hollow-fine-fibre membranes having smaller dimensions, various take-up speeds were used in this study. The mechanical properties and the inside/outside diameter of CA hollow-fine-fibre membrane using various take-up speeds are tabulated in Table 5-5. The fibre was spun from a dope containing 27% CA, 44% acetone and 29 formamide, with 70% acetone and 30% water as the bore fluid. The bore fluid rate and DER were kept at 3 ml/min and 10 ml/min respectively.

**Table 5-5:** Mechanical properties and fibre diameters as function of take-up speed

Sample numbers	Take-up speed (r/min)	Fibre ID/OD ( $\mu\text{m}$ )	Tensile stress (GPa)	Elongation at break (%)	Young's modulus (GPa)
M1	88	142/245	0.021	26.75%	0.077
M2	94	138/237	0.022	22.19%	0.099
M3	99	136/229	0.023	22.19%	0.102
M4	104	135/225	0.024	19.10%	0.123

It can be seen from Figure 5-8 and Table 5-5 that the inner and outer diameters of the hollow-fine fibres decreased with an increase in take-up speed, while the mechanical properties improved with increasing the take-up speed. This improvement in the mechanical properties of hollow-fine fibres probably occurred as result of the higher degree of orientation induced by the higher take-up speeds which then resulted in more closely packed molecular chains of the membrane polymer.<sup>108</sup>

**Figure 5-8:** SEM images of hollow-fine-fibre membrane with different dimensions (M1 to M4).

In addition, a too high take-up speed will simply cause the hollow-fine fibres to break and low take-up speed causes the fibre to run slowly in the coagulation bath and as consequence non-spherical (oval shape) fibres will be produced (Figure 5-9). The take-up speed was fixed at 104 r/min as this speed provides the required fibre dimension for brackish water desalination.

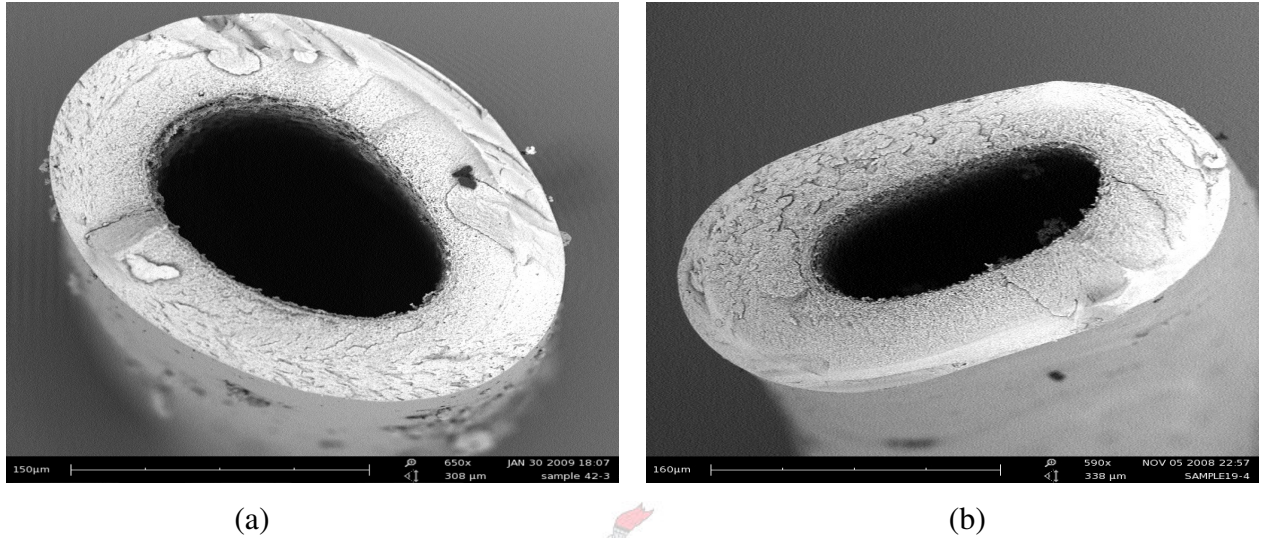


**Figure 5-9:** SEM images of hollow-fine-fibre membrane spun using lower take-up speeds (a) 60 r/min (b) 40 r/min respectively.

## 5.6 Collapse pressure determination of the produced fibre dimensions

Determination of the collapse pressure was carried out as described in Section 4.8.2. The fibres obtained during the above study were subjected to different applied pressures within the range of brackish water operating pressures. Figure 5-10 demonstrates the pressure failure of the hollow-fine-fibre membranes. RO water was used throughout and the water flux was measured over a range of different operating pressures. The data collected were plotted as a graph of permeate flux against different pressures to show the collapse profile from which the collapse pressure could easily be determined. The water flux gradually increased with increasing the applied pressure until it reached a point where it started to decrease. The decrease in water flux was thought to be a result of the membrane structure being compressed and can be interpreted as the pressure beyond which the membrane is susceptible to collapse. The graph also shows that the collapse pressure increased with decreasing the fibre dimensions. It can also be seen that the CA hollow-fine-fibre membranes retained a small amount of their flux after collapse due to the high elasticity of CA hollow-fine fibres. It is noticeable that the collapse pressure values of the spun fibre dimensions from the graph are slightly lower than the collapse pressure values obtained by calculations in section 3.3. This



is possibly due to that fibre porosity (module of elasticity) plays an important role in reducing the load-bearing within the membrane structure. It can be seen from the graph that the fibres with inside to outside diameter of 135/ 225, 136/229, 138/237 and 142/246 undergo gradual collapse at 24, 20, 20 and 18 bar respectively because the flux suddenly decreased. Therefore the spun fibres within the acceptable range obtained by collapse pressure and pressure drop calculations for brackish water showed a good ability to withstand the typical brackish water operating conditions of 20 – 25 bar.

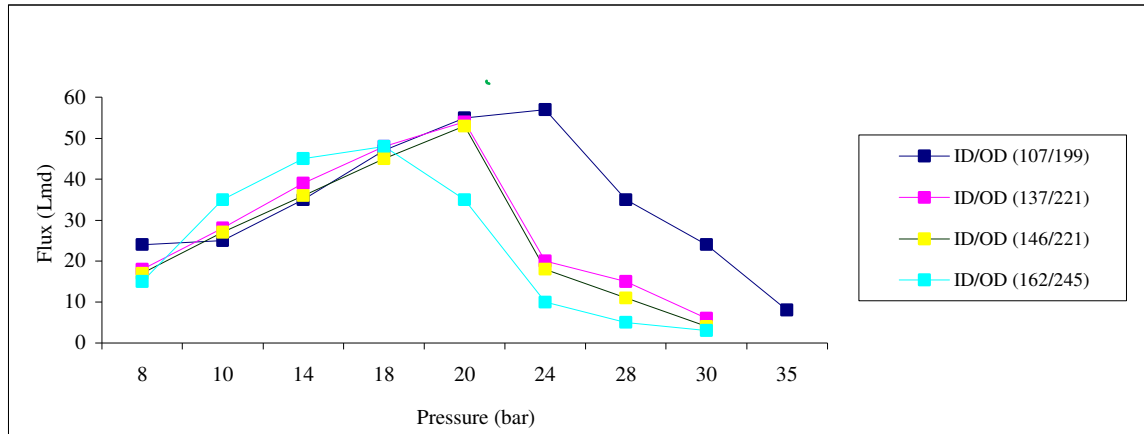


**Figure 5-10:** Collapse pressures of CA hollow-fine fibre with different ID/OD ratios.

For further validation of the collapse pressure values, calculations of collapse pressures were carried out using equation 3.1 (Chapter 3) on the fibre dimensions produced above with their real Young's modulus. The results are tabulated in Table 5-6.



**Table 5-6:** Calculated and measured collapse pressure values

Fibre dimensions ( $\mu\text{m}$ )	Young's modulus (GPa)	Calculated collapse pressures (bar)	Measured collapse* pressures (bar)
135/225	0.123	23	24
136/229	0.102	20	20
138/237	0.099	21	20
142/245	0.077	17	18

\* Determined experimentally as the point beyond which the flux decreases as the pressure increases, indicating probable collapse.

The results in Table 5-6 showed that there are only slight differences between the calculated and the measured collapse pressure values of the produced fibre dimensions within the region of fibre dimensions determined in Chapter 3. The results showed a good agreement between the determined and produced fibre dimensions in terms of their ability to withstand typical operating conditions of brackish water from 20 – 25 bar.

## 5.7 Effect of heat treatment

The last step in membrane fabrication is the direct immersion in hot water for a certain period of time. Unannealed RO membranes showed lower retention, generally not above 50%, and after annealing the retention increased with increasing annealing temperature.<sup>109</sup> In attempting to understand the effect of heat treatment, hollow-fine fibres were annealed at different temperatures ranging from 80 to 90 °C and times ranging from 20 to 35 min. The effect of heat treatment on the retention and flux of CA hollow-fine fibres is shown in Figure 5-11.

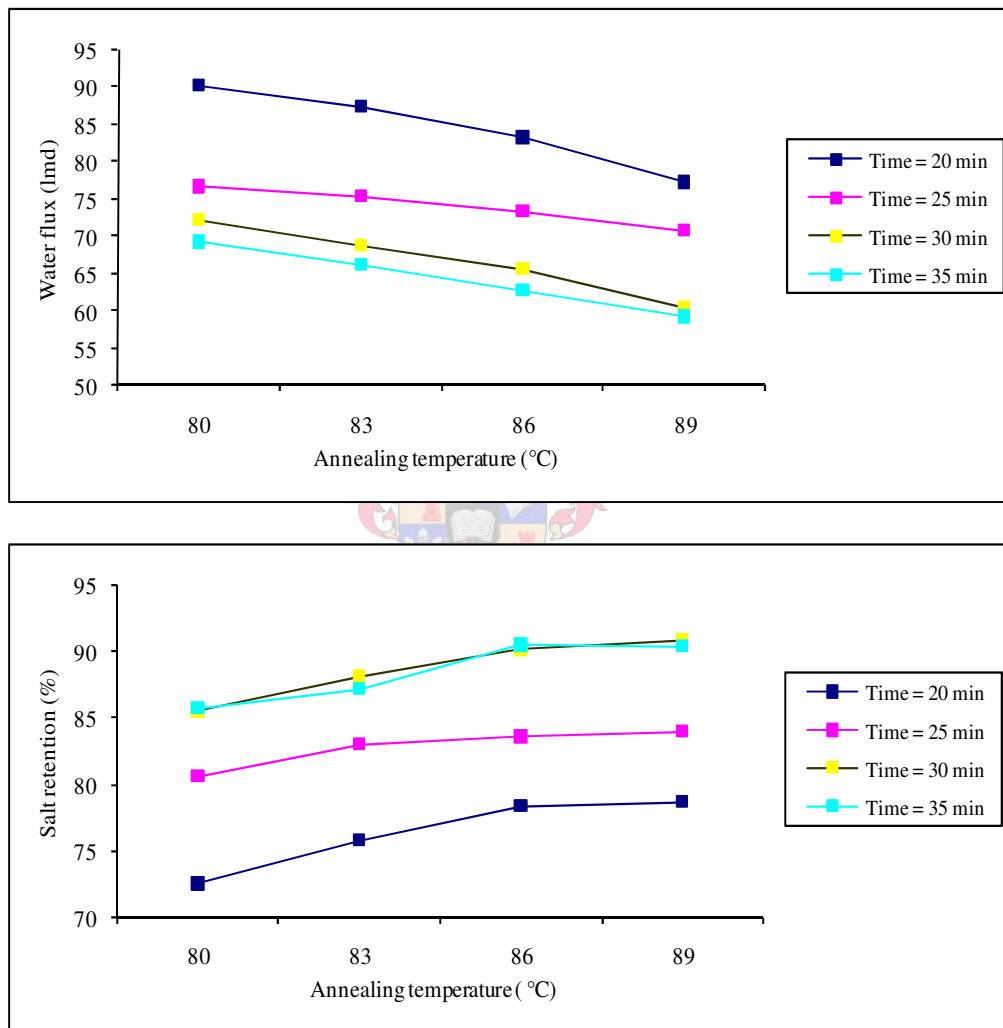


**Figure 5-11:** Effect of heat treatment on CA hollow-fine-fibre membrane performance.

It can be seen that the salt retention increased and the flux decreased with increasing the annealing temperature and time. This increase in retention was because of densification of skin layer due to segmental chain motion and loss of excluded free volume upon the heat treatment. The salt retention did not further improve with increasing time from 30 to 35 min

and temperature from 86 to 90 °C but the flux decreased gradually and continually with increasing time and temperature. This is possibly because the skin layer consolidates and grows in thickness with increasing time. The retention of CA hollow-fine fibres annealed at 86 °C for 30, min was 90% and flux was 65 L/m<sup>2</sup>.d. The hollow-fine-fibre membranes bundles were heat treated for a second time to see if there is any improvement in the salt retention. The heat treatment was 86 °C for times between 20 to 35 min after which these fibres showed good salt retention. Figure 5-12 shows the effect of second heat treatment on CA hollow-fine fibres. The fibres showed further increase in the salt retention while maintaining a good membrane flux, when annealed at 86 °C for 30 min for a second time.

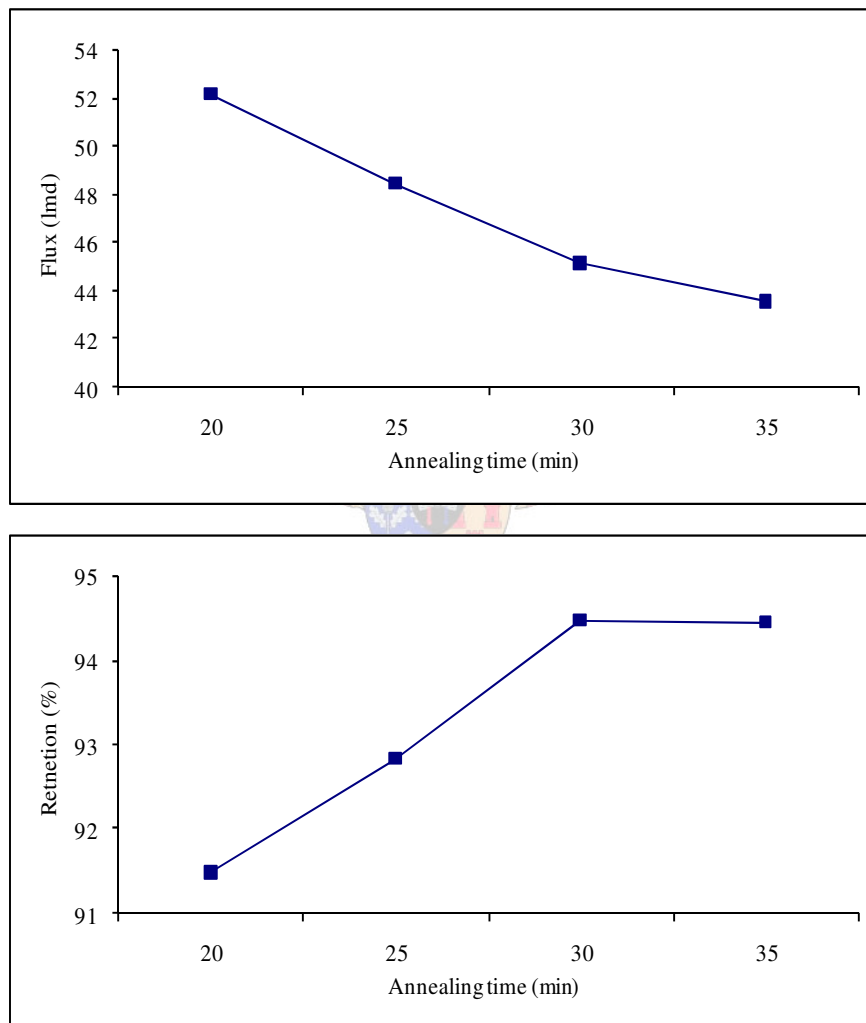


**Figure 5-12:** Effect of annealing time on CA hollow-fine-fibres membrane performance at the second annealing temperature at 86 °C.

The salt retention increased to about 94.5% and the flux decreased to 45 L/m<sup>2</sup>.d. Thus the process of a second annealing time for the fibre bundle yielded CA hollow-fine-fibre membranes with higher salt retention.

The first heating is carried out after relaxing the freshly spun fibre in fresh water for a day which is mainly done to remove excess solvent. There are two heat relaxation processes, firstly heat consolidation and densification of the upper-most skin layer, i.e. removing pores are tiny flaws and are undesirable, and secondly the tightening of the amorphous underlying area which hinders the flux. This underlayer will continuously tighten whether from temperature or time (as it is a viscoelastic phenomena).

Densifying the skin is problematic as retention asymptotically reaches a maximum after 30 min at 86 °C (see Figure 5.12). This is felt to be due to incomplete closure of the final pores. It was found that if the membranes were then left to relax at room temperature in water for 24 hours followed by the same heat treatment, 30 min at 86 °C, further consolidation of the skin and underlayer (the latter with loss of flux) resulted in an increased maximum retention. This has never been reported before in literature. It was not thought necessary to repeat this procedure a third or fourth time as the gain in retention still possible for CA is negligible and the flux will continue to drop.

One can surmise that in the skin layer, as the pores close, the OH groups, which are at a level of 2.45 degree of substitution, tend to hydrogen bond, leaving a stable pore or capillary and resulting in a maximum value for retention. During relaxation, rearrangement of CA molecules can occur to preferred orientations and a partial loss of the less stable H-bonded enclosed pores. The second heating leads to further tightening and rearrangement easing closing of the pores until only a small fraction of the OH groups persist to give unclosed pores and another plateau value occurs. 100% retention is not possible with CA. One can carry on tightening the skin layer but the flux suffers too much because of this and the tightening of the intermolecular space. Based on the above results the membranes bundle were annealed twice at 30 min for 86 °C and therefore this was not used as factor in the factorial experiments (Chapter 6).

## 5.8 Conclusion

The solvent to non-solvent ratio, bore fluid, dope extrusion rate, take-up speed, collapse pressure determination and effect of heat treatment determined in this chapter serve as the basis for the statistical analysis discussed in Chapter 6.

## ***Chapter 6***

# ***Statistical analysis using factorial design experiments for developing CA hollow-fine-fibre membranes***





## 6.1 Introduction

Factorial design and the associated analysis of variance are useful tools to characterize processes which are influenced by a number of factors. The methods allow the determination of statistically important factors and enable the experimenter to study the joint effect of the factors on a the response.<sup>138</sup> In this way a regression model for each of the measured can be generated. In this study a  $3^3$ -factorial design<sup>138</sup> is used to identify which factors and their interactions have the most important effect of the performance of CA hollow-fine-fibre membrane for brackish water desalinations.

## 6.2 Experimental design

Based on literature and preliminary results discussed Chapter 4, three important factors which affect the fabrication process were considered: solvent/non-solvent ratio, air gap distance and bore fluid composition. Each factor will be studied at three levels, and a  $3^3$  full factorial design was selected to achieve this goal because it consists of all possible combinations of the levels for all factors. It is also useful for investigating quadratic effects, which is not possible with 2 level design. The responses of interest are (flux) and (retention). The list of factors and their chosen levels for the experiment are shown in Table 6-1. The hollow-fine-fibre membrane performance was determined using an applied pressure of 20 bar and a feed solution of 2 000 ppm (NaCl).

Each trial was replicated twice since replication permits more degrees of freedom in the estimation of error variance and provides the means to determine variability between treatments and that due to random variation. The Design-Expert Software 7.1 was used to analyze the experimental data. The experimental results of the  $3^3$ -factorial design are shown in standard order in Table 6-2.

**Table 6-1:** Factors and levels for  $3^3$  levels factorial design

Label	Factors	Low level	Mid level	High level
		-1	0	1
A	Solvent/non-solvent mass ratio (m/m)	0.847	1.147	1.447
B	Air gap distance (mm)	40	80	120
C	Bore fluid ratio	50% acetone	60% acetone	70% acetone
	Acetone/water (m/m)	50% water	40% water	30% water

**Table 6-2:** Design data of the experiments and their replication with response values

Trials	Factor 1	Factor 2	Factor 3	Response 1	Response
	A:Solvent/Non-solvent (m/m)	B:Air gap (mm)	C:Bore fluid (m/m)	Salt retention (%)	Flux (L/m <sup>2</sup> .d)
1	0	0	0	97.5	62.4
2	0	0	1	94.5	50.0
3	0	-1	-1	96.3	53.4
4	0	0	1	94.0	49.0
5	1	0	-1	95.0	51.2
6	-1	1	-1	95.8	55.6
7	-1	1	-1	96.3	53.4
8	-1	1	0	97.0	62.3
9	0	1	1	95.0	53.0
10	-1	0	-1	96.4	50.2
11	1	-1	1	92.4	41
12	1	1	-1	95.4	53.5
13	-1	0	0	96.7	58.0
14	1	-1	1	93.4	42.0
15	1	1	0	96.7	55.6
16	1	1	-1	95.3	55.7
17	0	-1	-1	97.5	55.7
18	-1	-1	-1	95.7	49.4
19	1	1	1	94.5	45
20	1	-1	0	96.0	53.4
21	0	1	0	98.5	64.6
22	0	1	-1	97.6	55.7
23	1	1	0	96.0	60.0
24	1	-1	-1	95.6	51.2
25	1	0	1	94.2	42.4
26	-1	0	0	96.7	55.6
27	-1	1	1	94.0	48.0
28	1	0	0	96.0	53.4
29	0	-1	1	94.4	48.0
30	0	0	-1	97.2	58.0
31	-1	-1	0	96.6	60.0
32	1	1	1	95.0	43.6
33	0	1	-1	97.5	58.0
34	1	0	-1	94.9	51.2
35	0	0	-1	96.8	51.2
36	0	1	1	94.7	52.3
37	1	-1	-1	96.0	49.0
38	-1	-1	1	94.0	44.0
39	0	-1	0	97.4	61.5
40	1	0	0	95.8	53.4
41	0	1	0	97.6	62.3
42	1	-1	0	95.2	53.0
43	-1	0	1	94.0	47.0
44	-1	-1	0	96.3	51.2
45	-1	0	1	93.7	47.0
46	0	-1	1	94.0	49.0
47	-1	0	-1	96.3	49.3
48	-1	-1	-1	96.4	48.7
49	0	-1	0	96.8	59.3
50	0	0	0	97.2	60.0
51	-1	-1	1	92.0	42.0
52	1	0	1	93.5	44.0
53	-1	1	0	97.2	57.0
54	-1	1	1	94.8	50.0

## 6.3 Results and discussion

The salt retention and permeate flux responses for each experimental trial are shown in Table 6-2. These results were statistically analyzed using analysis of variance (ANOVA) to study the joint effect of each factor and their interactions on the membrane performance (retention and flux).

### 6.3.1 Analysis of variance (ANOVA)

This method was first developed by Fisher in 1930.<sup>139</sup> ANOVA is a statistical method used to evaluate which of the factors studied significantly affects the responses over the range studied. The relative importance of each factor and factor-factor interaction can be ranked in terms of their effect on the process output. Thus the information about how significant the effect of each factor on the experimental results, can be concluded from ANOVA. Tables 6.3 and 6.4 summarize the ANOVA of the three factors studied.

**Table 6-3:** Analysis of variance of the regression model for retention

Source	Sum of squares	df	Mean square	F-Value	Prob > F	
Model	98.44	9	10.94	51.34	< 0.0001	significant
A	1.93	1	1.93	9.04	0.0044	significant
B	4.97	1	4.97	23.32	< 0.0001	significant
C	44.22	1	44.22	207.55	< 0.0001	significant
AB	0.00	1	0.0017	0.0078	0.9299	not significant
AC	1.29	1	1.29	6.06	0.0178	significant
BC	2.21	1	2.21	10.39	0.0024	significant
A <sup>2</sup>	13.09	1	13.09	61.44	< 0.0001	significant
B <sup>2</sup>	0.13	1	0.13	0.63	0.4325	Not significant
C <sup>2</sup>	21.39	1	21.39	100.41	< 0.0001	significant
Residual	9.37	44	0.21			
Lack of fit	3.56	17	0.21	0.97	0.51	not significant
Pure error	5.81	27	0.22			
Correct Total	107.81	53				
Standard deviation	0.46		R-squared R <sup>2</sup>	0.91		
Mean	95.65		Adjusted R-squared	0.90		
Coefficient of variation C. V. %	0.48		Predicted R-squared	0.86		
PRESS	15.18		Adequate precision	23.88		

**Table 6-4:** Analysis of variance of the regression model for flux

Source	Sum of squares	df	Mean square	<i>F</i> -value	Prob > F	
Model	1732.21	9	192.47	49.13	< 0.0001	significant
A	29.66	1	29.66	7.57	0.0086	significant
B	138.98	1	138.98	35.47	< 0.0001	significant
C	355.32	1	355.32	90.69	< 0.0001	significant
AB	2.16	1	2.16	0.55	0.4617	not significant
AC	23.55	1	23.55	6.01	0.0183	significant
BC	0.19	1	0.19	0.05	0.828	not significant
A <sup>2</sup>	318.61	1	318.61	81.32	< 0.0001	significant
B <sup>2</sup>	10.58	1	10.58	2.70	0.1075	not significant
C <sup>2</sup>	704.12	1	704.12	179.72	< 0.0001	significant
Residual	172.39	44	3.92			
Lack of fit	43.61	17	2.57	0.54	0.9074	not significant
Pure error	128.78	27	4.77			
Correct total	1904.60	53				
Standard deviation	1.98		R-squared <i>R</i> <sup>2</sup>	0.91		
Mean	52.48		Adjusted R-squared	0.89		
Coefficient of variation C.V. %	3.77		Predicted R-squared	0.87		
PRESS	251.84		Adequate precision	26.24		

### 6.3.2 Checking the adequacy of both regression models

In tables 6-3, 6-4, the “Model *F*-values” are calculated from a model mean square divided by residual mean square; the residuals are defined as the differences between the experimental data and the predicted values for each point in the design. The Model *F*-value is the test for comparing model variance with residual (error) variance. If the variances are close to the same, the ratio will be close to one and it is less likely that any of the factors have a significant effect on the response. Similarly, an “*F*-value” for any individual factor term is calculated from a term mean square divided by a residual mean square. It is a test that compares a term variance with a residual variance. If the variances are close to the same, the ratio will be close to one and it is less likely that the term has a significant effect on the response. In Table 6-3 a “Model *F*-values” of 51.34 with a “Model *F*-values” 49.13 in Table 6-4 imply that the selected models are significant and there is only a 0.01% chance that a “Model *F*-values” this large could occur due to noise. Prob > F represents the probability of seeing the observed *F* value if the null hypothesis is true (there is no factor effect). Small probability values call for a rejection of the null hypothesis. The probability equals the proportion of the area under the curve of the *F*-distribution (with 9 and 27 degree of freedom) that lies beyond the observed *F*-value. Furthermore, the P-value is the probability that the test

statistic will take on a value that is at least as extreme as the observed value of the statistic when the null hypothesis is true. Thus, a P-value conveys much information about the weight of evidence against null hypothesis, and so a decision maker can draw a conclusion at any specified level of significance. More formally, we define the P-value as the smallest level of significance that would lead to the rejection of the null hypothesis.<sup>140</sup> In other words, if the  $\text{Prob} > F$  value is very small (less than 0.05), then the terms in the model have a significant effect on the response, providing at least 95% confidence for results. If the  $\text{Prob} > F$  value is greater than 0.1 then this is an indication that the model terms are not significant. The “lack-of-fit F-values” for both models implies that the lack of fit is not significantly related to pure error. These values of lack of fit are desirable as we want to know how well the models fit the experimental data.

“R-squared”, or more formally the coefficient of multiple determination, is defined as the sum of squares for the model divided by the total corrected sum of squares and indicates the proportion of the variability in the data explained by the analysis of variance model. The  $R^2$  values of models were calculated to be 0.91 in both instances, indicating that only 9% of the total variation was not explained. Thus the models were able to explain about 91% of the variability in salt retention and permeate flux data. The closer the value of  $R^2$  is to unity, the better is the correlation between the observed and predicted values.<sup>141</sup> In this study the predicted  $R^2$  of 0.86 and 0.87 are in reasonable agreement with the adjusted R-squared of 0.90 and 0.89 of both models. Adequate precision measures the signal to noise ratio. A ratio greater than 4 is desirable. Adequate precisions of 23.88 and 26.24 for both models indicate adequate model discrimination.<sup>138</sup> The coefficient of variation (CV) for the retention and flux were calculated to be 0.48 and 3.77%. The CV, the ratio of the standard error of estimate to the mean value of the observed response (as a percentage), is a measure of reproducibility of the model and, as a general rule, a model can be considered reasonably reproducible if its CV is not greater than 10%.<sup>142</sup> The predicted sum of squares (PRESS), which is a measure of how a particular model fits each point in the design, was 15.18 and 251.84. According to Table 6-3 the main factors of A, B, C, the interaction of AC, BC, and the second orders of  $A^2$ ,  $C^2$  are significant model terms. In Table 6-4 the main factors of A, B, C, the interaction of AC and the second orders of  $A^2$ ,  $C^2$  are significant model terms. The other factors are less significant but cannot be neglected due to their little influence on responses as well.

The results of each of these overall responses are included in the analysis procedure and an equation that describes the influence of the factors on the overall responses was found. The following equations are the final regression models in terms of the actual and coded factors.

Table 6-5 tabulates the differences between the actual and predicted response values according to the equations.

$$\text{Salt retention (coded)} = 97.16 - 0.23 \times A + 0.37 \times B - 1.11 \times C + 0.00838 \times A \times B + 0.23 \times A \times C + 0.30 \times B \times C - 1.04 \times A^2 + 0.11 \times B^2 - 1.42 \times C^2$$

$$\text{Flux (coded)} = + 60.63 - 0.91 \times A + 1.97 \times B - 3.14 \times C - 0.30 \times A \times B - 0.98 \times A \times C + 0.088 \times B \times C - 5.15 \times A^2 + 0.94 \times B^2 - 8.16 \times C^2$$

In order to check data for normality, even when there is fairly small number of observations, it is best to construct normal probability plots of the residuals. Here “residual” means the difference in the observed values (obtained from the experiments) and the predicted value or fitted values. The normal probability plot shows the residuals plotted against a cumulative normal percentile derived from the normal probability distribution for the ranking location of the residuals. This provides a visual method to illustrate if the residuals are actually normally distributed. If the residuals fall approximately along a straight line, the residuals are then normally distributed. In contrast, if the residuals do not fall fairly close to a straight line, the residuals are then not normally distributed and hence the data do not come from a normal population. In Table 6-5 the residuals are ranked in ascending order from the lowest to highest in order to plot the normal probability plot and their cumulative probability points are calculated  $P_k = (K - 0.5)/n$ , where K is the sequence number from 1 to n and n is the number of entries in the list. Figure 6-1 shows the normal probability plots of the residuals. There is no indication of nonnormality, nor is there any evidence pointing to possible outliers. It can be concluded that the normal distribution provides an excellent model for the data.

The next residual plot which we examine was the plot of residuals versus the predicted values in Figure 6-2. The plot of the residuals versus the ascending predicted response values indicated that there is no expanding variance phenomenon. The residual values seem to be randomly scattered above and below zero over the range of the data and do not indicate any problems with the model. The reference line at 0 emphasizes that the residuals are split about 50-50 between positive and negative. There are no systematic patterns or unusual structures apparent in this plot. Plots in which the residuals do not exhibit any systematic structure indicate that the model fits the data well. In contrast, plots of the residuals that exhibit systematic structure indicate that the form of the function can be improved in some way.<sup>138</sup>

Therefore, Figure 6-2 indicates that the model fits and, there is no reason to suspect any violation of the independence or constant variance assumption.

**Table 6-5:** Comparison of the actual and predicted responses of retention and flux

Trial	Actual retention	Predicted retention	Residual	Actual flux	Predicted flux	Residual
1	97.5	97.1	0.34	62.4	60.6	1.77
2	94.5	94.6	-0.13	50.0	49.3	0.67
3	96.3	96.8	-0.58	53.4	54.6	-1.26
4	94.0	94.6	-0.63	49.0	49.3	-0.33
5	95.0	95.3	-0.34	51.2	49.5	1.66
6	95.8	96.4	-0.64	55.6	55.4	0.13
7	96.3	96.4	-0.14	53.4	55.4	-2.07
8	97.0	96.8	0.18	62.3	60.5	1.72
9	95.0	95.4	-0.41	53.0	52.3	0.67
10	96.4	96.2	0.13	50.2	51.3	-1.17
11	92.4	93.0	-0.61	41.0	43.4	-2.42
12	95.4	95.5	-0.13	53.5	51.0	2.41
13	96.7	96.3	0.35	58.0	56.3	1.61
14	93.4	93.0	0.39	42.0	43.4	-1.42
15	96.7	96.3	0.33	55.6	56.2	-0.60
16	95.3	95.5	-0.23	55.7	51.0	4.61
17	97.5	96.8	0.62	55.7	54.6	1.04
18	95.7	96.3	-0.61	49.4	49.1	0.26
19	94.5	94.3	0.13	45.0	44.9	0.02
20	96.0	95.6	0.39	53.4	54.8	-1.41
21	98.2	97.6	0.86	64.6	63.5	1.06
22	97.6	97.0	0.57	55.7	58.4	-2.73
23	96.0	96.3	-0.37	60.0	56.2	3.80
24	95.6	95.3	0.23	51.2	49.8	1.32
25	94.2	93.5	0.62	42.4	43.2	-0.86
26	96.7	96.3	0.35	55.6	56.3	-0.79
27	94.0	94.3	-0.36	48.0	49.3	-1.37
28	96.0	95.8	0.11	53.4	54.5	-1.17
29	94.4	94.0	0.34	48.0	48.2	-0.20
30	97.2	96.8	0.35	58.0	55.6	2.39
31	96.6	96.0	0.51	60.0	54.0	5.93
32	95.0	94.3	0.63	43.6	44.9	-1.38
33	97.5	97.0	0.47	58.0	58.4	-0.43
34	94.9	95.3	-0.44	51.2	49.5	1.66
35	96.8	96.8	-0.05	51.2	55.6	-4.41
36	94.7	95.4	-0.71	52.3	52.3	-0.03
37	96.0	95.3	0.63	49.0	49.8	-0.88
38	94.0	93.0	0.97	44.0	42.8	1.32
39	97.4	96.8	0.51	61.5	59.6	1.90
40	95.8	95.8	-0.09	53.4	54.5	-1.17
41	97.6	97.6	-0.04	62.3	63.5	-1.24
42	95.2	95.6	-0.41	53.0	54.8	-1.81
43	94.0	93.5	0.41	47.0	45.0	1.92
44	96.3	96.0	0.21	51.2	54.0	-2.87
45	93.7	93.5	0.11	47.0	45.0	1.92
46	94	94.0	-0.06	49.0	48.2	0.80
47	96.3	96.2	0.03	49.3	51.3	-2.07
48	96.4	96.3	0.09	48.7	49.1	-0.44
49	96.8	96.8	-0.09	59.3	59.6	-0.30
50	97.2	97.1	0.04	60.0	60.6	-0.63
51	92.0	93.0	-1.03	42.0	42.8	-0.68
52	93.5	93.5	-0.08	44.0	43.2	0.74
53	97.2	96.8	0.38	57.0	60.5	-3.58
54	94.8	94.3	0.44	50.0	49.3	0.63



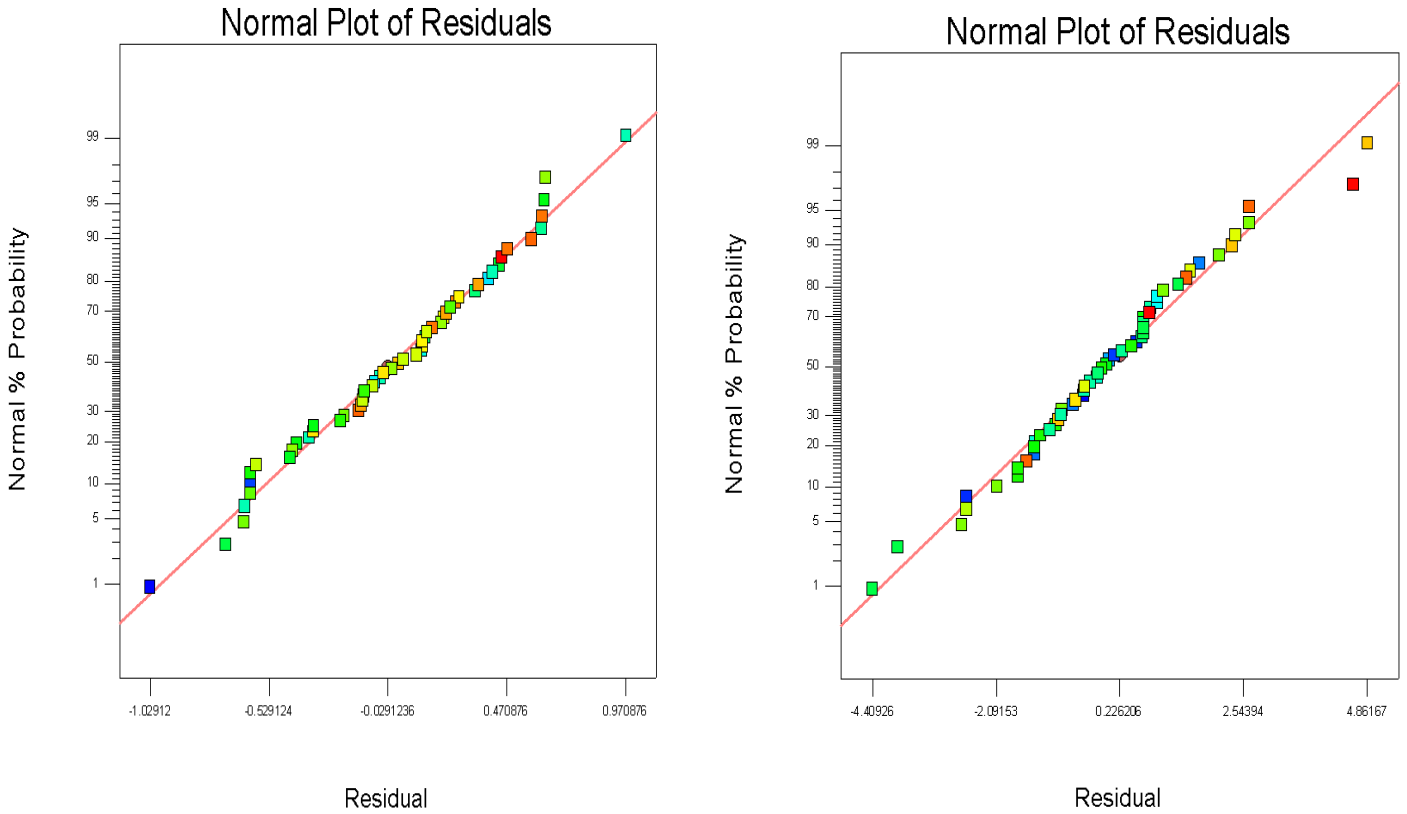


**Figure 6-1:** Normal plot of residuals for retention (left) and flux (right). Colouring is merely indicative of different data points

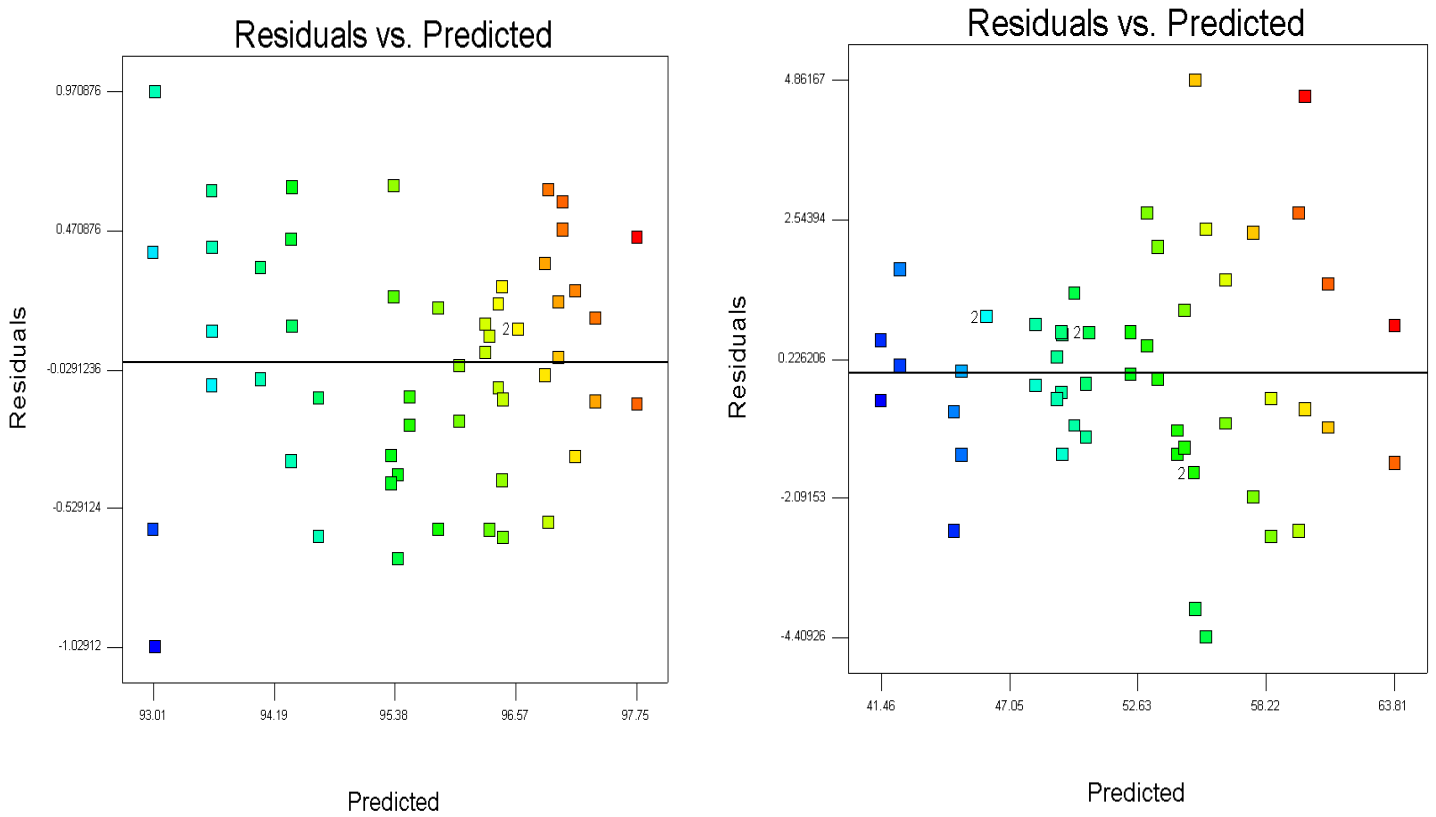
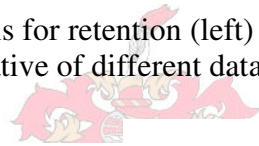


**Figure 6-2:** Plots of residuals versus predicted response values for retention (right) and flux (left). Colouring is merely indicative of different data points



### 6.3.3 Effect of factors and interactions on the performance of CA hollow-fine-fibre membranes

The 3D response surface plots described by the regression models and these graphs were drawn to illustrate the effect of the independent factors and the interaction effects on the response variables. These graphs in accordance to the regression model fitted, implying that the interaction between the two factors were significant. Figures 6-3 and 6-4 depict the effect of solvent/non-solvent and bore fluid ratio on both membrane retention and flux. The retention and flux which were obtained from earlier experiments support the finding from the analysis of variance which shows that solvent/non-solvent and bore fluid ratio are important factors that affect the membrane performance. The retention and flux plots show an improvement in salt retention and water flux as the solvent/non-solvent ratio in the solution was decreased from 1.447 to 1.147 (factor A) while decreasing the solvent concentration (factor c) in the bore fluid. The decrease in solvent/non-solvent ratio will result in a high formamide ratio in the spinning solution, which will shift the composition path of the spinning solution in the direction of the liquid-liquid demixing gap and as result a porous membrane will be produced. The decrease of acetone in the bore fluid from 70 to 60 and 50% (m/m) will improve the flux and retention of the produced hollow-fine fibres. High solvent concentration in the bore fluid and dope solution produced a very thick dense layer when the extruded fibres undergoes rapid phase separation from both sides. The formation of an impermeable skin is due to the high gelation of super saturated top layer of the spinning solution. Lowering the solvent concentration by increasing the non-solvent content in both bore fluid and the spinning solution will slow down and control the two different processes of gelation and the phase separation process and hence more porous hollow-fine fibres could be produced with improved flux and retention.

Figure 6-5 and 6-6 illustrate the interaction plot between solvent/non-solvent ratio and air gap distance on both retention and flux. It is clear that both flux and retention were increased with decreasing the solvent/non-solvent ratio and increasing the air-gap distance to 120 mm. It was discussed in (Section 2.8.2.5) that the air gap is responsible for the formation of a thin skin on the outside of the fibre and the bulk of membrane structure is formed in the coagulation bath. Then increasing the non-solvent content in the spinning solution with 12 cm air-gap distance will produce very thin skin layer with more pores in it. As the composition bath of the spinning solution will become close to the liquid-liquid demixing state with high non-solvent content and therefore spinodal outer layer should result in a

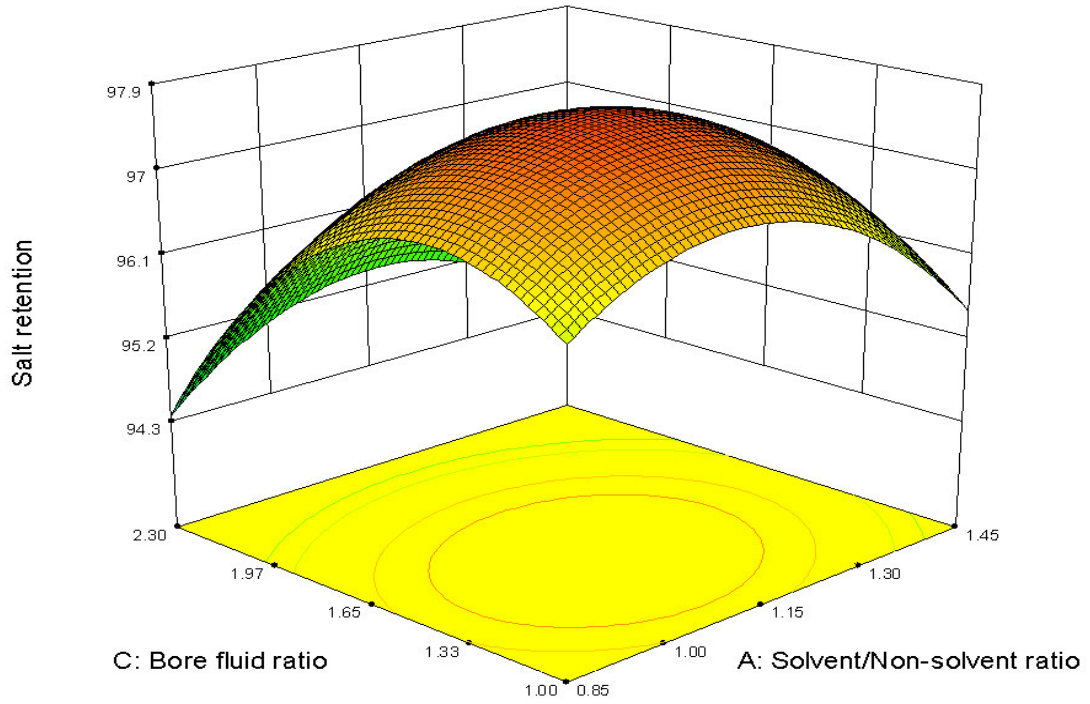


**Figure 6-3:** Effect of solvent/non-solvent and bore fluid ratio on salt retention.

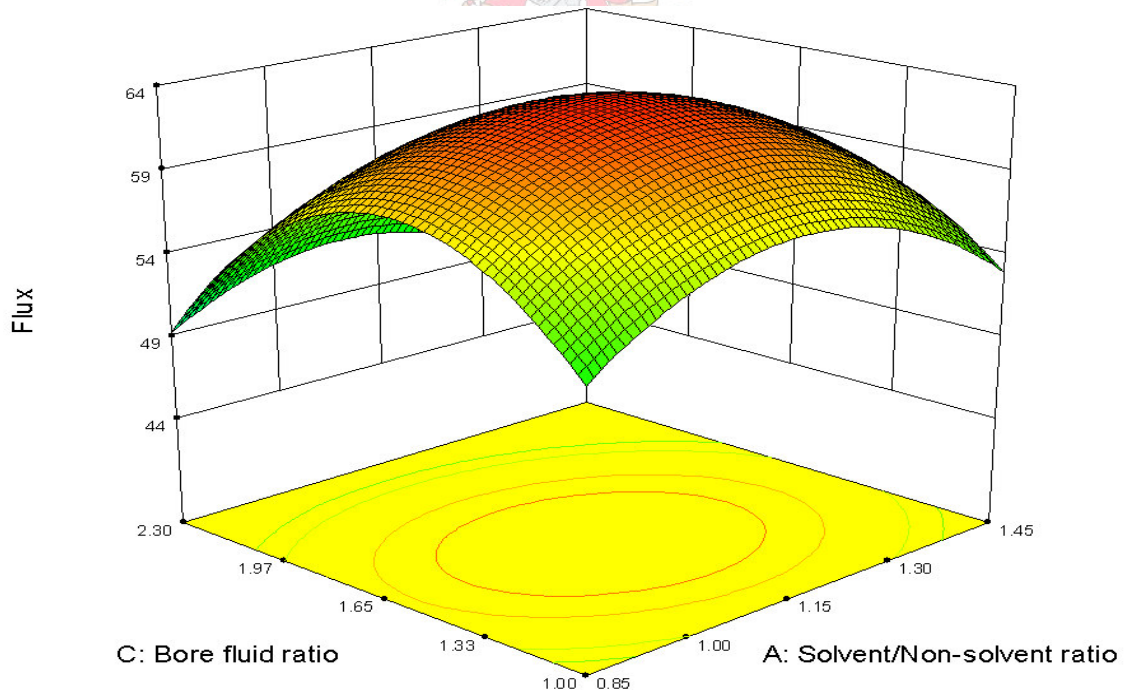


**Figure 6-4:** Effect of solvent/non-solvent and bore fluid ratio on water flux.

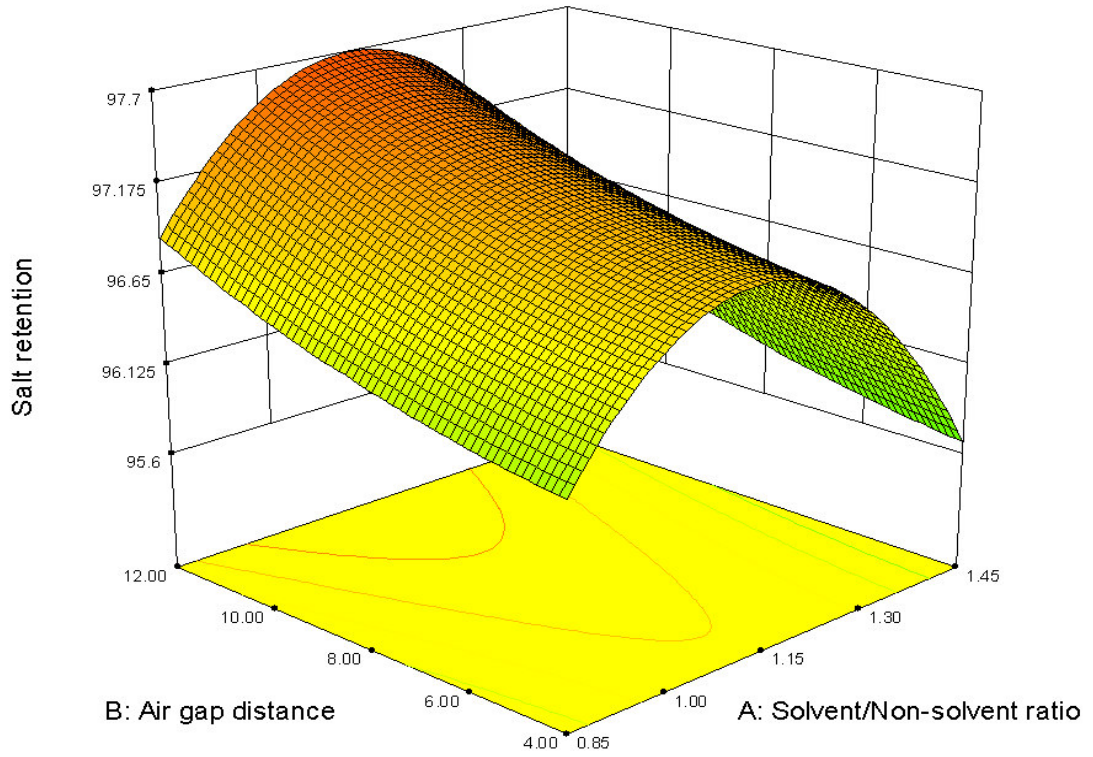


**Figure 6-5:** Response surface plot of the effects of solvent/non-solvent ratio and air gap distance on salt retention of CA hollow-fine-fibre membranes.

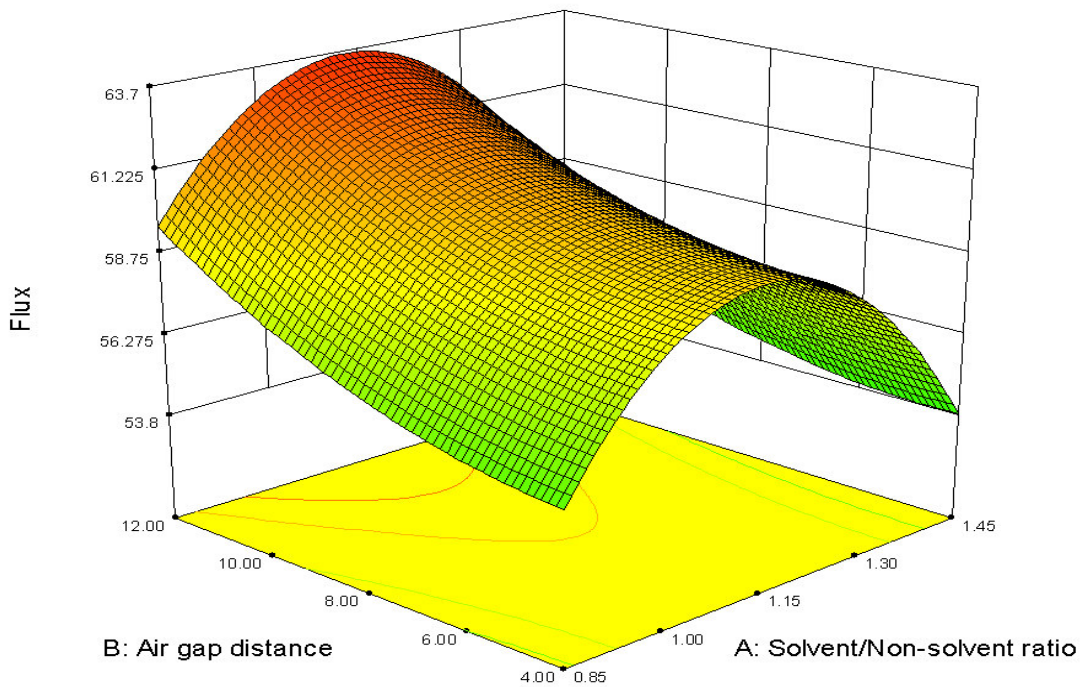


**Figure 6-6:** Response surface plot of the effects of solvent/non-solvent ratio and air gap distance on water flux of CA hollow-fine-fibre membranes.

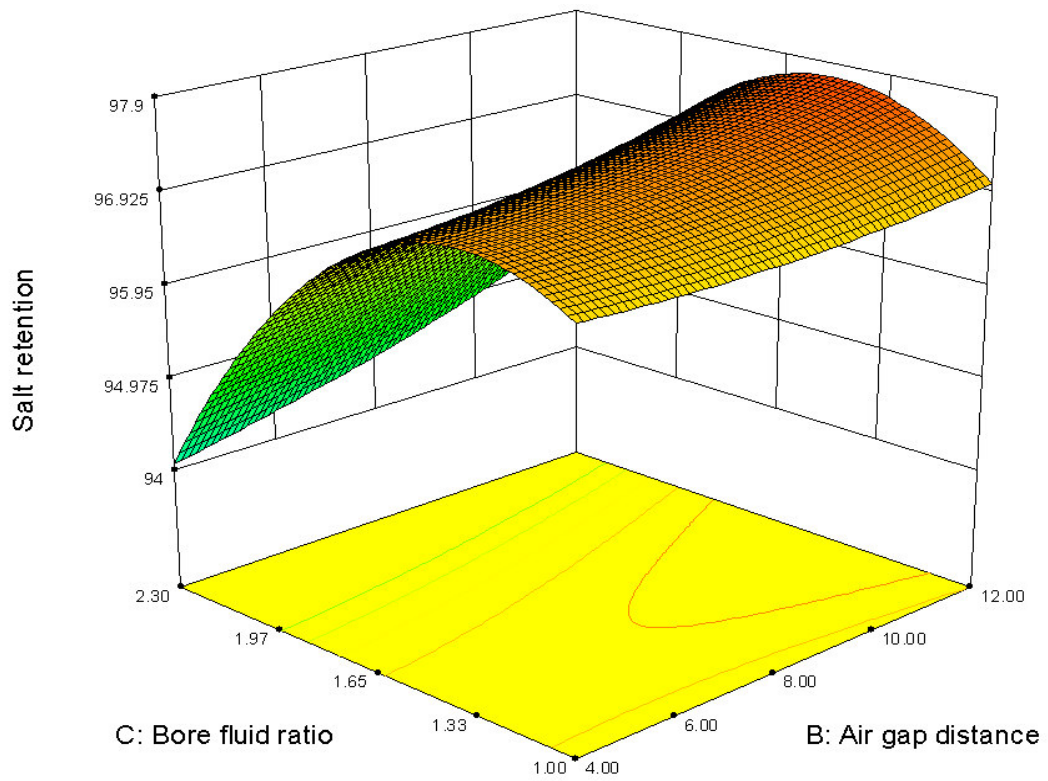


**Figure 6-7:** Response surface plot of the effects of air gap distance and bore fluid ratio on salt retention of CA hollow-fine-fibre membranes.

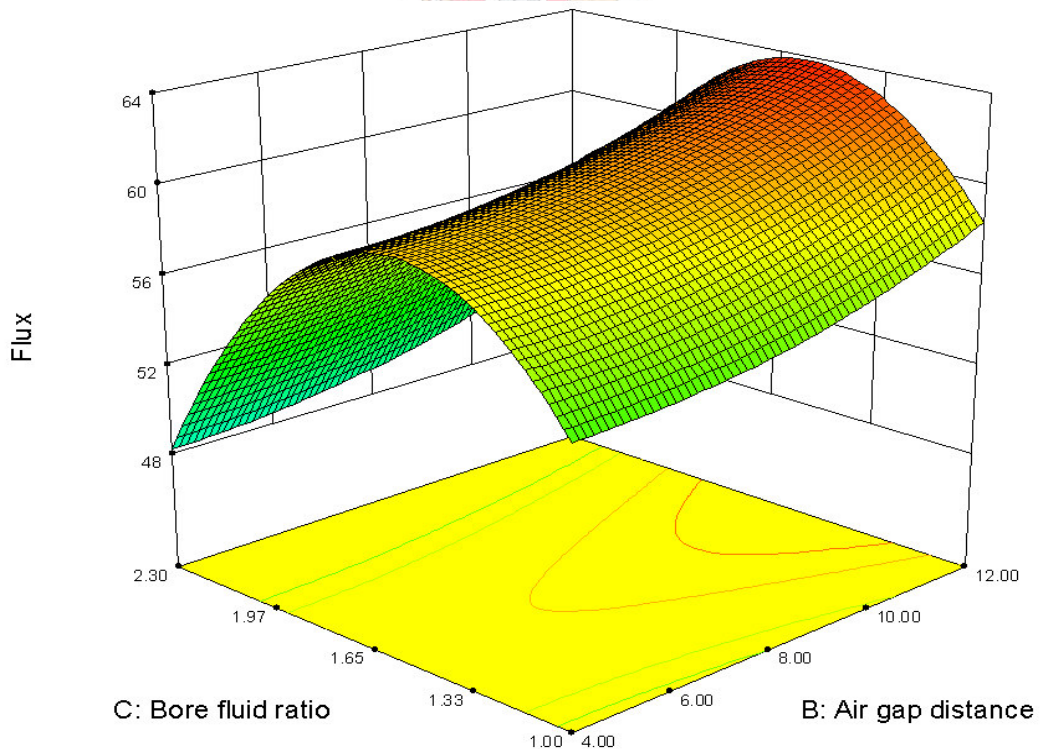


**Figure 6-8:** Response surface plot of the effects of air gap distance and bore fluid ratio on flux of CA hollow-fine-fibre membranes.



micro-porous skin layer. As explained previously in (Chapter 5), fibres spun with different air gap distances experience elongational stress with higher take-up speeds that induce molecular orientation and cause polymer molecules to pack more closely to one another. For a small air gap distance 4 cm, there was too little time for orientation and with a high take-up speed leading to a much tighter structure resulted. With an air gap of 12 cm the orientation will have small relaxation time before entering the gelation bath and leading to a less dense outer skin and subsequently high flux and retention.

Figure 6-7 and 6-8 illustrate the interaction plot between the air gap distances and bore fluid ratio on both retention and flux. It can be seen the bore fluid ratio had a large effect on flux. This can be explained that higher air gap distance results in enough time for the mass transfer at the inner surface, which means enough time for bore liquid/solvent exchange. As a result, an open porous structure will be formed on the inner surface leading to an increase in the flux.

#### 6.4 Model validation

In order to verify the adequacy of the model developed, three confirmation experiments were conducted within the range of the levels studied. Each of the experiments was repeated three times from different dope solutions and the average was taken for the retention and flux of each experiment. For each of confirmations, the responses were determined experimentally and calculated by using the regression equation. The results of these validation experiments and the model predicted values are shown in Table 6-6.

**Table 6-6:** Confirmation runs with their responses

Solvent/Non-solvent (m/m)	Air gap distance mm	Bore fluid ratio (m/m)	Retention %	Flux L/m <sup>2</sup> .d
1	60	1.2	97.92	60.14
1	60	1.2	97.68	62.36
1	60	1.2	97.43	59.52
1.147	80	1.5	98.04	60.14
1.147	80	1.5	97.80	64.59
1.147	80	1.5	98.17	62.36
1.302	100	1.8	97.56	55.68
1.302	100	1.8	97.07	55.68
1.302	100	1.8	96.82	57.91

Test conditions: (2 000 ppm NaCl and 20 bar)

The average values are shown in Table 6-7 for each set together with their predicted values calculated from the regression model. The results showed that our regression model yields

reasonable results for the flux and retention with small residual between predicted and actual data. Therefore our regression equation can be expected to apply in the preparation of CA hollow-fine-fibre membranes with better performance.

**Table 6-7:** Actual and predicted responses of retention and flux for the confirmation runs

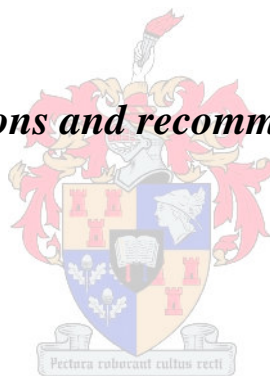
Solvent/Non-solvent ratio %(m/m)	Air gap distance m/m	Bore fluid ratio %(m/m)	Actual retention %	Predicted retention %	Residual	Actual flux L/m <sup>2</sup> .d	Predicted flux L/m <sup>2</sup> .d	Residual
1	6	1.2	97.68 ± 0.25	97.15	0.66	60.67 ± 1.49	57.23	3.44
1.147	8	1.5	98.00 ± 0.19	97.34	0.53	62.36 ± 2.23	60.92	1.44
1.302	10	1.8	97.15 ± 0.38	96.56	0.58	56.42 ± 1.29	57.95	-1.52

## 6.5 Conclusions

In this study, the ability of a factorial design to perform a comparative investigation of the importance of individual factors and their interactions on the membrane performance was demonstrated. It was concluded in this statistical analysis, that the solvent/non-solvent ratio, bore fluid ratio, air gap distance and the interaction between solvent/non-solvent and bore fluid, air gap distance, and bore fluid ratio had a significant influence on both the flux and retention of CA hollow-fine-fibre membranes for brackish water desalination. According to 3<sup>3</sup> factorial designs the regression analysis showed a goodness of fit to the experimental data. Therefore, the model was considered adequate for the prediction of good membrane performance (salt retention in the range of 96 – 98% and permeate flux in the range of 60 – 64 L/m<sup>2</sup>.d.

## *Chapter 7*

### *Conclusions and recommendations*

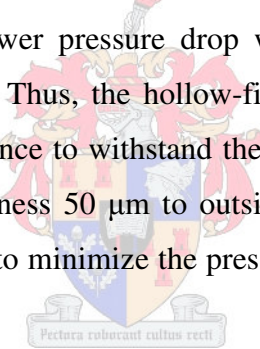


## 7.1 Conclusions

The main objective of this research was the development of a CA hollow-fine-fibre membrane for brackish water desalination with good performance from first principles. The influence of different variables pertaining to the fabrication process was studied and the overall conclusions of the research are as follows:

(a) Prediction of fibre dimensions by using collapse pressure and pressure drop calculations.

The relationships between the collapse pressure and pressure drop calculations were considered in order to determine an acceptable range of fibre dimensions capable to withstand brackish water operating conditions of 20 – 25 bar with smaller pressure drop. The collapse pressure calculations showed that outside diameters, mechanical properties and membrane wall thickness play an important role in determining the membrane operating pressures. A fibre dimensions in the range of 222 – 247  $\mu\text{m}$  showed good resistance against collapse of brackish water operating conditions. The hollow-fine fibres with range obtained above (222 – 247  $\mu\text{m}$ ) also showed a lower pressure drop within the brackish water operating conditions during the calculations. Thus, the hollow-fine-fibre membranes in the range of (222 – 247  $\mu\text{m}$ ) showed high resistance to withstand the brackish water operating conditions at relatively low ratio of wall thickness 50  $\mu\text{m}$  to outside diameter and thereby provide an advantageously large bore diameter to minimize the pressure drop to permeate passing within the bore.



(b) Effect of process parameters on the fibre morphology

The spinning parameters such as solvent/nonsolvent ratio, bore fluid ratio, dope extrusion rate, take-up speeds and heat treatment was studied in terms of their effect on the fibre morphology. The elimination of macrovoids from the morphology of hollow-fine-fibre membranes was achieved in two ways. Firstly, increasing the formamide ratio in the polymer solution and secondly, decreasing the water activity in the bore fluid by adding a solvent (acetone) to water.

The presence of solvent in the bore fluid decreased the water activity and produced hollow-fine-fibre membranes with a sponge-like structure that improved the membrane flux and retention performance. SEM images showed that the fibres consist of a very thin dense surface layer, followed by a fine porous sub-layer, with increasingly larger pore sizes as the distance from the outer interface increases.



An increase of dope extrusion rate induces a high shear stress inside the spinneret wall and subsequently increases the molecular orientation in skin layer of asymmetric hollow-fine-fibre membranes. This effect improved the retention of the membranes while leading to a slight reduction in flux. Both the inner and outer diameter of the hollow fibre decreased with increasing the take-up speeds resulting in a fibre dimensions within the required region for brackish water operating pressure. The mechanical strength of the fibres increased with increasing take-up speeds. This could be attributed to the higher orientation caused by higher take-up speeds. CA hollow-fine-fibre membrane showed good salt retention at an annealing temperature of 86 °C and annealing period of two subsequent times.

(c) Validation of determined fibre dimensions by using collapse pressure tests.

Different hollow-fine-fibre dimensions were spun by different take-up speeds in the range of the dimensions required for brackish water desalination. Collapse pressure tests were carried out to validate the fibre dimensions required for brackish water desalination. The spun fibre dimensions showed a reasonable agreement with the determined fibre dimensions. The produced hollow-fine fibres with inside to outside diameter of 135/ 225, 136/229, 138/237 and 142/246 µm showed collapse pressures beyond 24, 20, 20 and 18 bar respectively within a reasonable region of brackish water operating conditions.

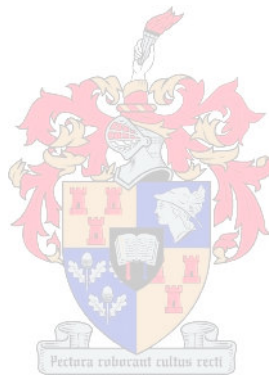
(d) Use of statistical analysis to generate fabrication formulation for producing hollow-fine-fibre membranes with good salt retention and flux.

A three-level three-factor factorial design was used to study the important process parameters and their interaction effects with respect to both permeability and selectivity. The most significant factors were solvent/non-solvent ratio, air gap distance, bore fluid ratio and interaction between solvent/non-solvent and bore fluid ratio. The 3<sup>3</sup> factorial design showed that CA hollow-fine-fibre membrane capable of brackish water desalination of good performance can be produced. The salt retention of these membranes ranged from 96 to 98 % and the permeate flux of 60 to 64 L/m<sup>2</sup>.d. A regression equation was also developed and can be used to predict the performance within the limit of the factors studied.

## 7.2 Recommendations for future work

1) Develop large working modules that contain thousands of hollow-fine-fibre membranes.

- 2) Use the newest technology in ultrafiltration and use the ultrafiltration water as feed for long term testing of these modules. Study wear, tear (breakage and collapse), performance (retention and flux) and fouling (pore and surface blocking) as a function of time.
- 3) Most important is the need to automate the membrane production to make it repeatable and computer controllable.
- 4) Search for more friendly solvent systems e.g. alcohol instead of formamide in the preparation of CA hollow-fine-fibre membranes.



## References

1. Baker, R. W., *Membrane Technology and Applications*, 2nd Ed, John Wiley & Sons, Chichester, 2004.
2. Lonsdale, H. K., *Desalination by Reverse Osmosis*, Merten, U. (Ed.), MIT Press, Cambridge, MA (1966).
3. Dresner, L. and Johanson, J. S., *Principles of Desalination*, Academic Press, New York, 1975.
4. Sourirajan, S., *Reverse osmosis: A new field of applied chemistry and chemical engineering*, American Chemical Society Symposium, 1981, 11-62.
5. Lonsdale, H. K., *Desalination by Reverse Osmosis*, Merten, U. (Ed.), MIT Press, Cambridge, MA, 1966.
6. Loeb, S. and Sourirajan, S., *New water desalting process developed at University of California*, University of California, Los Angeles, UCLA Report 60-60, 1960.
7. Riley, R. L., Merten, U. and Gardner, J. O., *Replication electron microscopy of cellulose acetate osmotic membranes*, *Desalination*, 1966, 1, 30-34.
8. Petersen, R. J. and Cadotte, J. E., *Thin Film Composite Reverse Osmosis Membranes*, *Handbook of Industrial Membrane Technology*, Porter, M. C. (Ed.), Noyes Publications, Park Ridge, 1990.
9. Riley, R. L., *Membrane Separation Systems*, Baker, R. W., Cussler, E. L., Eykamp, W., Koros, W. J., Riley, R. L. and Strathmann, H. (Ed.), Noyes Data Corporation, New Jersey, 1991.
10. Allanson, J. T., *Drinking Water from the Sea: Reverse Osmosis, the Modern Alternative*, Allanson, J. T. and Charnely, R. (Ed.), Institute of Marine Engineers, London, 1983.
11. Sammon, D. C., *Membrane process*, *Pure and Applied Chemistry*, 1974, 37, 423-436.
12. Loeb, S. and Sourirajan, S., *Sea water demineralization by means of osmotic membranes*, *Advances in Chemistry Series*, 1963, 38, 117-132.
13. Frith, C. F., *Electronic-Grade Water Production Using Reverse Osmosis Technology*, *Reverse Osmosis Technology: Applications for High-Purity Water Production*, Parekh, B. S. (Ed.), Marcel Dekker, New York, 1988.
14. Osada, Y. and Nakagawa, T., *Reverse Osmosis*, *Membrane Science and Technology*, Marcel Dekker, New York, 1992.
15. Reid, C. E. and Breton, E. J., *Water and ion flow across cellulosic membranes*, *Journal of Applied Polymer Science*, 1959, 1, 133-143.
16. Sourirajan, S., *Mechanism of demineralization of aqueous sodium chloride solutions by flow, under pressure, through porous membranes*, *Industrial and Engineering Chemistry Fundamentals* 1963, 2, 51-55.
17. Glueckauf, E., *The distribution of electrolytes between cellulose acetate membranes and aqueous solutions*, *Desalination*, 1976, 18, 155-172.
18. Lonsdale, H. K., Merten, U. and Riley, R. L., *Transport properties of cellulose acetate osmotic membranes*, *Journal of Applied Polymer Science*, 1965, 9, 1341-1362.
19. Banks, W. and Sharples, A., *Studies on desalination by reverse osmosis. III. Mechanism of solute rejection*, *Journal of Applied Chemistry*, 1966, 16, 153-158.
20. Amjad, Z., *Reverse Osmosis: Membrane Technology*, *Water Chemistry and Industrial Applications*, Amjad, Z. (Ed.), Kluwer Academic, New York, 1993.
21. Lacey, R. E. and Loeb, S., *Industrial Processing with Membranes*, Lacey, R. E. and Loeb, S. (Ed.), John Wiley & Sons, New York, 1972.
22. Cadotte, J. E. and Rozelle, L. T., *In-Situ-Formed Condensation Polymers for Reverse Osmosis Membranes*, NTIS Report No. PB-229337, 1972.

23. Lonsdale, H. K. and Podall, H. E., Reverse osmosis membrane research. Plenum Press, New York, 1972.
24. Loeb, S. and Sourirajan, S., High flow porous membranes for separating water from saline solutions, U.S. Patent 3,133,132, 1964.
25. Blais, P., Polyamide Membranes, In: Reverse Osmosis and Synthetic Membranes, Sourirajan, S. (Ed.), National Research Council of Canada, Ottawa, 1977.
26. Richter, J. W. and Hoehn, H. H., Selective aromatic nitrogen-containing polymeric membranes, U.S. Patent 3,567,632, 1971.
27. Orofino, T. A., Development of hollow filament technology for reverse osmosis desalination systems, Office of Saline Water and Development, Progress Report No. 549, 1970.
28. Kesting, R. E., Phase Inversion Membranes, In: Synthetic Polymeric Membranes, John Wiley & Sons, New York, 1985.
29. Zeman, L. and Fraser, T., Formation of air-cast cellulose acetate membranes. Part I. Study of macrovoid formation, Journal of Membrane Science, 1993, 84, 93-106.
30. Kesting, R. E., Concerning the microstructure of dry-RO membranes, Journal of Applied Polymer Science, 1973, 17, 1771-1784.
31. Strathmann, H., Production of Microporous Media by Phase Inversion Process, In: Material Science of Synthetic Membranes, Lloyd, D. R. (Ed.), American Chemical Society, Washington D.C, 1985.
32. Lau, W. W., Guiver, M. D. and Matsuura, T., Phase separation in carboxylated polysulfone/solvent/water systems, Journal of Applied Polymer Science, 1991, 42, 3215-3221.
33. Castro, A. J., Method for making microporous products, U.S. Patent 4,247,498, 1980.
34. Riley, R. L., Lonsdale, H. K. and LaGrange, L. D., Development of ultrathin membranes, Office of Saline Water Research and Development, Progress Report No 386, 1969.
35. Hilderbrand, J. and R. Scott, R., Solubility of Non-Electrolytes, 3rd Ed, Reinhold, New York, 1949.
36. Rabek, J. F., Experimental Methods in Polymer Chemistry, 1st Ed, John Wiley & Sons, Chichester, 1980.
37. Hansen, C. M., The universality of the solubility parameter, Industrial and Engineering Chemistry Product Research and Development 1969, 8, 2-11.
38. Hansen, C. M. and Skaarup, K., The three dimensional solubility parameter, Journal of Coatings Technology, 1967, 39, 505-510.
39. Ott, E. and Spurlin, H., Cellulose and Cellulose Derivatives, Part II, Interscience, New York, 1954.
40. Hansen, C. M. and Beerbower, A., Solubility Parameters, In Kirk-Othmer Encyclopedia of Chemical Technology Supplementary volume, 2nd Ed, Standen, A, Interscience, New York, 1971.
41. Anderson, J. E. and Ullman, R., Mathematical analysis of factors influencing the skin thickness of asymmetric reverse osmosis membranes, Journal of Applied Physics, 1973, 44, 4303-4311.
42. Krantz, W. B., Ray, R. J., Sani, R. L. and Gleason, K. J., Theoretical study of the transport processes occurring during the evaporation step in asymmetric membrane casting, Journal of Membrane Science, 1986, 29, 11-36.
43. Cohen, C., Tanny, G. B. and Prager, S., Diffusion-controlled formation of porous structures in ternary polymer systems, Journal of Polymer Science: Polymer Physics Edition, 1979, 17, 477-489.
44. Reuvers, A. J., van den Berg, J. W. A. and Smolders, C. A., Formation of membranes by means of immersion precipitation, Part I. A model to describe mass transfer during immersion precipitation, Journal of Membrane Science, 1987, 34, 45-65.

45. Binder, K., Spinodal Decomposition, In: *Materials Science and Technology: A Comprehensive Treatment*, Haasen, P. (Ed.), VCH, New York, 1991.
46. Cahn, J. W., Spinodal decomposition, *Transactions of the Metallurgical Society of AIME*, 1968, 242, 166-180.
47. van de Witte, P., Dijkstra, P. J., van den Berg, J. W. A. and Feijen, J., Review, phase separation processes in polymer solutions in relation to membrane formation, *Journal of Membrane Science*, 1996, 117, 1-31.
48. Mulder, M., *Basic Principles of Membrane Technology*, Kluwer Academic Publishers, The Netherlands, 1996.
49. Bokhorst, H., Altena, F. W. and Smolder, C. A., Formation of asymmetric cellulose acetate membranes, *Desalination*, 1981, 38, 349-360.
50. Mulder, M. H. V., Oude Hendrikman, J., Wijmans, J. C. and Smolder, C. A., A rationale for the formation of asymmetric pervaporation membranes, *Journal of Applied Polymer Science* 1985, 30, 2805-2820.
51. Guenet, J. M., *Thermoreversible Gelation of Polymers and Bpolymers*, Academic Press, London, 1992.
52. Miles, M. J., *Gelation, Developments in Crystalline Polymers-2*, Bassett, D. C. (Ed.), Elsevier Applied Science, New York, 1988.
53. Brones, L., Altena, F. W., Smolder, C. A. and Koenhen, D. M., Asymmetric membrane structure as a result of phase separation, *Desalination*, 1980, 32, 33-45.
54. Altena, F. W. and Smolders, C. A., Phase separation phenomena in solutions of cellulose acetate, I. Differential scanning calorimetry of cellulose acetate in mixtures of dioxane and water, *Journal of Polymer Science: Polymer Symposium*, 1981, 69, 1-10.
55. Binder, K., Spinodal decomposition, In: *Materials science and technology: A comprehensive treatment*, Haasen, P. (Ed.), VCH, New York, 1991.
56. Kamide, K., Iijima, H. and Matsuda, S., Thermodynamics of formation of porous polymeric membrane by phase separation method I. Nucleation and growth of nuclei, *Polymer Journal*, 1993, 1113-1131.
57. James, P. F., Liquid-phase separation in glass-forming systems, *Journal of Materials Science*, 1975, 10, 1802-1825.
58. Cahn, J. W. and Charles, R. J., The initial stages of phase separation in glasses, *Physics and Chemistry of Glasses*, 1965, 6, 181-191.
59. Reuvers, A. J. Membrane formation. Diffusion induced demixing processes in ternary systems. Ph.D. dissertation, University of Twente, The Netherlands, 1987.
60. Reuvers, A. J. and Smolders, C. A., Formation of membranes by means of immersion precipitation. Part II. The mechanism of formation prepared from the system cellulose acetate-acetone-water, *Journal of Membrane Science*, 1987, 34, 67-86.
61. Mahon, H. I., Permeability separatory apparatus, permeability separatory membrane element, method of making the same and process utilizing the same, U.S. Patent 3,228,876, 1966.
62. Mahon, H. I., Permeability separator and process using hollow fibre, U.S. Patent 3,228,877, 1966.
63. Ho, W. S. W., Recent developments and applications for hollow fibre membranes, *Journal of the Chinese Institute of Chemical Engineers*, 2003, 34, 75-89.
64. Gabelman, A. and Hwang, S. T., Hollow fibre membrane contactors, *Journal of Membrane Science*, 1999, 159, 61-106.
65. Dance, E. L., Davis, T. E., Mahon, H. I., McLain, E. A. and Skiens, W. E., Development of Cellulose Triacetate Hollow Fibre Reverse Osmosis Modules for Brackish Water Desalination, Research and Development Report for Contract DI-14-01-0001-2248 to Dow Chemical Co, 1971.
66. Ziabiciki, A., *Fundamentals of Fibre Formation*, John Wiley & Sons, New York, 1976.



67. Mohamed, S. and William, N. G., An experimental study of the complete-mixing model for radial flow hollow fibre reverse osmosis systems, *Desalination*, 1984, 49, 57-88.
68. Mahon, H. I. and Lipps, B. J., *Hollow Fibre Membranes*, In: *Encyclopedia of Polymer Science and Engineering*, John Wiley & Sons, New York, 1971.
69. Cabasso, I., *Membranes*, *Encyclopedia of Polymer Science and Engineering* Kroschwitz, J. I. (Ed.), John Wiley & Sons, New York, 1987.
70. Li, S. G., Koops, G. H., Mulder, M. H. V., Vandenboomgaard, T. and Smolder, C. A., Wet spinning of integrally skinned hollow-fibre membranes by a modified dual-bath coagulation method using a triple orifice spinneret, *Journal of Membrane Science*, 1994, 94, 329-340.
71. Antonson, C. R., Gardner, R. J., King, C. F. and Ko, D. Y., Analysis of gas separation by permeation in hollow fibres, *Industrial & Engineering Chemistry Process Research and Development*, 1977, 16, 463-469.
72. Jae-Jin, K., Jeong, R. H., Un, Y. K. and Sung, S. K., Operation parameters of melt spinning of polypropylene hollow fibre membranes, *Journal of Membrane Science*, 1995, 25-36.
73. Baum, B., Holley, W. and White, R. A., *Hollow Fibres in Reverse Osmosis, Dialysis, and Ultrafiltration*, In: *Membrane Separation Process*, Meares, P. (Ed.), Elsevier, Amsterdam, 1976.
74. Kesting, R. E., Process for spinning dry-fibre cellulose acetate hollow fibre membranes, U. S. Patent 4,035,459, 1977.
75. Strathmann, H., *Handbook of Industrial Membrane Technology*, In: *Synthetic Membranes and their Preparation*, Porter, M. C. (Ed.), Noyes Publications, New Jersey, 1990.
76. Mustaffar, M. I., Ismail, A. F. and Illias, R. M., Study on the effect of polymer concentration on hollow fibre ultrafiltration membrane performance and morphology, In: *Regional Symposium on Membrane Science and Technology*, Malaysia, 2004.
77. Sourirajan, S. and Govindon, T. S., Proceedings of the first international symposium on water desalination, Office of Saline Water, Washington, D.C., 1965,1, 251-274.
78. Manjikian, S., Loeb, S. and McCutchan, J. W., Proceedings of the first International Symposium on Water Desalination, Office of Saline Water, Washington, DC, 1965, 159-173.
79. Hans, H. G., Statistical design of experiments for optimizing the casting variables for cellulose acetate membranes, *Reverse Osmosis and Synthetic Membranes*, National Research Council Canada, Ottawa, 1977, 111-128.
80. Ji, H. H., Haiping, D., PuChen, Y. and Zhen, W., Spinning of the cellulose acetate hollow fibre by dry-wet technique of 3C-shaped spinneret, *Journal of Applied Polymer Science*, 1996, 62, 129-133.
81. Mckinney, R., An experimental approach to the preparation of hollow fibre membranes, *Desalination*, 1987, 62, 37-47.
82. Idris, A., Ismail, A. F., Gordeyev, S. A. and Shilton, S. J., Rheology assessment of cellulose acetate spinning solution and its influence on reverse osmosis hollow fibre membrane performance, *Polymer Testing*, 2003, 22, 319-325.
83. So, M. T., Eirich, F. R., Strathmann, H. and Baker, R. W., Preparation of asymmetric Loeb-Sourirajan membranes, *Journal of Polymer Science, Part C: Polymer Letters*, 1973, 11, 201.
84. So, M. T., Eirich, F. R., Strathmann, H. and Baker, R. W., Preparation of anisotropic Loeb-Sourirajan Membranes, *Polymer letters*, 1973, 201-205.
85. Kesting, R. E., *Synthetic Polymeric Membranes: A Structural Perspective*, Wiley-Interscience, New York, 1985.
86. Pinnau, I., Wind, J. and Peineman, K. V., Ultrathin multicomponent poly(ether sulfone) membrane for gas separation made by dry/wet phase inversion, *Industrial and Engineering Chemistry Research*, 1990, 29, 2028-2032.

87. Manjikian, S., Desalination membranes from organic casting solutions, *Industrial and Engineering Chemistry Product Research and Development*, 1967, 6, 23-32.
88. Jacobs, E. P., Statistical and numerical techniques in the optimization of membrane fabrication variables, PhD Thesis, University of Stellenbosch, South Africa, 1988.
89. Qin, J. J., Wang, R. and Chung, T. S., Investigation of shear stress effect within a spinneret on flux, separation and thermomechanical properties of hollow fibre ultrafiltration membranes, *Journal of Membrane Science*, 2000, 175, 197-213.
90. Pesek, S. C. and Koros, W. J., Aqueous quenched asymmetric polysulfone hollow fibres prepared by dry/wet phase separation, *Journal of Membrane Science*, 1994, 88, 1-19.
91. Shieh, J. J. and Chung, T. S., Effect of liquid-liquid demixing on the membrane morphology, gas permeation, thermal and mechanical properties of cellulose acetate hollow fibres, *Journal of Membrane Science*, 1998, 140, 67-79.
92. Qin, J. J., Li, Y., Lee, L. S. and Lee, H., Cellulose acetate hollow fibre ultrafiltration membranes made from CA/PVP 360 K/NMP/water, *Journal of Membrane Science*, 2003, 218, 173-183.
93. Pinnau, I. and Koros, W. J., Defect free ultra high flux asymmetric membranes, U.S. patent 4,902,422, 1990.
94. Pesek, S. C. and Koros, W. J., Aqueous quenched asymmetric polysulphone membranes prepared by dry/wet phase separation, *Journal of Membrane Science*, 1993, 81, 71-88.
95. Pinnau, I., Wind, J. and Pieneman, K. V., Ultrathin multicomponent polyethersulphone membranes for gas separation made by dry/wet phase inversion, *Industrial and Engineering Chemistry Research*, 1990, 29, 2028-2032.
96. Chung, T. S. and Xu, Z. L., Effect of air-gap distance on the morphology and thermal properties of polyethersulfone hollow fibres, *Journal of Applied Polymer Science*, 1997, 66, 1067-1077.
97. Aptel, P., Abidine, N., Ivaldi, F. and Lafaille, J. P., Polysulphone hollow fibres-effect of spinning conditions on ultrafiltration properties, *Journal of Membrane Science*, 1985, 22, 199-215.
98. Liu, T., Zhang, D., Xu, S. and Sourirajan, S., Solution-spin hollow fibre polysulfone and polyethersulfone ultrafiltration membranes, *Separation Science and Technology* 1992, 27, 161-172.
99. Wang, D., Li, K. and Teo, W. K., Preparation and characterization of polyetherimide asymmetric hollow fibre membranes for gas separation, *Journal of Membrane Science*, 1998, 138, 193-201.
100. Chung, T. S., Xu, Z. L. and Lin, W. H., Fundamental understanding of the effect of air-gap distance on the fabrication of hollow fibre membranes, *Separation and Purification Technology*, 1999, 72, 379-395.
101. Ismail, A. F., Dunkin, I. R., Gallivan, S. L. and Shilton, S. J., Production of super selective polysulfone hollow fibre membranes for gas separation, *Polymer*, 1999, 40, 6499-6506.
102. Chau, J. L., Wang, S. S. and Guo, C. L., Pilot production of polysulfone hollow fibre for ultra-filtration using orthogonal array experimentation, *Industrial and Engineering Chemistry Research*, 1995, 34, 803-919.
103. Ismail, A. F., Mustaffar, M. I., Illias, R. M. and Abdullah, M. S., Effect of dope extrusion rate on morphology and performance of hollow fibres membrane for ultrafiltration, *Separation and Purification Technology*, 2006, 49, 10-19.
104. Idris, A., Noordin, M. Y., Ismail, A. F. and Shilton, S. J., Study of shear rate influence on the performance of cellulose acetate reverse osmosis hollow fibre membranes, *Journal of Membrane Science*, 2002, 202, 205-215.
105. Shilton, S. J., Bell, G. and Ferguson, J., The rheology of fibre spinning and the properties of hollow fibre membranes for gas separation, *Polymer*, 1994, 35, 5327-5334.

106. Qin, J. and Chung, T. S., Effect of dope flow rate on the morphology, separation performance, thermal and mechanical properties of ultrafiltration hollow fibre membranes, *Journal of Membrane Science*, 1999, 157, 35-51.
107. Ekiner, O. M. and Vassilatos, G., Polymeric membranes, U.S. Patent 5,102,600, 1992.
108. Chou, W.-L. and Yang, M.-C., Effect of take-up speed on physical properties and permeation performance of cellulose acetate hollow fibres, *Journal of Membrane Science*, 2005, 250, 259-267.
109. Gittens, G. J., Hitchcock, P. A., Sammon, D. C. and Wakley, G. E., The structure of cellulose acetate membranes for reverse osmosis. Part I. Membranes prepared from a dioxane based dope, *Desalination* 1970, 8, 369-391.
110. Nguyen, T. D., Chan, K., Matsuura, T. and Sourirajan, S., Effect of shrinkage on pore size and pore size distribution of different cellulose reverse osmosis membranes, *Industrial & Engineering Chemistry, Product Research and Development*, 1984, 23, 501-508.
111. Lacey, R. E. and Loeb, S., *Industrial Processing with Membranes*, Lacey, R. E. and Loeb, S. (Ed.), John Wiley & Sons, New York, 1972.
112. Doshi, M. R., Gill, W. N. and Kabadi, V. N., Optimal design of hollow fibre modules, *American Institute of Chemical Engineers Journal*, 1977, 765-768.
113. Case, J., *The Strength of Materials: A Treatise on the Theory of Stress Calculations for Engineers*, Edward Arnold London, 1983.
114. Hanbury, W. T. and Yuceer, A., Constriction of B10 hollow fibre diameters under operating conditions, *Desalination*, 1985, 54, 27-44.
115. De Nevers, N., *Fluid mechanics for chemical engineers*, 3rd Ed, McGraw-Hill, New York, 2005.
116. Hermans, J. J., Hydrodynamics of hollow fibre reverse osmosis modules, *Membrane Digest*, 1978, 1, 45.
117. Hermans, J. J., Physical aspects governing the design of hollow fibre modules, *Desalination*, 1972, 26, 45-62.
118. Chen, C. and Petty, C. A., Flow characteristics of semipermeable hollow fibres undergoing reverse osmosis, *Desalination*, 1973, 12, 281-293.
119. Evangelista, F. and Jonsson, G., Explicit design of hollow fibre reverse osmosis systems, *Proceedings of the 1990 International Congress on Membranes and Membrane Processes*, Chicago, USA, 1990.
120. Sekino, M., Precise analytical model of hollow fibre reverse osmosis modules, *Journal of Membrane Science*, 1993, 85, 241-252.
121. Ohya, H., Nakajima, H., Tagaki, K., Kagawa, S. and Negishi, Y., An analysis of reverse osmotic characteristics of B9 hollow fibre module, *Desalination*, 1977, 21, 257-274.
122. Strove, V. M., Smart, J. and Lioyd, D. R., Performance Optimization of Hollow Fibre Reverse Osmosis Membranes. Part I. Development of Theory, *Journal of Membrane Science*, 1995, 103, 257-270.
123. Smart, J., Starov, V. M. and Lioyd, D. R., Performance optimization of hollow fibre reverse osmosis membranes. Part II. Comparative study of flow configurations, *Journal of Membrane Science*, 1996, 119, 117-128.
124. Chanda, M. and Salil, K. R., *Plastics technology handbook*. 3rd ed.; Marcel Dekker, New York, 1998.
125. Gercek, H., Poisson's ratio values for rocks, *International Journal of Rock Mechanics and Mining Sciences* 2007, 44, 1-13.
126. Fischer, F., Rigacci, A., Pirard, R., Berthon-Fabry, S. and Achard, P., Cellulose-based aerogels, *Polymer* 2006, 47, 7636-7645.
127. Chunxiu, L. and Renbi, B., Preparation of chitosan/cellulose acetate blend hollow fibres for adsorptive performance, *Journal of Membrane Science*, 2005, 267, 68-77.
128. William, N. G. and Bansal, B., Hollow fibre reverse osmosis systems analysis and design, *AIChE Journal*, 1973, 19, 823-831.



129. Porter, M. C., Concentration polarization with membrane ultrafiltration, *Industrial and Engineering Chemistry Product Research and Development* 1972, 11, 234-248.
130. Nader, M. A. and Abderrahim, A., Modeling an industrial reverse osmosis unit, *Desalination*, 1999, 126, 33-93.
131. Kimura, S. and Sourirajan, S., Analysis of data in reverse osmosis with porous cellulose acetate membranes used, *American Institute of Chemical Engineers Journal*, 1976, 13, 497-503.
132. Malm, C. J., Tanghe, L. J. and Laird, B. C., Preparation of cellulose acetate- Action of sulfuric acid, *Industrial & Engineering Chemistry*, 1946, 38, 77-82.
133. Frommer, M. A. and Lancet, D., Reverse osmosis membrane research, Lonsdale, H. and Podall, H. E. (Ed.), Plenum Press, 1972.
134. Smolders, C. A., Reuvers, A. J., Boom, R. M. and Wienk, I. M., Microstructures in phase-inversion membranes. Part 1. Formation of macrovoids, *Journal of Membrane Science*, 1992, 73, 259-275.
135. Frommer, M. A. and Messalem, R. M., Mechanism of membrane formation. VI. Convective flows and large void formation during membrane precipitation, *Industrial and Engineering Chemistry Product research and development*, 1973, 12, 328-333.
136. Idris, A., Ismail, A. F., Noordin, M. Y. and Shilton, J. S., Optimization of cellulose acetate hollow fibre reverse osmosis membrane production using Taguchi method, *Journal of Membrane Science*, 2002, 223-237.
137. Wang, D., Li, K. and Teo, W. K., Highly permeable polyethersulfone hollow fibre gas separation membranes prepared using water as non-solvent additive, *Journal of Membrane Science*, 2000, 176, 147-158.
138. Montgomery, D. C., *Design and Analysis of Experiment*, John Wiley & Sons, New York, 1997.
139. Fisher, F., *The Design of Experiments*, Hafner, New York, 1971.
140. Thomas, P. R., *Modern Engineering Statistics*, John Wiley & Sons, New Jersey, 2007.
141. Khuri, A. I. and J.A. Cornell, J. A., *Response Surfaces: Design and Analyses*, Marcel Dekker Inc, New York, 1987.
142. Beg, Q., Sahai, V. and Gupta, R., Statistical media optimization and alkaline protease production from *Bacillus mojavensis* in bioreactor, *Process Biochemistry*, 2003, 39, 203-209.

**Appendix A: Solubility parameters of solvents with reference to Figure 2-6**

Number	Name	$\delta_d$	$\delta_p$	$\delta_h$
13	Cyclohexane	8.2	0	0.1
16	Toluene	8.8	0.7	1.0
24	Methylene Chloride	8.9	3.1	3.0
27.1	1,1-dichloroethylene	8.3	3.3	3.2
28	Ethylene dichloride	9.3	3.6	2.0
29	Choloroform	8.7	1.5	2.8
29.1	1,1-dichloroethane	8.1	4.0	0.2
32	Trichloroethylene	8.8	1.5	2.6
36	Carbon tetrachloride	8.7	0	0.3
37	1, 1,1-trichloroethane	8.3	2.1	1.0
38	Tetrachloroethylene	9.3	3.2	1.4
39	Chlorobenzene	9.3	3.2	1.4
39.2	1,1,2,2-tetrachloroethane	9.2	2.5	4.6
51.2	Tetrahydrofuran	8.2	2.8	3.9
51.3	1,4-dioxane	9.3	0.9	3.6
52	Diethyl ether	7.1	1.4	2.5
53	Bis (2-chloroethyl) ether	9.2	4.4	2.8
55	Acetone	7.6	5.1	3.4
56	Methyl ethyl ketone	7.8	4.4	2.5
57	Cyclohexane	8.7	3.1	2.5
60	Methyl i-butyl ketone	7.5	3.0	2.0
66.2	Methyl acetate	7.6	3.5	3.7
69	Ethyl acetate	7.7	2.6	3.5
69.1	Trimethyl phosphate	8.2	7.8	5.0
75.1	Triethyl phosphate	8.2	5.6	4.5
76	Diethyl phthalate	8.6	4.7	2.2
77	Tricresyl phosphate	9.3	6.0	2.2
81	Acetonitrile	7.5	8.8	3.0
90	Pyridine	9.3	4.3	2.9
93	Aniline	9.5	2.5	5
98	Formamide	8.4	12.8	9.3
99	Dimethylformamide	8.5	6.7	5.5
99.1	Dimethylacetamide	8.2	5.6	5.0
99.3	Hexamethyl phosphramide	9.0	4.2	5.5
120	Methanol	7.4	6.0	10.9
122	1-propanol	7.7	4.3	9.5
127	Cyclohexanol	8.5	2.0	6.6
140	Formica acid	7.0	5.8	8.1
141	Acetic acid	7.1	3.9	6.6
148	Water	7.6	7.8	20.7
149	Ethylene glycol	8.3	5.4	12.7
150	Glycerol	8.5	5.9	14.3
150.1	Propylene glycol	8.2	4.6	11.4
152	Triethylene glycol	7.8	6.1	9.1
144	Phenol	8.8	2.9	7.3
101	DMSO	9.0	8.0	5.0
66	Ethylene carbonate	9.5	10.6	2.5

## Appendix B: FORTRAN Codes

```
pressure drop calculation

real Jv
Dimension Jv(100), Pp(100)

l=1
d1=0.00072
d0=0.000172
Dz=0.01
m=100

Pb=25e5
alfa=0.55
R=1000
u=0.000798
A=4.294e-10

S=3.14*d0*1

Pp(0)=101325

flux=1.03E-06

aJv1=flux/m

do j = 1, m
  Jv(j)=A*((Pb-Pp(j))-(alfa*A-B)*(Cb-Cp))/R
  F=0.0
  do i = 1, j
    F=F+Jv(i)
  end do
  F=aJv1*(m-j)
  Pp(j)=Pp(j-1)+128*u*Dz**2*d0*F/d1**4
  write(*,*) Pp(j)
end do

end
```



## Appendix C: Results of the tensile test

**UNIVERSITY OF STELLENBOSCH  
TEXTILE SCIENCE LABORATORY**

Operator name:

yarn tests sabs 2062 EUGENE NOV 2007

Sample Identification: TAWARI 1

Test Date: 04 August 2009

Test Method Number: 15

Interface Type: 4200/4300/4400

SAMPLE: 165

Ramp Rate: 20.0000 kN/min

OPERATOR:

Second Speed: 250.0000 mm/min

COMMENT:

Third Speed: 0.0000 mm/min

Sample Rate (pts/secs): 6.6670

Temperature: 20 C

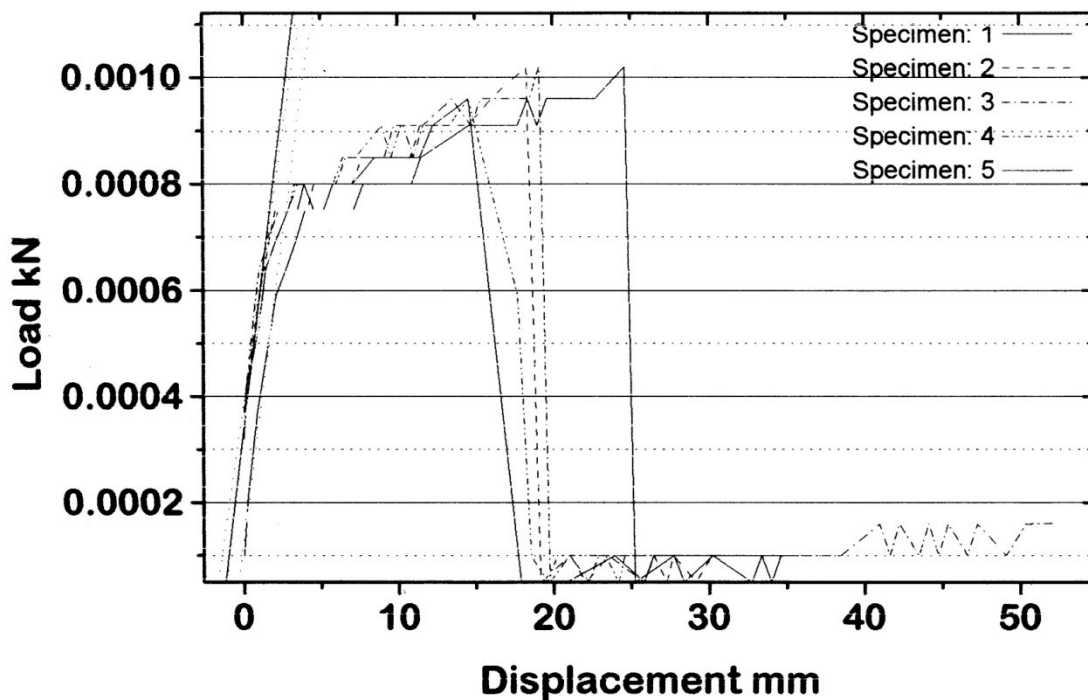
Humidity (%): 65

Dimension 4: 0.0000

Grip Distance: 120.0000 mm

	MAX LOAD (N)	Displment at Max. Load (mm)	Modulus (AutYoung) (MPa)	Slope (AutYoung) (N/mm)	Stress at Max. Load (MPa)	Strain at Max. Load (mm/mm)
1	1.020	24.500	505.395	0.224	19.212	0.204
2	1.020	18.430	557.543	0.247	19.212	0.154
3	1.020	19.230	453.621	0.201	19.212	0.160
4	1.020	17.190	542.562	0.240	19.212	0.143
5	0.960	17.180	416.443	0.184	18.082	0.143
Mean	1.008	19.306	495.113	0.219	18.986	0.161
S.D.	0.027	3.031	59.509	0.026	0.505	0.025
C.V.	2.662	15.700	12.019	12.019	2.662	15.700
Median	1.020	18.430	505.395	0.224	19.212	0.154
Mean +2.00 SD	1.062	25.368	614.130	0.272	19.996	0.211
Mean -2.00 SD	0.954	13.244	376.096	0.166	17.975	0.110
Minimum	0.960	17.180	416.443	0.184	18.082	0.143
Maximum	1.020	24.500	557.543	0.247	19.212	0.204

**Sample ID: TAWARI 1**



**UNIVERSITY OF STELLENBOSCH**  
**TEXTILE SCIENCE LABORATORY**

Operator name:

yarn tests sabs 2062 EUGENE NOV 2007

Sample Identification: TAWARI 2

Test Date: 04 August 2009

Test Method Number: 15

Interface Type: 4200/4300/4400

SAMPLE: 103

Ramp Rate: 20.0000 kN/min

OPERATOR:

Second Speed: 250.0000 mm/min

COMMENT:

Third Speed: 0.0000 mm/min

Sample Rate (pts/secs): 6.6670

Temperature: 20 C

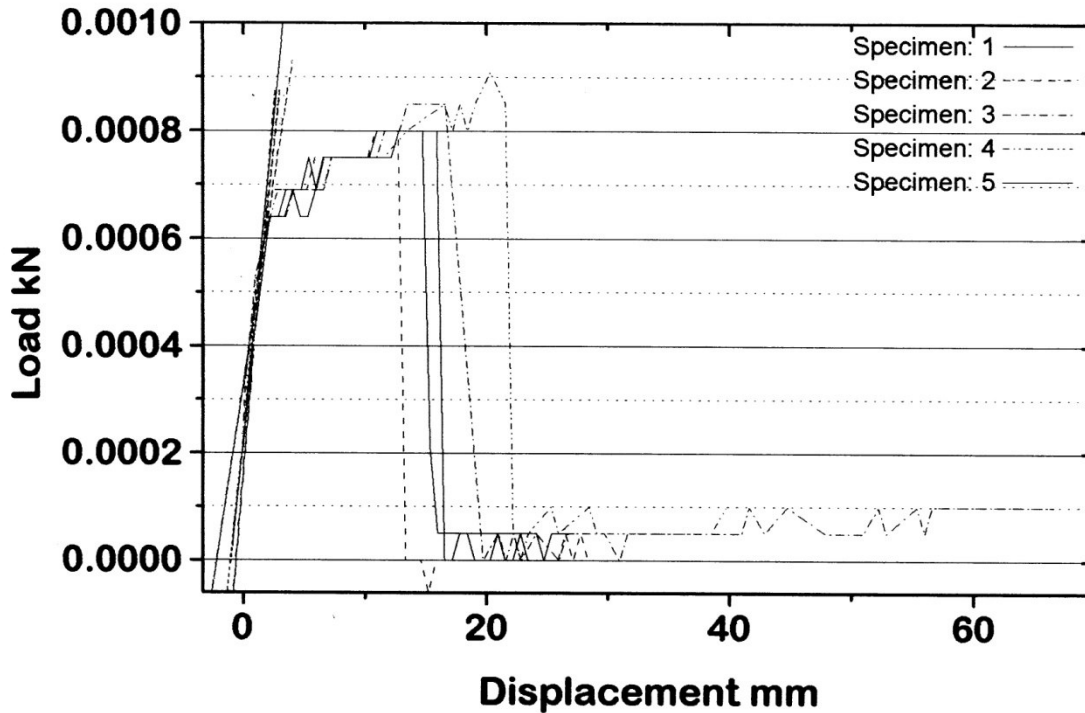
Humidity (%): 65

Dimension 4: 0.0000

Grip Distance: 120.0000 mm

	MAX LOAD (N)	displcmnt at Max.Load (mm)	Modulus (AutYoung) (MPa)	Slope (AutYoung) (N/mm)	Stress at Max.Load (MPa)	Strain at Max.Load (mm/mm)
1	0.800	15.850	490.202	0.217	15.068	0.132
2	0.800	12.910	615.821	0.272	15.068	0.108
3	0.910	18.820	336.675	0.149	17.140	0.157
4	0.910	21.290	518.200	0.229	17.140	0.177
5	0.850	15.100	501.553	0.222	16.010	0.126
Mean	0.854	16.794	492.490	0.218	16.085	0.140
S.D.	0.055	3.285	100.296	0.044	1.037	0.027
C.V.	6.446	19.561	20.365	20.365	6.446	19.561
Median	0.850	15.850	501.553	0.222	16.010	0.132
Mean +2.00 SD	0.964	23.364	693.082	0.307	18.159	0.195
Mean -2.00 SD	0.744	10.224	291.898	0.129	14.011	0.085
Minimum	0.800	12.910	336.675	0.149	15.068	0.108
Maximum	0.910	21.290	615.821	0.272	17.140	0.177

**Sample ID: TAWARI 2**





**UNIVERSITY OF STELLENBOSCH**  
**TEXTILE SCIENCE LABORATORY**

Operator name:

yarn tests sabs 2062 EUGENE NOV 2007

Sample Identification: TAWRI3

Test Date: 04 August 2009

Test Method Number: 15

Interface Type: 4200/4300/4400

SAMPLE: 101

Ramp Rate: 20.0000 kN/min

OPERATOR:

Second Speed: 250.0000 mm/min

COMMENT:

Third Speed: 0.0000 mm/min

Sample Rate (pts/secs): 6.6670

Temperature: 20 C

Humidity (%): 65

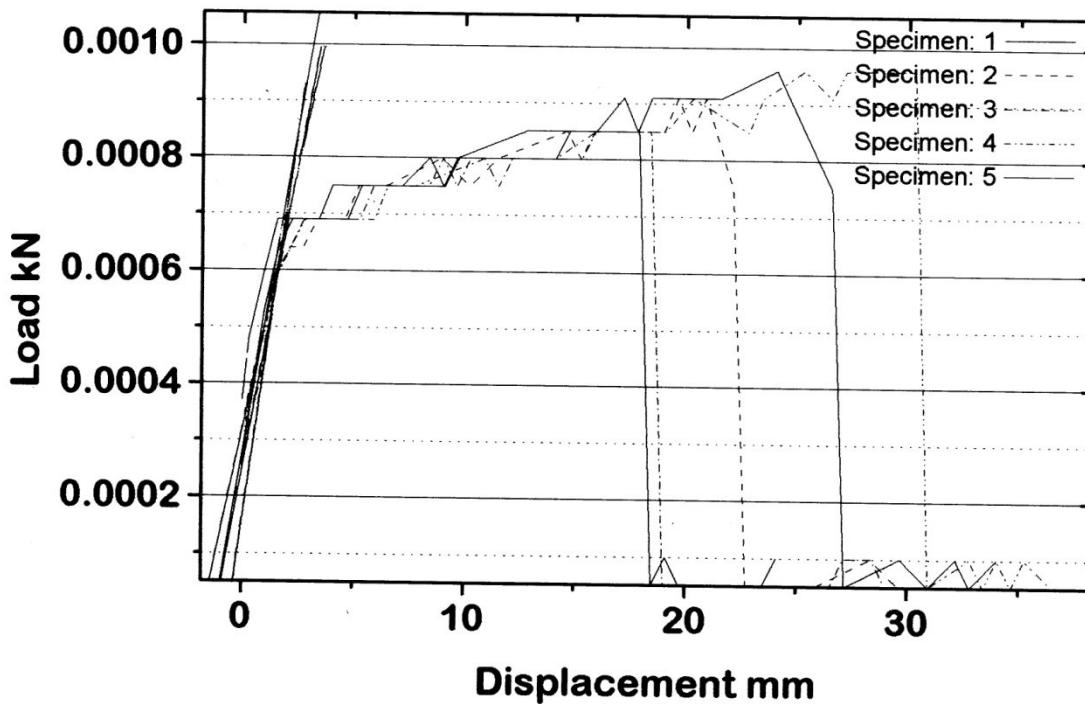
Dimension 4: 0.0000

Grip Distance: 120.0000 mm

	MAX LOAD (N)	Displcmnt at Max.Load (mm)	Modulus (AutYoung) (MPa)	Slope (AutYoung) (N/mm)	Stress at Max.Load (MPa)	Strain at Max.Load (mm/mm)
1	0.850	17.970	626.269	0.277	16.010	0.150
2	0.910	21.790	419.617	0.186	17.140	0.182
3	0.850	18.300	488.201	0.216	16.010	0.152
4	1.020	30.350	522.857	0.231	19.212	0.253
5	0.960	26.210	333.551	0.148	18.082	0.218
Mean	0.918	22.924	478.099	0.212	17.290	0.191
S.D.	0.073	5.319	109.970	0.049	1.380	0.044
C.V.	7.983	23.201	23.002	23.002	7.983	23.201
Median	0.910	21.790	488.201	0.216	17.140	0.182
Mean +2.00 SD	1.065	33.561	698.039	0.309	20.051	0.280
Mean -2.00 SD	0.771	12.287	258.158	0.114	14.530	0.102
Minimum	0.850	17.970	333.551	0.148	16.010	0.150
Maximum	1.020	30.350	626.269	0.277	19.212	0.253



**Sample ID: TAWRI3**





**UNIVERSITY OF STELLENBOSCH**  
**TEXTILE SCIENCE LABORATORY**

Operator name:  
Sample Identification: TAWRI4  
Test Method Number: 15

yarn tests sabs 2062 EUGENE NOV 2007

Test Date: 04 August 2009  
Interface Type: 4200/4300/4400  
Ramp Rate: 20.0000 kN/min  
Second Speed: 250.0000 mm/min  
Third Speed: 0.0000 mm/min  
Sample Rate (pts/secs): 6.6670  
Temperature: 20 C  
Humidity (%): 65  
Dimension 4: 0.0000  
Grip Distance: 120.0000 mm

SAMPLE: 170  
OPERATOR:  
COMMENT:

	MAX LOAD (N)	Displment at Max.Load (mm)	Modulus (Aut Young) (MPa)	Slope (Aut Young) (N/mm)	Stress at Max.Load (MPa)	Strain at Max.Load (mm/mm)
1	0.910	18.170	486.341	0.215	17.140	0.151
2	0.960	24.420	615.462	0.272	18.082	0.203
3	0.960	30.610	488.237	0.216	18.082	0.255
4	1.020	31.730	622.153	0.275	19.212	0.264
5	1.020	27.870	644.381	0.285	19.212	0.232
Mean	0.974	26.560	571.315	0.253	18.345	0.221
S.D.	0.047	5.473	77.451	0.034	0.879	0.046
C.V.	4.794	20.607	13.557	13.557	4.794	20.607
Median	0.960	27.870	615.462	0.272	18.082	0.232
Mean +2.00 SD	1.067	37.506	726.217	0.321	20.104	0.313
Mean -2.00 SD	0.881	15.614	416.413	0.184	16.586	0.130
Minimum	0.910	18.170	486.341	0.215	17.140	0.151
Maximum	1.020	31.730	644.381	0.285	19.212	0.264



**Sample ID: TAWRI4**

